

AEDC-TR-78-35
AFATL-TR-78-55

ARCHIVE COPY
DO NOT LOAN

cy.1

**AERODYNAMIC CHARACTERISTICS OF A 1/24-SCALE
F-111 AIRCRAFT WITH VARIOUS EXTERNAL
STORES AT MACH NUMBERS
FROM 0.5 TO 1.3**



C. F. Anderson
ARO, Inc., a Sverdrup Corporation Company

PROPELLION WIND TUNNEL FACILITY
ARNOLD ENGINEERING DEVELOPMENT CENTER
AIR FORCE SYSTEMS COMMAND
ARNOLD AIR FORCE STATION, TENNESSEE 37389

July 1978

Final Report for Period 23 December 1977 — 9 January 1978

Approved for public release; distribution unlimited.

Property of U. S. Air Force
AEDC LIBRARY
F40600-77-0-0003

Prepared for

AIR FORCE ARMAMENT LABORATORY/DLJCA
EGLIN AIR FORCE BASE, FLORIDA 32542

AEDC TECHNICAL LIBRARY

5 0720 00034 2073

NOTICES

When U. S. Government drawings, specifications, or other data are used for any purpose other than a definitely related Government procurement operation, the Government thereby incurs no responsibility nor any obligation whatsoever, and the fact that the Government may have formulated, furnished, or in any way supplied the said drawings, specifications, or other data, is not to be regarded by implication or otherwise, or in any manner licensing the holder or any other person or corporation, or conveying any rights or permission to manufacture, use, or sell any patented invention that may in any way be related thereto.

Qualified users may obtain copies of this report from the Defense Documentation Center.

References to named commercial products in this report are not to be considered in any sense as an endorsement of the product by the United States Air Force or the Government.

This report has been reviewed by the Information Office (OI) and is releasable to the National Technical Information Service (NTIS). At NTIS, it will be available to the general public, including foreign nations.

APPROVAL STATEMENT

This report has been reviewed and approved.



GREGORY COWLEY, 2d Lt, USAF
Project Manager, Research Division
Directorate of Test Engineering

Approved for publication:

FOR THE COMMANDER



CHAUNCEY D. SMITH, JR, Lt Colonel, USAF
Director of Test Operations
Deputy for Operations

UNCLASSIFIED

REPORT DOCUMENTATION PAGE		READ INSTRUCTIONS BEFORE COMPLETING FORM
1 REPORT NUMBER AEDC-TR-78-35 AFATL-TR-78-55	2 GOVT ACCESSION NO.	3 RECIPIENT'S CATALOG NUMBER
4 TITLE (and Subtitle) AERODYNAMIC CHARACTERISTICS OF A 1/24-SCALE F-111 AIRCRAFT WITH VARIOUS EXTERNAL STORES AT MACH NUMBERS FROM 0.5 TO 1.3		5 TYPE OF REPORT & PERIOD COVERED Final Report, 23 Dec 1977 - 9 Jan 1978
7 AUTHOR(s) C. F. Anderson, ARO, Inc.		6 PERFORMING ORG. REPORT NUMBER
9 PERFORMING ORGANIZATION NAME AND ADDRESS Arnold Engineering Development Center Air Force Systems Command Arnold Air Force Station, TN 37389		10. PROGRAM ELEMENT, PROJECT, TASK AREA & WORK UNIT NUMBERS Program Element 65807F System 06ZA, Task 01
11 CONTROLLING OFFICE NAME AND ADDRESS Air Force Armament Laboratory/DLJCA Eglin Air Force Base, Florida 32542		12. REPORT DATE July 1978
		13 NUMBER OF PAGES 129
14 MONITORING AGENCY NAME & ADDRESS (if different from Controlling Office)		15 SECURITY CLASS. (of this report) UNCLASSIFIED
		15a DECLASSIFICATION/DOWNGRADING SCHEDULE N/A
16 DISTRIBUTION STATEMENT (of this Report) Approved for public release; distribution unlimited.		
17 DISTRIBUTION STATEMENT (of the abstract entered in Block 20, if different from Report)		
18 SUPPLEMENTARY NOTES Available in DDC.		
19 KEY WORDS (Continue on reverse side if necessary and identify by block number) F-111 aircraft external stores aerodynamic characteristics wind tunnel tests transonic flow		
20 ABSTRACT (Continue on reverse side if necessary and identify by block number) This report presents and discusses the results of transonic wind tunnel tests conducted to evaluate the effects of external stores on the aerodynamic characteristics of the F-111 aircraft at wing sweep angles of 26, 45, and 54 deg. The analysis includes evaluation of the incremental changes in the drag, static margin, and lateral-directional derivatives associated with the various store configurations. Wind tunnel coefficient data for a clean		

UNCLASSIFIED

UNCLASSIFIED

20. ABSTRACT (Continued)

baseline configuration are also presented. Data are presented with pylons alone, GBU-10, GBU-15CCW, GBU-15CCW with extended Pave Tack pod, AGM-65, Rockeye, SUU-30H/B, and MK-82SE stores. Data are presented for Mach numbers ranging from 0.5 to 1.3 at angles of attack from -2 to 16 deg at zero sideslip angle, and for sideslip angles from -10 to 10 deg at angles of attack of 5, 10, and 15 deg.

PREFACE

The work reported herein was conducted by the Arnold Engineering Development Center (AEDC), Air Force Systems Command (AFSC), at the request of the Air Force Armament Laboratory (AFATL/DLJCA) under Program Element 65807F. The Armament Development and Test Center (ADTC) project monitor was Lt. Thomas Speer. The results of the test were obtained by ARO, Inc., AEDC Division (a Sverdrup Corporation Company), operating contractor for the AEDC, AFSC, Arnold Air Force Station, Tennessee, under ARO Project Number P41C-O4A. Data reduction was completed on February 3, 1978, and the manuscript was submitted for publication on May 16, 1978.

CONTENTS

	<u>Page</u>
1.0 INTRODUCTION	5
2.0 APPARATUS	5
2.1 Test Facility and Model Support System	5
2.2 Test Articles	5
2.3 Instrumentation	6
3.0 TEST DESCRIPTION	6
3.1 Test Conditions, Procedures, and Test Program	6
3.2 Data Reduction and Corrections	7
3.3 Data Uncertainty	8
4.0 TEST RESULTS	8
4.1 Aerodynamic Characteristics of the Baseline Configuration	8
4.2 Effects of Reynolds Number, Transition Grit, and Afterbody Modifications	9
4.3 Aerodynamic Hysteresis Effects	10
4.4 Effects of External Store Loadings	10
5.0 SUMMARY OF RESULTS	12

ILLUSTRATIONS

Figure

1. Tunnel Installation	13
2. F-111 Model	14
3. External Store Suspension Equipment	20
4. External Stores	23
5. Boundary-Layer Transition Grit Pattern	30
6. Pylon/Store Configuration Identification	31
7. Tunnel Flow Angularity	32
8. Aerodynamic Characteristics of the F-111 Aircraft, Clean Configuration	33
9. Static Stability Derivatives and Drag Coefficients of the F-111 Aircraft, Clean Configuration	51
10. Reynolds Number Effects	56
11. Transition Grit Effects, $\Lambda = 26$ deg	62
12. Sting Fairing Effects, $\Lambda = 26$ deg	65

<u>Figure</u>	<u>Page</u>
13. Typical Hysteresis Effects, $\alpha = 15$ deg, $\Lambda = 45$ deg, $M_\infty = 1.2$	68
14. Effects of External Stores on the Static Margin	74
15. Effects of External Stores on the Drag Coefficient	84
16. Effects of External Stores on the Static Directional Stability Derivative	94
17. Effects of External Stores on the Effective Dihedral	104

TABLES

1. Part Number Index	114
2. Aerodynamic Coefficient Uncertainties	127
3. Incremental Drag Coefficients	128
NOMENCLATURE	129

1.0 INTRODUCTION

Wind tunnel tests were conducted to evaluate the effects of various external store loadings on the performance and stability of an F-111 aircraft model. The tests were conducted in the Aerodynamic Wind Tunnel (4T) of the AEDC Propulsion Wind Tunnel Facility (PWT) using a 1/24-scale F-111 aircraft model. Static longitudinal stability, drag, and static lateral-directional stability data were obtained for the clean aircraft model, model with pylons alone, and model with various external store configurations. These data were obtained for wing sweep angles of 26, 45, and 54 deg at Mach numbers from 0.5 to 1.3. Angle of attack was varied from -2 to 16 deg at zero sideslip angle. Sideslip angle was varied from -10 to 10 deg at angles of attack of 5, 10, and 15 deg.

2.0 APPARATUS

2.1 TEST FACILITY AND MODEL SUPPORT SYSTEM

Tunnel 4T is a continuous flow, closed-loop, variable density wind tunnel equipped with a sonic nozzle. The normal Mach number range is from 0.1 to 1.3; however, removable nozzle block inserts can be installed to give Mach numbers of 1.6 and 2.0. The stagnation pressure can be varied from 300 to 3,700 psfa. The test section is 4 ft square and 12.5 ft long with perforated, variable porosity (0.5- to 10-percent open) walls. A detailed description of the tunnel and its capabilities may be found in the Test Facilities Handbook.¹

The model support system consists of a pitch sector and sting which provide a pitch capability from -8 to 28 deg with respect to the tunnel centerline. The pitch center is located at tunnel station 108. The model support system has a remote-control roll system that allows the model to be rolled ± 180 deg.

A schematic of the test section showing the model location is presented in Fig. 1, and model details and installation photographs are presented in Fig. 2.

2.2 TEST ARTICLES

The test articles were 1/24-scale models of the F-111 aircraft, AGM-65, Rockeye, MK-82SE, SUU-30H/B, GBU-10, and GBU-15CCW stores, an extended Pave Tack pod, and associated suspension equipment. The F-111 model had flow-through ducts and was equipped with Type II inlets (no splitter plates) containing fixed 10-deg inlet spikes and

¹Test Facilities Handbook (Tenth Edition). "Propulsion Wind Tunnel Facility, Vol. 4." Arnold Engineering Development Center, May 1974.

nozzle plugs. The aft fuselage and exhaust nozzles were modified to allow insertion of the balance and sting. The model had a fairing above and below the sting between the exhaust nozzles; however, it was removed to avoid fouling the sting. Limited data were obtained with steel shimstock fairings installed between the exhaust nozzles to evaluate the effects of removing the sting fairing on the aerodynamic coefficients. The model is shown with and without the fairing in Fig. 2. The model stabilator was held constant at zero deg with respect to a waterline throughout the test.

The LAU-88 triple rail launchers used with the AGM-65 stores were modified by deleting the stop normally installed at the aft end of each rail to allow for the installation of store balance sting mounts; however, the AGM-65 stores were bolted directly to the launchers for the current test. Basic details and dimensions of the models are presented in Figs. 2 through 4. The transition grit pattern used in evaluating possible boundary-layer transition effects is shown in Fig. 5. Only limited testing was conducted with transition grit installed on the model.

Pylons were installed at the pivot stations (3 through 6) for all testing except for data obtained for the clean configurations. BRU-3AA racks were installed only on those pylons carrying MK-82SE, SUU-30H/B, or Rockeye stores. The pylon loadings for all configurations tested are presented in Fig. 6.

The Pave Tack pod is semisubmerged in the weapons bay when extended. A model representing the exposed portion of the extended Pave Tack pod was attached to the centerline of the weapons bay at MS 12.78 when required.

2.3 INSTRUMENTATION

A six-component, internal strain-gage balance was used to measure the forces and moments on the F-111 model. Two base pressure measurements were made using transducers and orifice tubes which extended just aft of the base of the nozzle plugs.

3.0 TEST DESCRIPTION

3.1 TEST CONDITIONS, PROCEDURES, AND TEST PROGRAM

Static stability data were obtained for all configurations at Mach numbers from 0.5 to 1.3 at a constant total pressure of 1,200 psfa. Limited data were also obtained at 2,000 psfa for $M_\infty = 0.5, 0.9$, and 1.3 with $\Lambda = 26$ and 54 deg with the clean model in order to evaluate possible Reynolds number effects. Transition grit effects were evaluated with the clean model at $p_t = 1,200$ psfa for Mach numbers from 0.6 to 0.95 with $\Lambda = 26$ deg. The nominal test conditions were:

M_{∞}	p_t , psfa	$Re \times 10^{-6}$, per foot
0.5	1,200	1.71
0.5	2,000	2.80
0.7	1,200	2.11
0.8	1,200	2.30
0.9	1,200	2.41
0.9	2,000	4.09
0.95	1,200	2.44
1.05	1,200	2.50
1.10	1,200	2.53
1.20	1,200	2.55
1.30	1,200	2.55
1.30	2,000	3.99

The test procedures were conventional in nature, consisting of varying the model angle of attack incrementally at zero sideslip angle, or varying the model angle of sideslip at a constant angle of attack. The test program that was completed during these tests is presented in Table 1 and provides a key to all the wind tunnel data obtained.

3.2 DATA REDUCTION AND CORRECTIONS

Wind tunnel force and moment data were reduced to coefficient form in the stability axis system. Base drag was calculated using an average of two nozzle plug pressure measurements and was used to calculate forebody coefficients. However, all data presented in this report are measured coefficients. Moments were referenced to MS 21.951 (45-percent MAC at $\Lambda = 16$ deg), WL 7.396, and BL 0 (see Fig. 2).

The angle of attack and angle of sideslip were corrected for sting and balance deflections caused by the aerodynamic loads. The model was tested both upright and inverted at the three wing sweep angles to provide the data to correct for tunnel flow angularity. On the basis of these data, the angle of attack was corrected as indicated by the curve faired through the data presented in Fig. 7. Corrections for the components of model weight, normally termed static tares, were also applied to the data.

3.3 DATA UNCERTAINTY

The data uncertainties determined for a confidence level of 95 percent are presented in Table 2. The aerodynamic coefficient uncertainties include the uncertainties of Mach number and dynamic pressure together with the uncertainty contribution associated with the balance and instrumentation system. Model angle-of-attack uncertainty has been estimated to be ± 0.1 deg and model roll angle ± 0.4 deg.

4.0 TEST RESULTS

The static stability and drag characteristics of the clean F-111 aircraft model are presented together with data showing the incremental effects of various external stores on the drag and on the static longitudinal and lateral-directional stability derivatives. All aerodynamic coefficients are presented for the baseline (clean) configuration; however, only incremental data are presented to show the effects of external stores. The incremental data were obtained by subtracting coefficients and derivatives of the baseline configuration from the coefficients and derivatives of the configurations with stores.

Drag increments were calculated at specific lift coefficients from nonlinear curve fits of the lift and drag coefficients. The static margins were evaluated by taking the slope of a linear least-squares curve fit of C_m versus C_L for nominal angles of attack from -2 to 6 deg. Lateral-directional derivatives were also evaluated from linear least-squares curve fits of the data for nominal sideslip angles from -4 to 4 deg.

All moment coefficients and stability derivatives are referenced to a standard moment reference center located at 45 percent of the MAC with the wing at 16 deg sweep angle (see Fig. 2).

4.1 AERODYNAMIC CHARACTERISTICS OF THE BASELINE CONFIGURATION

The static aerodynamic characteristics of the clean F-111 model are presented in Fig. 8. Although the characteristics are generally well behaved, the lift coefficient variation with angle of attack exhibited unusual changes in slope at $M_\infty = 0.9$ and 0.95 with $\Lambda = 26$ deg. Also, the rolling-moment coefficient was less well behaved at $M_\infty \geq 0.8$ for $\Lambda = 26$ deg. The reason for the rolling-moment coefficient behavior is not known; however, hysteresis checks made at $\alpha = 15$ deg indicate that the data repeated within the data uncertainty when the model was yawed in both directions. Hysteresis is responsible for the shift in the C_n curves at $\alpha = 15$ deg at supersonic Mach numbers (Fig. 8e) and is discussed further in Section 4.3.

The data presented in Fig. 8 are summarized in Fig. 9 in terms of static longitudinal and lateral-directional stability parameters and drag coefficients at specific values of the lift coefficient. These data show that the F-111 model has essentially neutral static longitudinal stability at $\Lambda = 26$ deg. Static longitudinal stability increases with increasing wing sweep angle and with increasing Mach number for $M_\infty > 0.9$.

The static margin was calculated by a linear fit of the C_L versus C_m curves in order to provide a single figure representative of the static longitudinal stability over a moderate angle-of-attack range. This procedure provides a reasonable approximation for $\Lambda = 45$ and 54 deg; however, both C_L and C_m have significant nonlinearities at low angles of attack at $\Lambda = 26$ deg. Therefore, static margins for $\Lambda = 26$ deg were also calculated by determining the slope of a nonlinear curve fit of C_L versus C_m at specific values of C_L to show the effects of nonlinearities on the static margin (Fig. 9b). The linear curve fit represents a reasonable approximation of the static margin in the angle-of-attack range of interest for Mach numbers through 0.8. At $M_\infty = 0.9$ and 0.95, at $\Lambda = 26$ deg, SM and ΔSM should be used with caution because of the nonlinearities in C_L and C_m .

As shown in Fig. 9, the F-111 model was directionally stable at all conditions tested except at $\alpha = 15$ deg at $M_\infty = 1.05$ and 1.1, where the model became directionally unstable. The F-111 model also had favorable effective dihedral except at $\alpha = 5$ deg for Mach numbers near 0.8 and 0.9 at $\Lambda = 26$ deg.

4.2 EFFECTS OF REYNOLDS NUMBER, TRANSITION GRIT, AND AFTERBODY MODIFICATIONS

The effects of Reynolds number were investigated by testing the clean model at $p_t = 2,000$ psfa at $M_\infty = 0.5$, 0.9, and 1.3 for $\Lambda = 26$ and 54 deg (Fig. 10). At present Reynolds number effects are evident for angles of attack above 8 deg at $M_\infty = 0.5$ and at all angles of attack at $M_\infty = 0.9$ for $\Lambda = 26$ deg. At $\Lambda = 54$ deg, increasing Reynolds number had no effect at $M_\infty = 0.9$; at $M_\infty = 1.3$, increasing Reynolds number decreased C_L , increased C_m , and had little effect on C_D for angles of attack above 8 deg. The addition of transition grit (Fig. 11) had no significant effect on the aerodynamic coefficients of the clean model at $\Lambda = 26$ deg, indicating that the changes produced by increasing total pressure are not necessarily boundary-layer transition effects.

High balance dynamic loads limited the testing that could be accomplished at $p_t = 2,000$ psfa. Since the primary purpose of the test was to evaluate the incremental changes in aerodynamic coefficients by adding external stores to the F-111 aircraft, and the effects produced by increasing total pressure are not believed to affect the incremental data, all store effect data were obtained at $p_t = 1,200$ psfa and without transition grit.

The model was designed with fairings above and below the sting between the nozzle ducts. These fairings were deleted to prevent the sting from fouling the model (Fig. 2c). The effects of removing the fairings were investigated at $\Lambda = 26$ deg by welding steel shimstock between the nozzle ducts as shown in Fig. 2c. The effects of the sting fairings on C_L , C_m , and C_D are shown in Fig. 12. As expected, the principal effect of the sting fairings was to increase the nose-down pitching moment at all Mach numbers. There was also a slight increase in C_L at angles of attack above 6 deg at $M_\infty = 0.95$. All data presented in this report were obtained with the sting fairing removed except for the data presented in Fig. 12.

4.3 AERODYNAMIC HYSTERESIS EFFECTS

Aerodynamic hysteresis occurs when the value of an aerodynamic coefficient depends on the past history of the model motion, and this phenomenon makes analysis and application of the data difficult. Aerodynamic hysteresis had been observed in pitch and yaw polars at angles of attack below 20 deg during recent transonic wind tunnel tests of a fighter configuration. Therefore, a brief survey was conducted to determine whether aerodynamic hysteresis occurred within the angle-of-attack and sideslip range of the current test.

Hysteresis effects were investigated by pitching and yawing the model in both directions. No significant hysteresis effects were observed for pitch polars; however, significant hysteresis effects were observed in yaw polars with the clean configuration for $\alpha = 15$ deg at supersonic Mach numbers. Typical hysteresis effects obtained while yawing the model from -10 to 10 to -10 deg for the clean aircraft and with 12 SUU-30H/B stores, at $M_\infty = 1.2$ and $\alpha = 15$ deg, are presented in Fig. 13. At these test conditions, all aerodynamic coefficients except C_N exhibited some hysteresis for the clean configuration, with yawing moment showing the most pronounced effect. Only limited hysteresis data were taken with external stores; however, the data suggest that the addition of pylons, with or without external stores, significantly reduced hysteresis effects during yaw polars. Because test time was limited, all yaw polars could not be run in both directions. Therefore, most of the yaw polars were run with increasing β , and all yaw data presented in the remainder of this report were obtained while increasing β from -10 to 10 deg.

4.4 EFFECTS OF EXTERNAL STORE LOADINGS

The effects of pylons and various loadings of external stores on the static margin are presented in Fig. 14. Pylons-alone and single-carriage store effects are shown in Figs. 14a through d, and multiple-carriage store effects are shown in Figs. 14e through j. All

external store loadings were generally destabilizing, except at $M_\infty = 0.8$ and 0.9 with $\Lambda = 26$ deg. Single-carriage loads were generally less destabilizing than multiple-carriage loads. Adding the extended Pave Tack pod to the model with four GBU-15CCW stores had little effect on the static longitudinal stability at subsonic Mach numbers and produced a slight increase in static longitudinal stability at supersonic Mach numbers.

Incremental drag data showing the effects of pylons and various external store loadings on the drag of the clean F-111 model are presented in Fig. 15. The variations of the incremental drag coefficients exhibit the normal transonic drag rise. The incremental drag coefficients also decrease with increasing wing sweep angle. Drag increments produced by the various external stores at representative level flight values of C_L are also presented in tabulated format in Table 3.

The effects of various external store loadings on the static directional stability derivative are presented in Fig. 16 in the form of incremental changes in the static directional stability derivative. Most pylon store configurations had little effect on static directional stability except at $M_\infty = 0.9$ and 0.95 where the GBU-10, GBU-15CCW, and AGM-65 stores generally degraded the static directional stability at $\alpha = 15$ deg. At supersonic Mach numbers, pylon store configurations generally increased the static directional stability (positive $\Delta C_{n\beta}$). The static directional stability contribution of all pylon store configurations increased with increasing Mach number and wing sweep angle at supersonic Mach numbers. Adding the extended Pave Tack pod to the fuselage centerline degraded the static directional stability at all wing sweep angles, angles of attack, and Mach numbers.

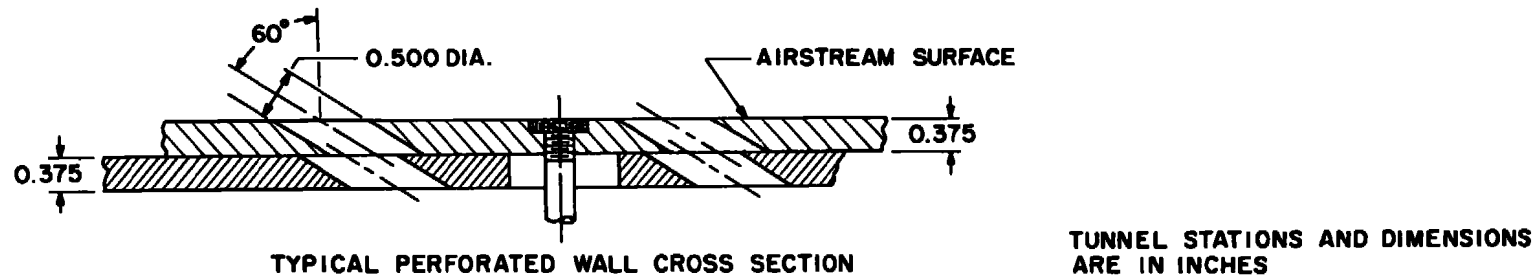
The effects of external store configurations on the effective dihedral are presented in Fig. 17. At $\Lambda = 26$ deg, pylon stores generally increased the effective dihedral (negative $\Delta C_{\ell\beta}$) at $\alpha = 5$ deg. At higher angles of attack, most pylon store configurations decreased the effective dihedral. In particular, the incremental data in Figs. 17c and d, when compared to the clean configuration data in Fig. 9e, show that the GBU-15CCW with and without the extended Pave Tack pod degraded $C_{\ell\beta}$ sufficiently to change the effective dihedral from favorable to unfavorable at $\alpha = 15$ deg at $M_\infty = 0.7$.

Increasing the wing sweep angle decreased the effect of pylon stores on the effective dihedral. However, at $\Lambda = 45$ deg, the low effective dihedral of the clean aircraft at $\alpha = 5$ and 10 deg for $M_\infty > 0.9$ allowed all pylon store configurations to reduce the effective dihedral to near zero. Adding the extended Pave Tack pod to the aircraft with four GBU-15CCW stores had no significant effect on the effective dihedral.

5.0 SUMMARY OF RESULTS

Transonic wind tunnel tests were conducted to determine the effects of external stores on the aerodynamic characteristics of the F-111 aircraft. The results obtained are summarized as follows:

1. For the moment reference point chosen, the clean aircraft model exhibited near-neutral longitudinal stability for a 26-deg wing sweep angle and was directionally unstable at high angles of attack at Mach numbers 1.05 and 1.10.
2. The clean aircraft model exhibited hysteresis effects during yaw polars for all coefficients except the normal-force coefficient. The yawing-moment coefficient exhibited the most hysteresis effects. Addition of pylons, or pylons and stores, significantly reduced hysteresis effects.
3. Generally, all pylon store and pylon configurations tested decreased the static longitudinal stability, except for Mach numbers 0.8 and 0.9 at wing sweep angles of 26 deg, where pylons, single carriage, and AGM-65 store configurations increased the static longitudinal stability.
4. Adding pylon stores generally had little effect on the static directional stability at subsonic Mach numbers except at $M_\infty = 0.9$ and 0.95, where the GBU-10, GBU-15CCW, and AGM-65 were destabilizing at high angles of attack. All external stores increased the static directional stability at supersonic Mach numbers.
5. Most pylon store configurations produced a favorable dihedral effect at an angle of attack of 5 deg and an unfavorable dihedral effect at higher angles of attack at a wing sweep angle of 26 deg. Increasing wing sweep angle decreased the effect of pylon stores on the effective dihedral.
6. Adding the extended Pave Tack pod increased the static longitudinal stability at Mach numbers above 1.0, increased the drag coefficient, decreased the static directional stability, and had no significant effect on the effective dihedral.



13

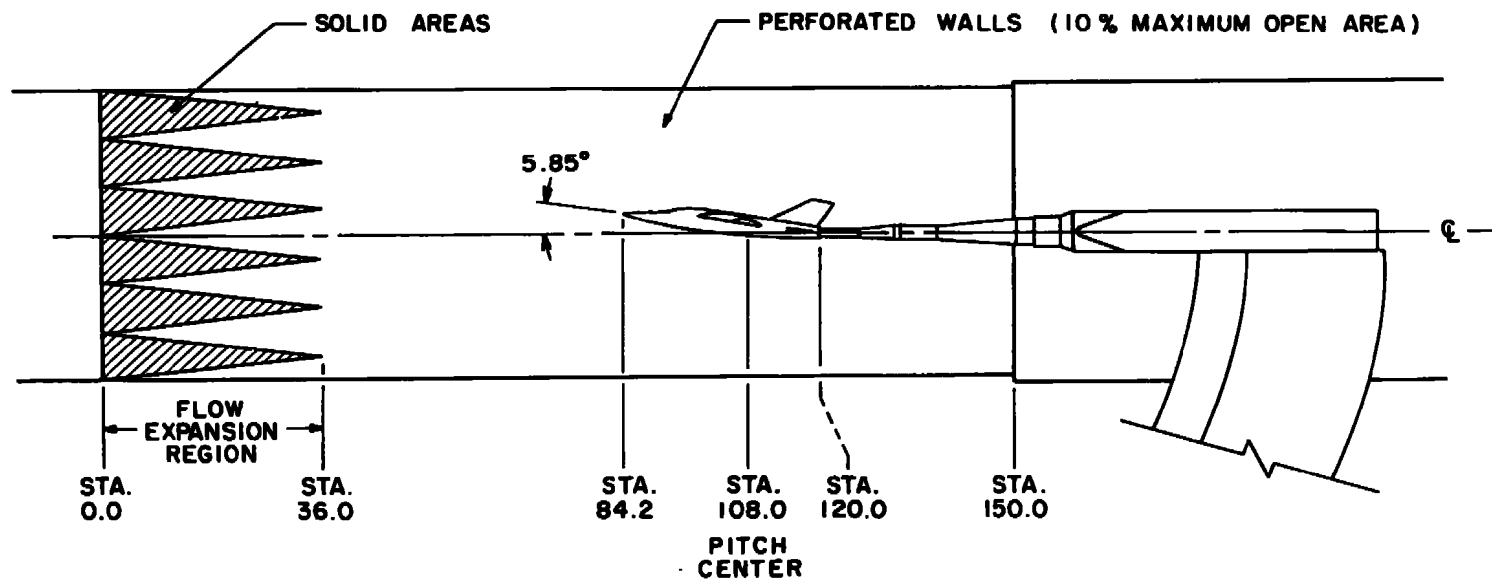
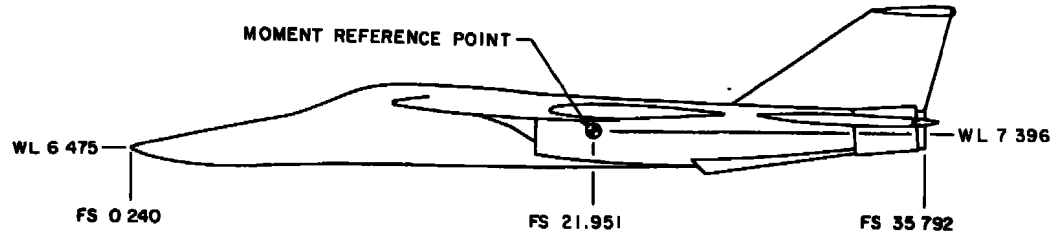
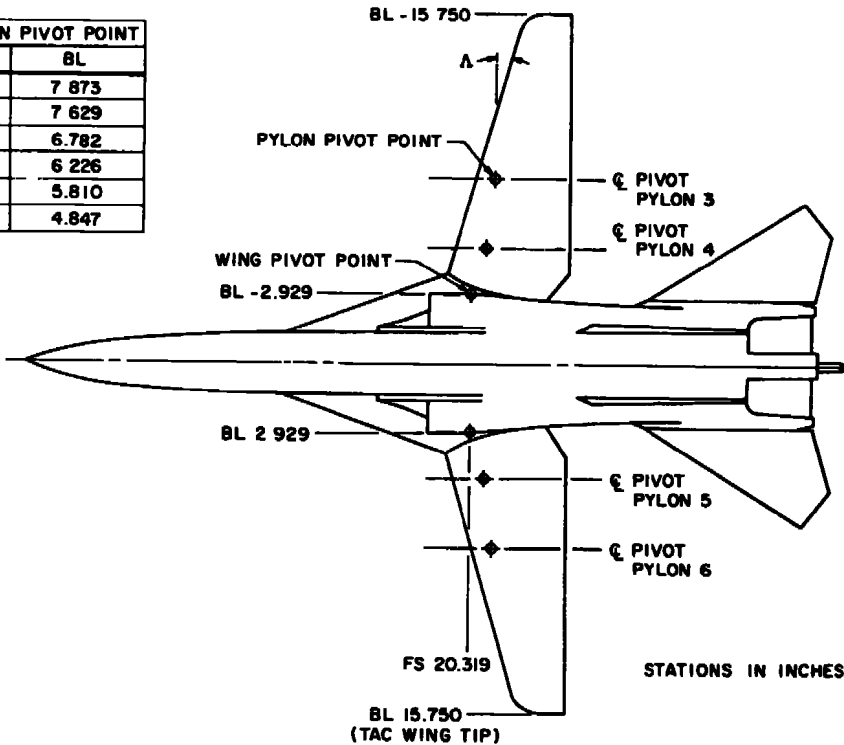


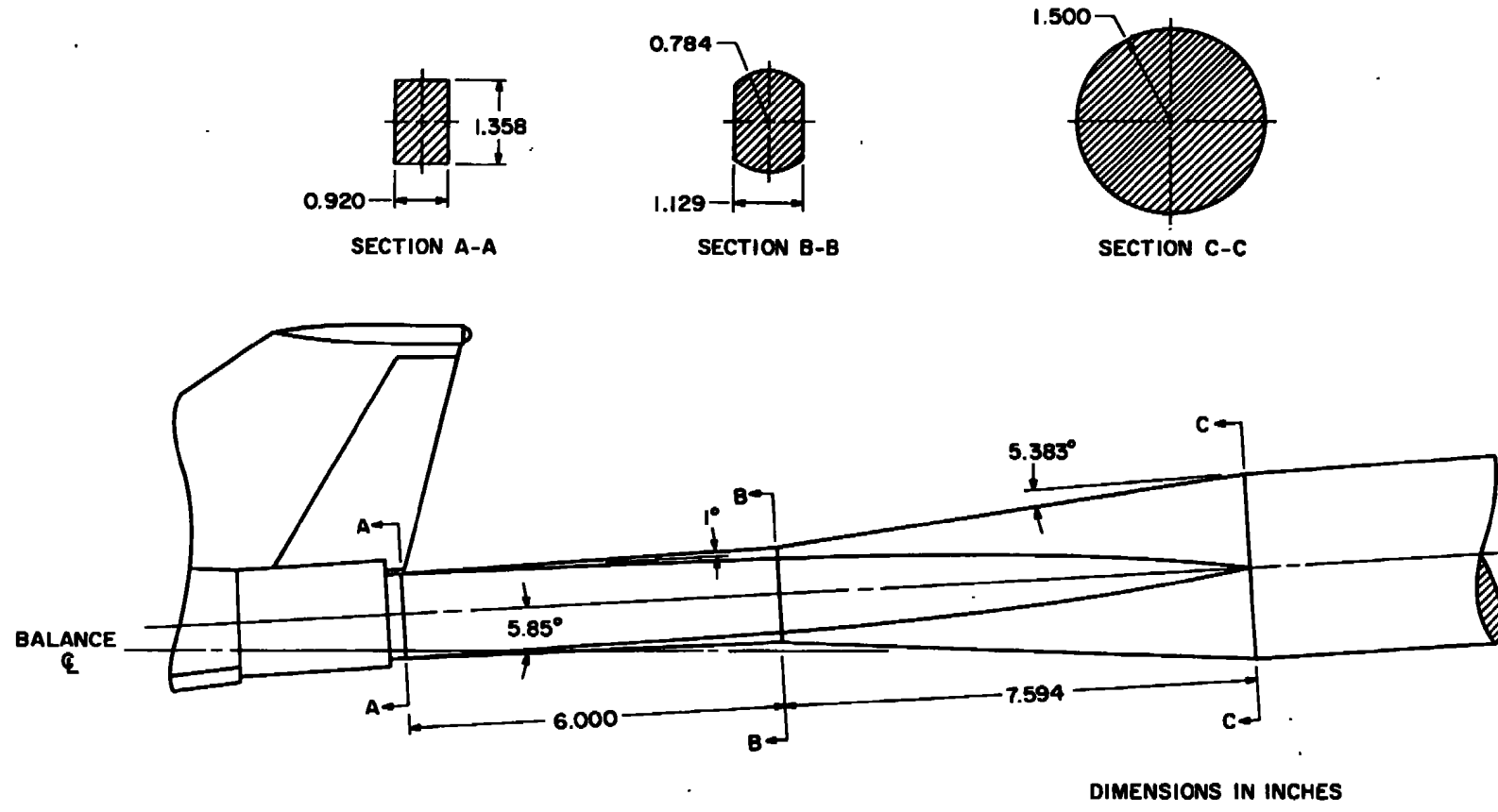
Figure 1. Tunnel installation.



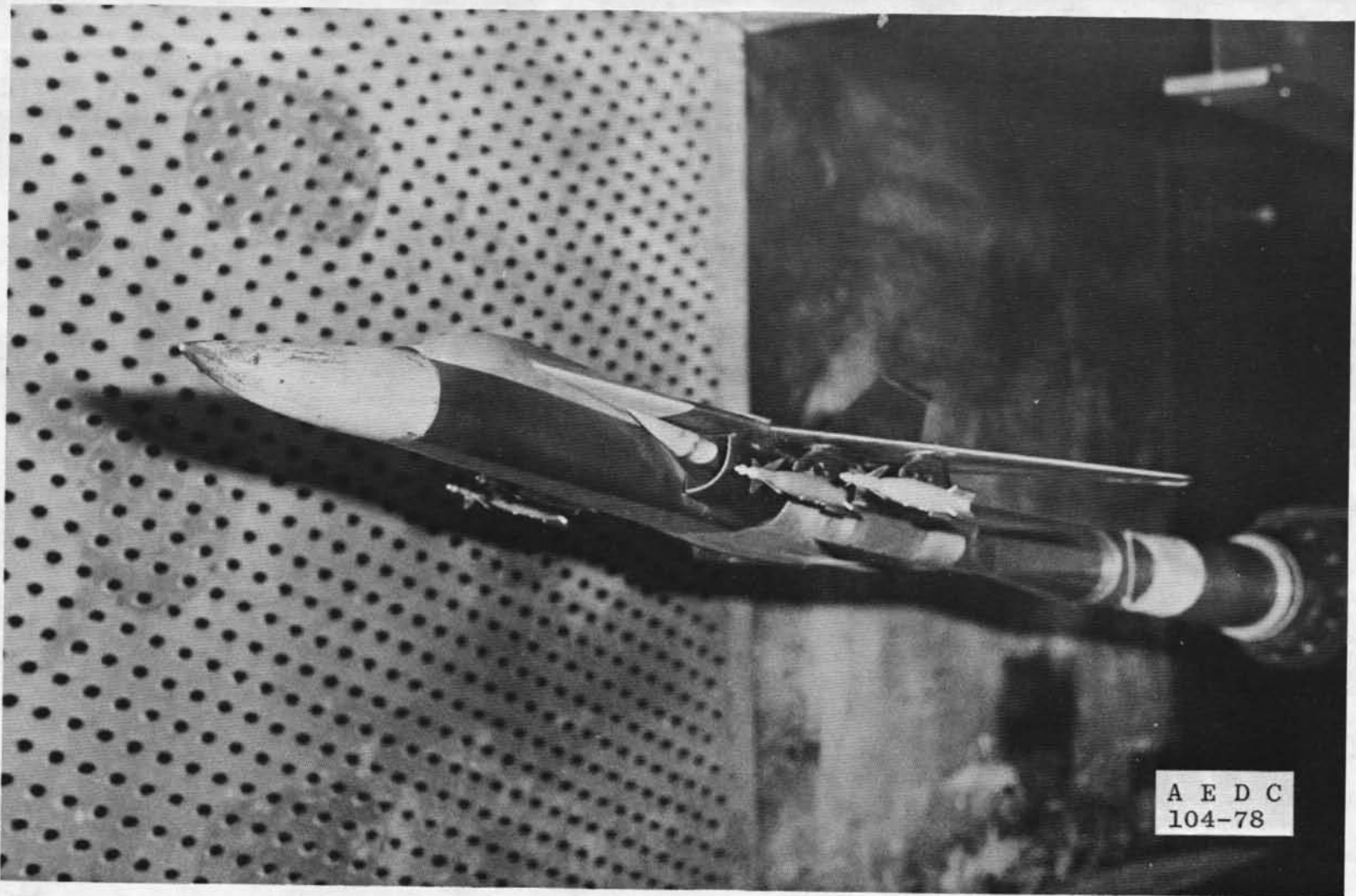
A	INBD PYLON PIVOT POINT		OUTBD PYLON PIVOT POINT	
	FS	BL	FS	BL
16(Ref)	20.962	4 913	21 291	7 873
26	21.297	4.771	22.135	7 629
45	21.843	4.352	23 566	6.782
54	22 047	4.096	24 129	6 226
60	22 160	3.910	24 452	5.810
72.5	22.238	3.488	24 978	4.847



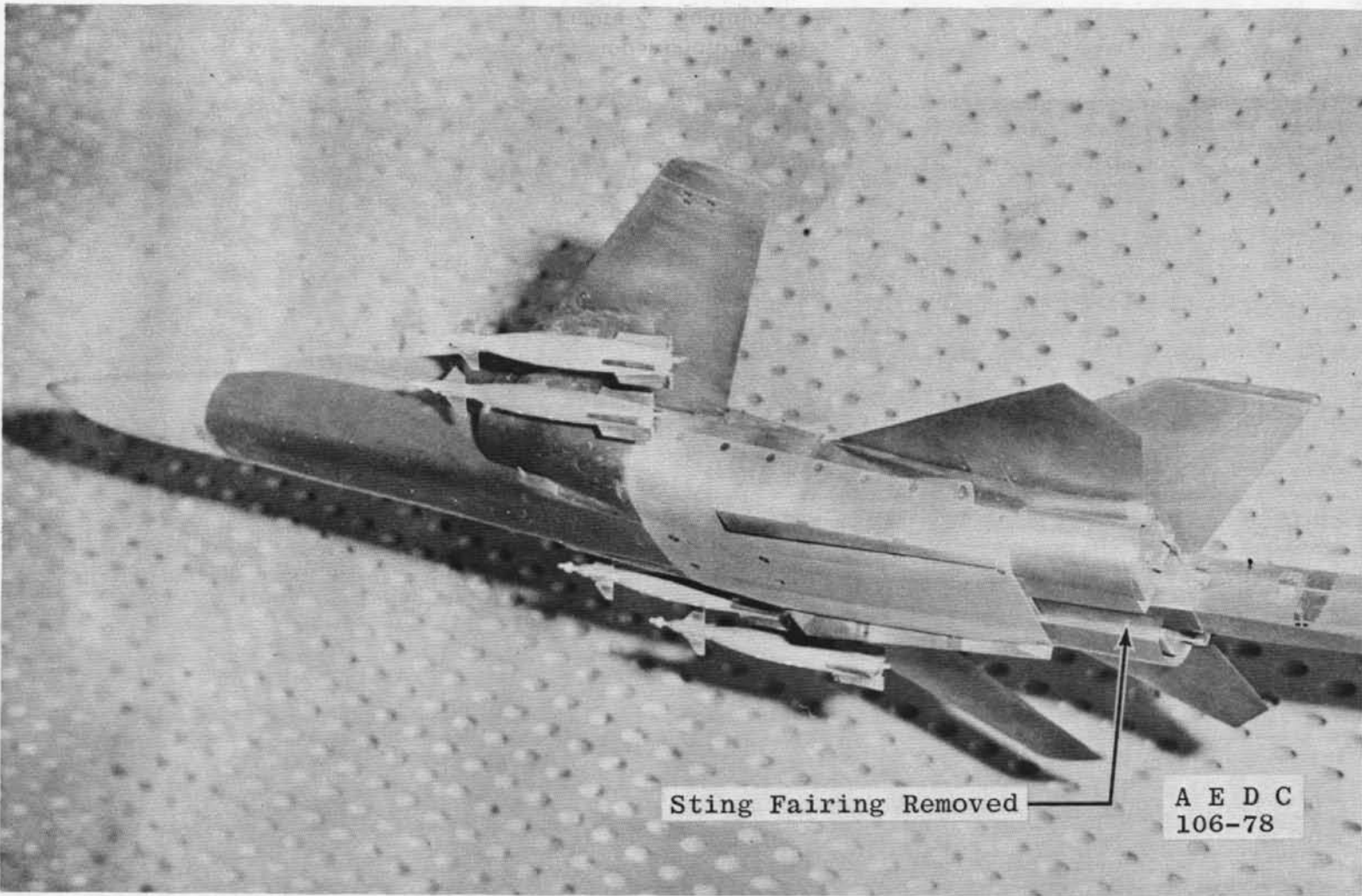
a. General arrangement
Figure 2. F-111 model.



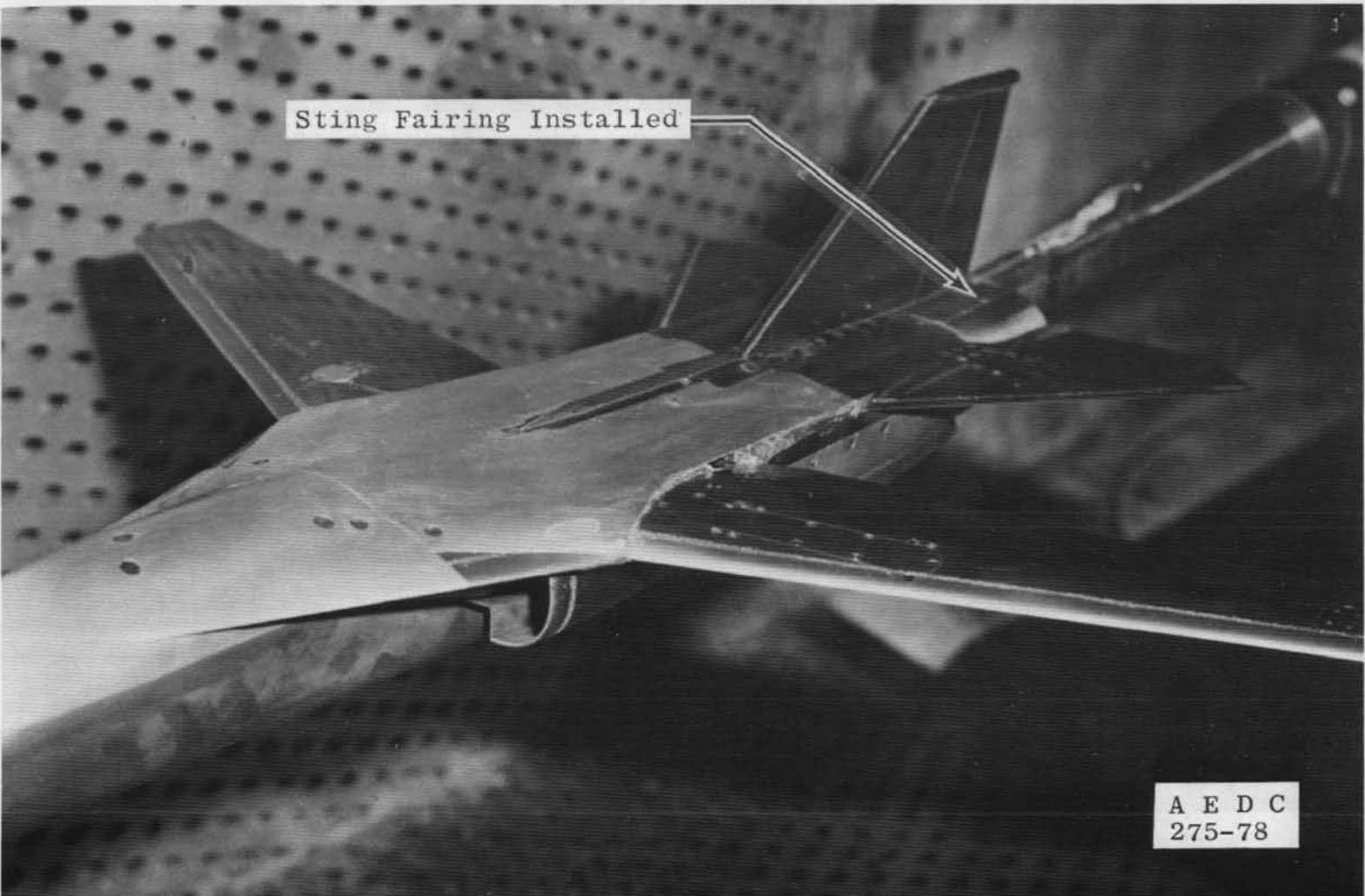
b. Model base details
Figure 2. Continued.



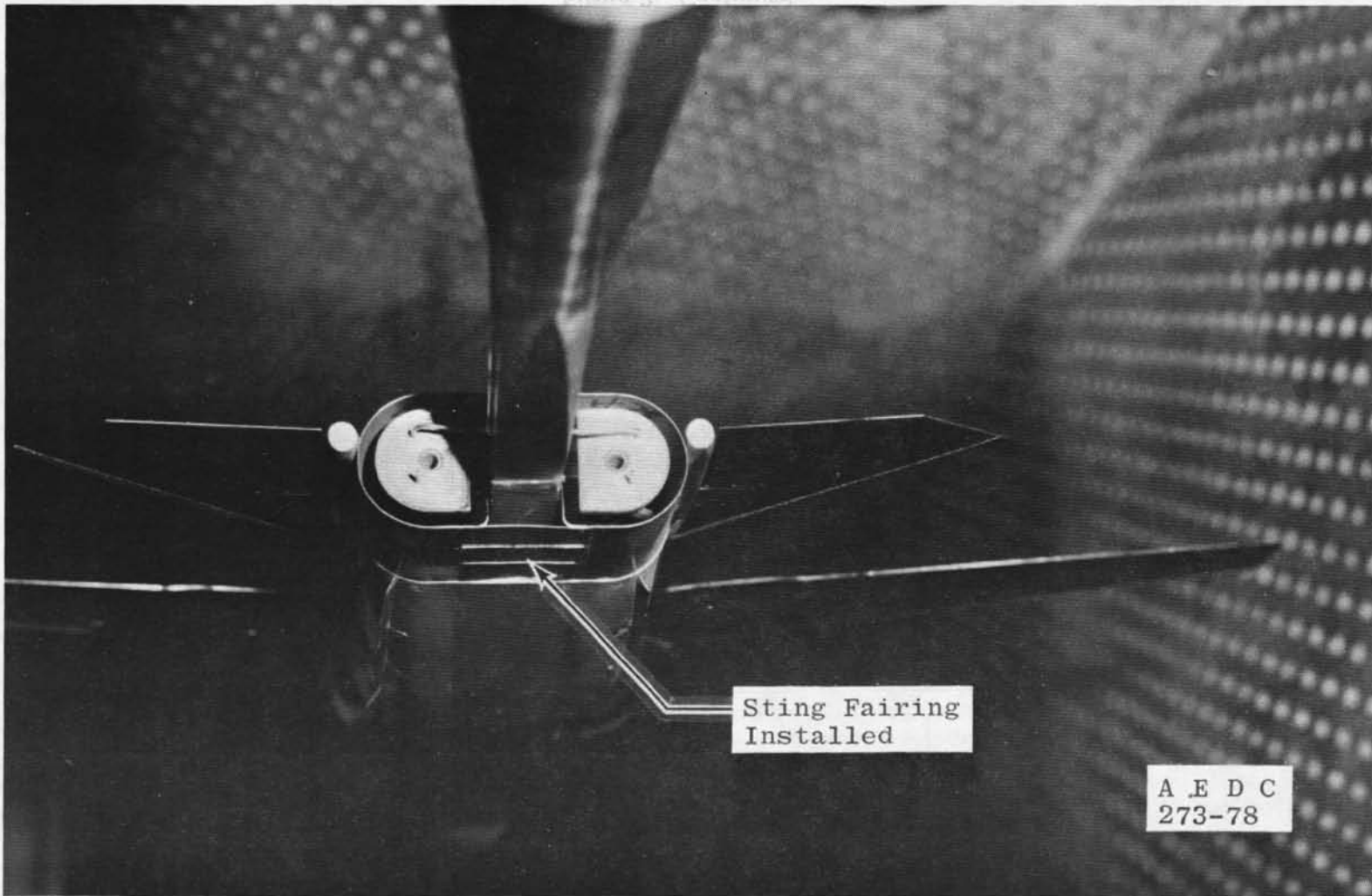
c. Model photographs
Figure 2. Continued.



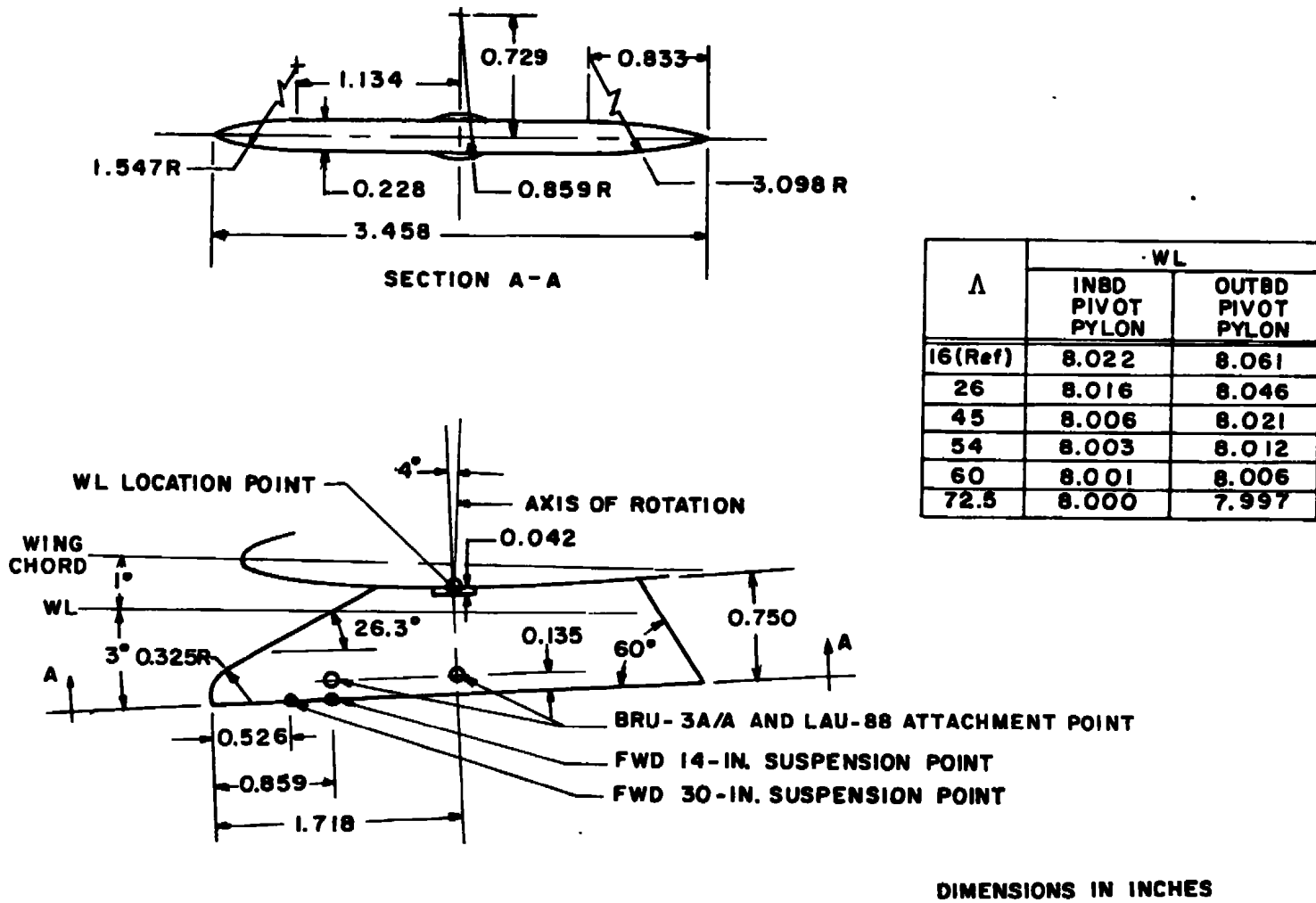
c. Continued
Figure 2. Continued.



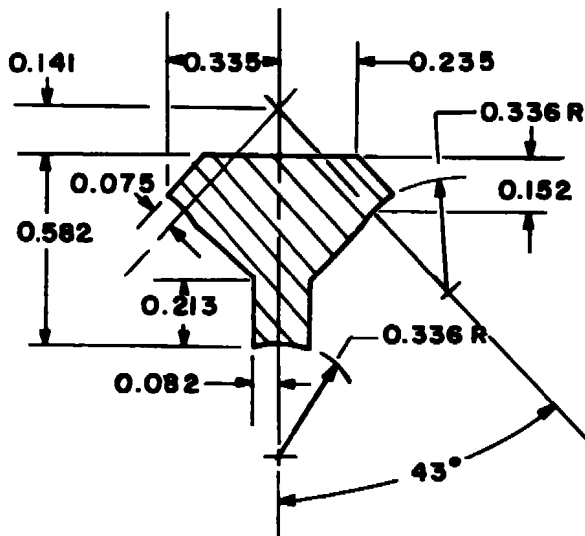
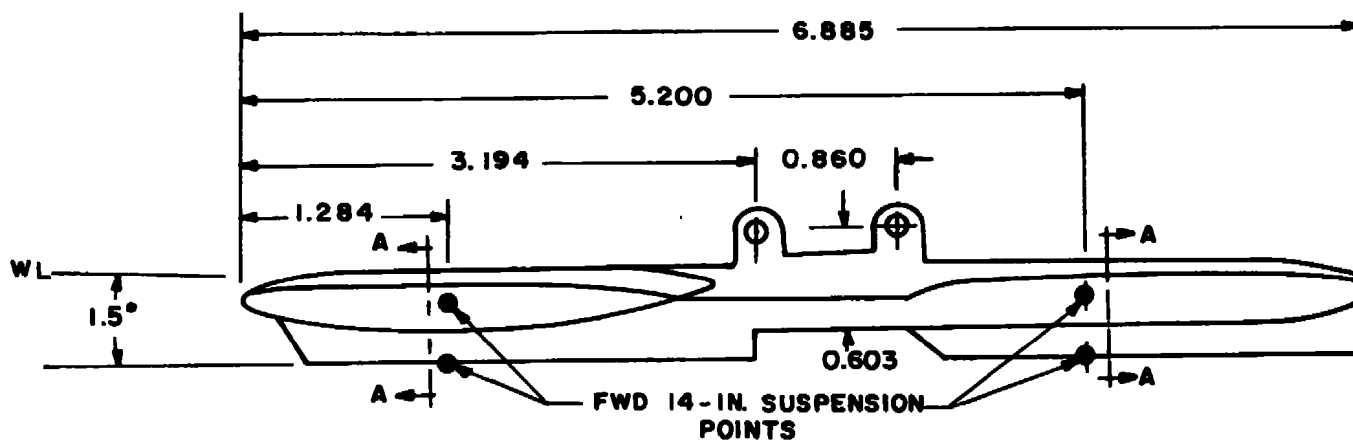
c. Continued
Figure 2. Continued.



c. Concluded
Figure 2. Concluded.

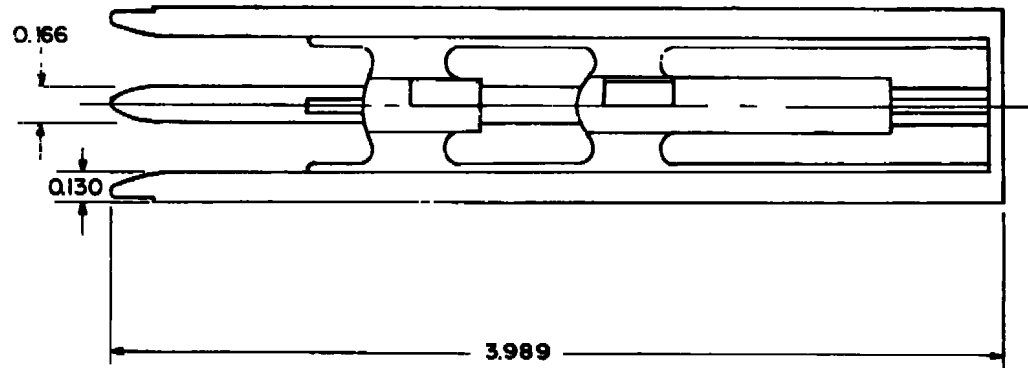


a. Pylon
Figure 3. External store suspension equipment.

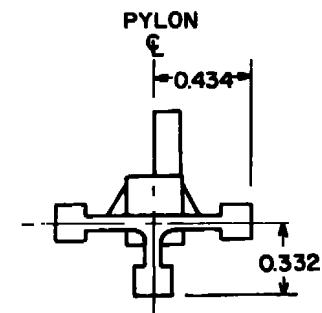
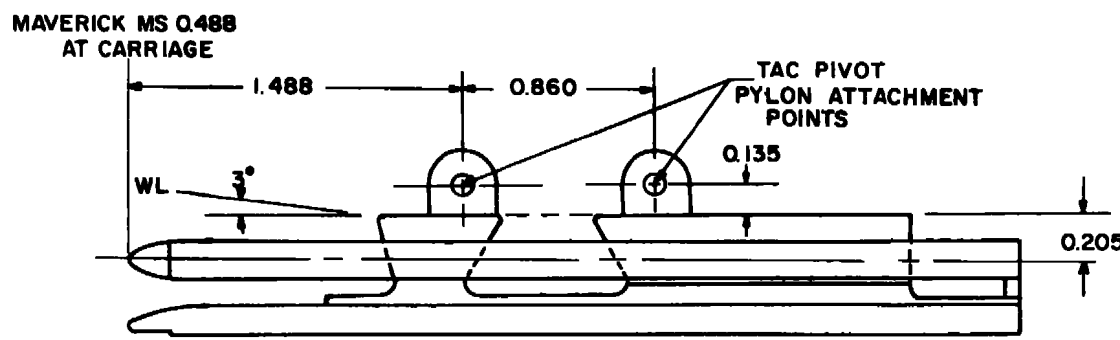


SECTION A-A
DIMENSIONS IN INCHES

b. BRU-3A/A rack
Figure 3. Continued.

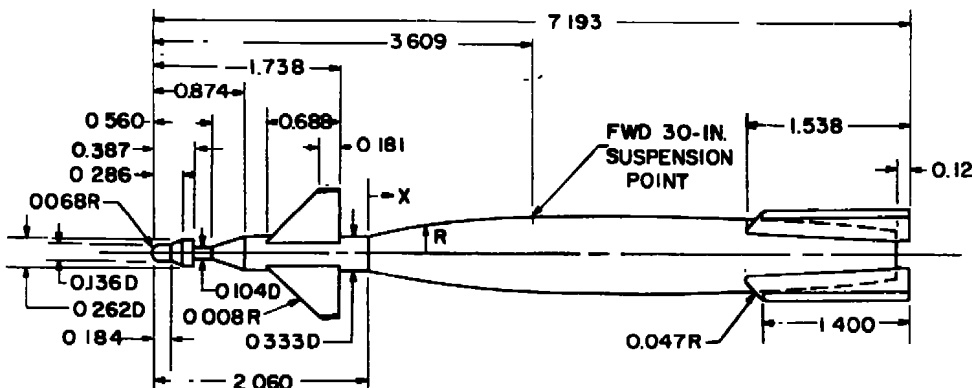


DIMENSIONS IN INCHES



c. LAU-88 triple-rail launcher
Figure 3. Concluded.

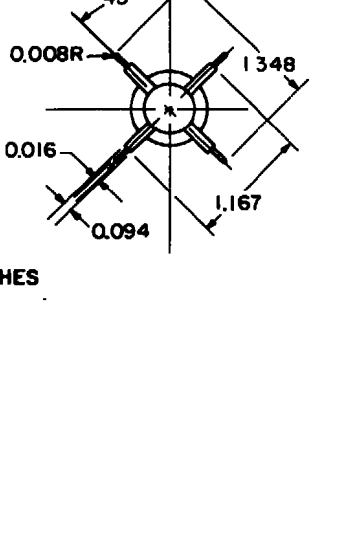
X, in.	R, in.
0	0 167
0 132	0 202
0 275	0 233
0 417	0 258
0 560	0 279
0 703	0 305
0 846	0 313
0 989	0 326
1 132	0 339
1 275	0 350
1 417	0 360
1 560	0 368
1 703	0 373
1 846	0 375
CONST DIAM	
2 846	0 375
2 989	0 373
3 132	0 370
3 275	0 365
3 417	0 358
3 560	0 350
3 794	0 334
CONST SLOPE	
5 012	0 233

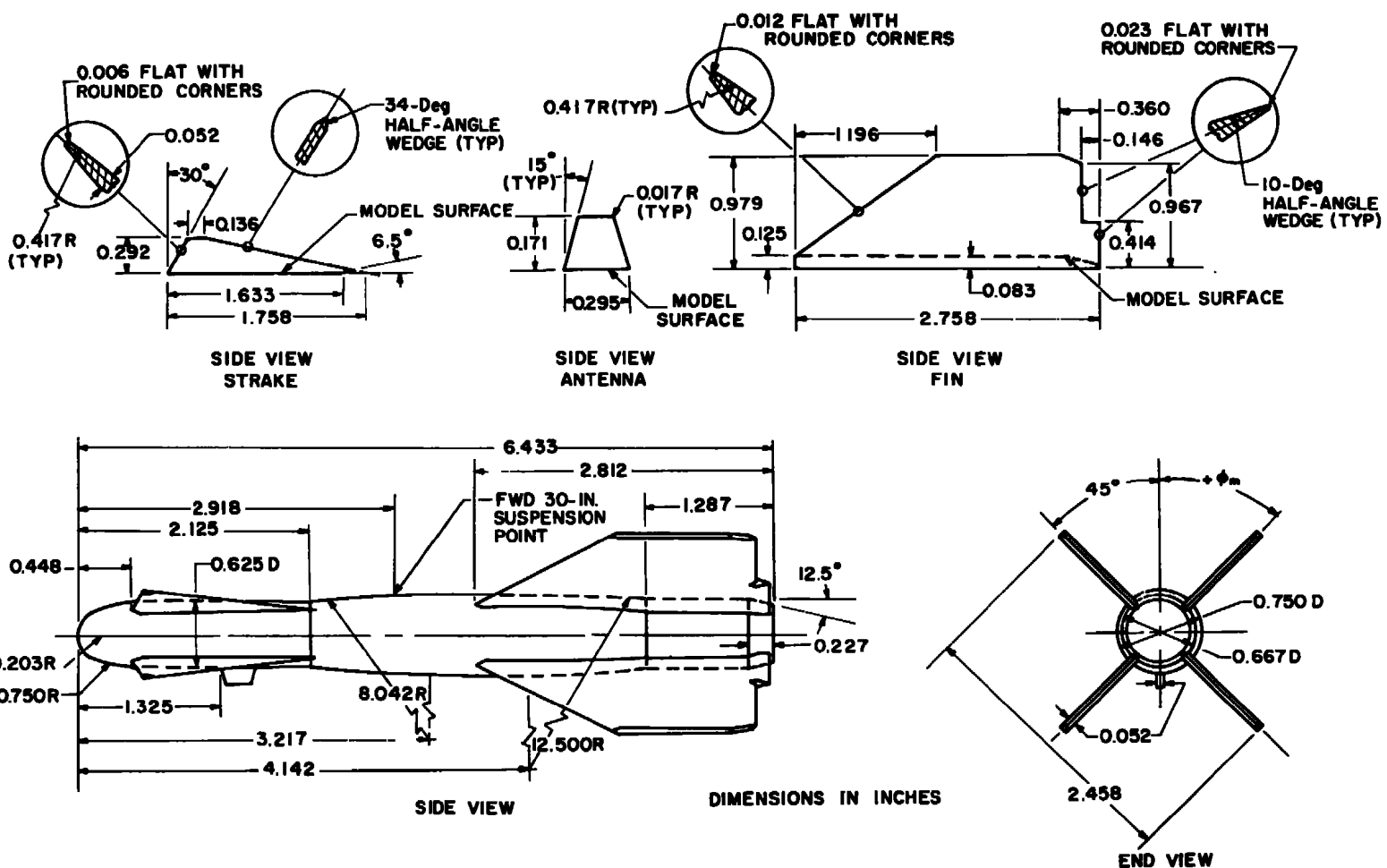


DIMENSIONS IN INCHES

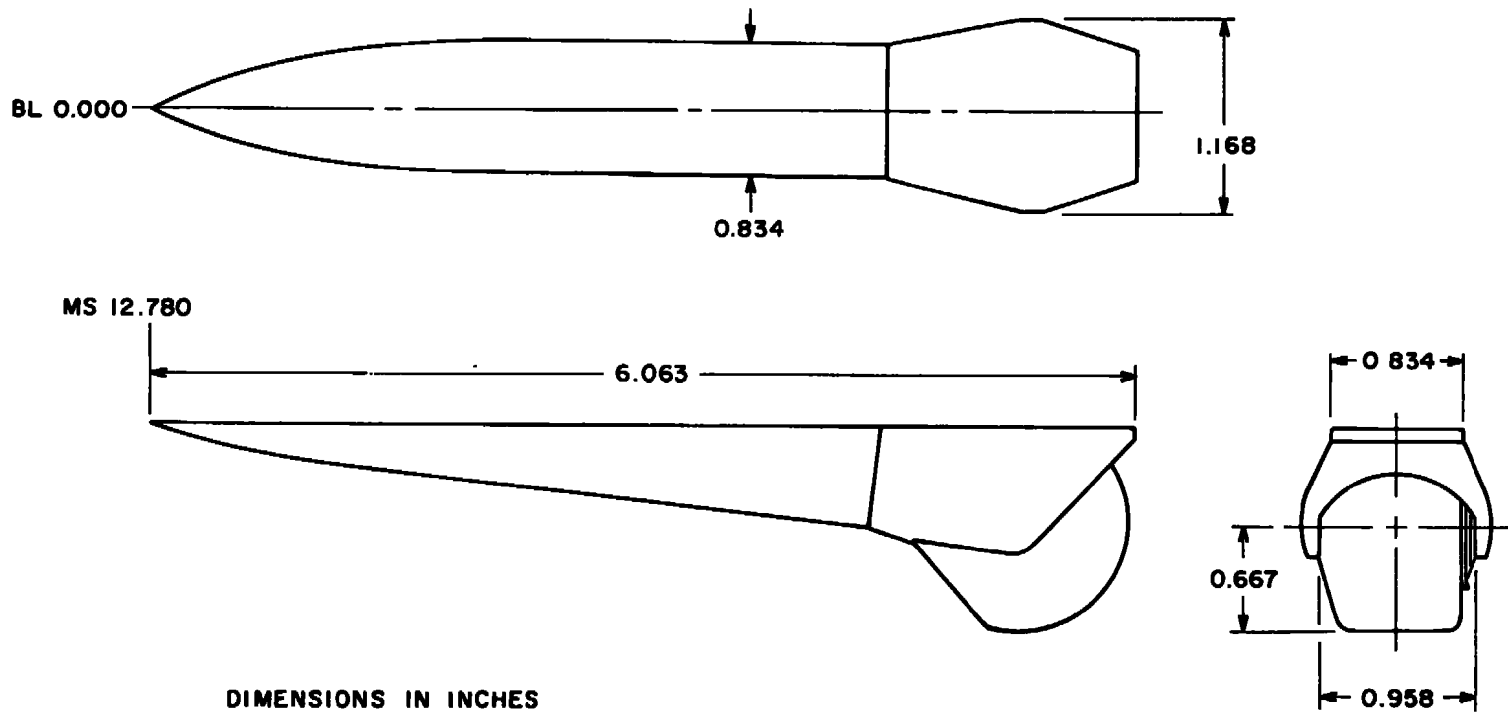
a. GBU-10

Figure 4. External stores.

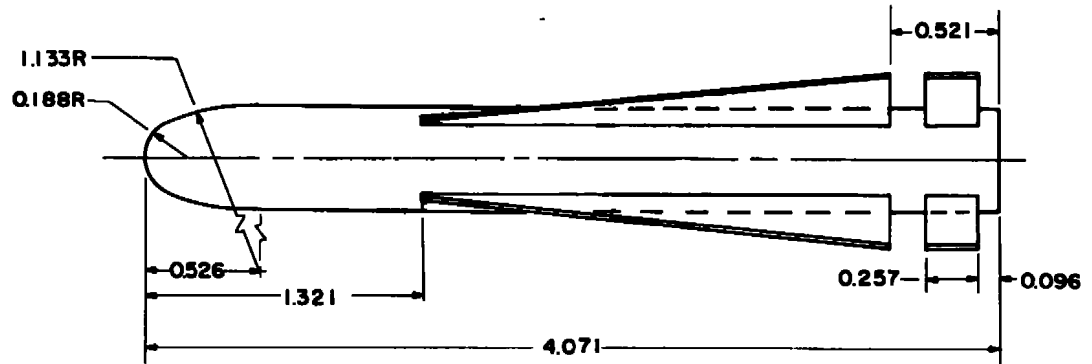




b. GBU-15CCW
Figure 4. Continued.

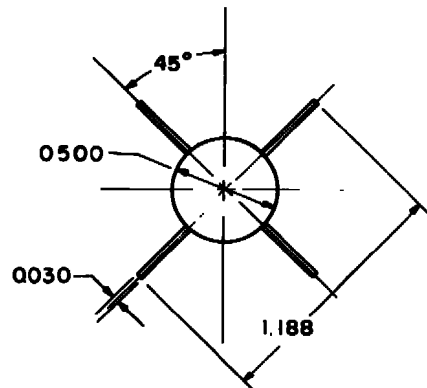


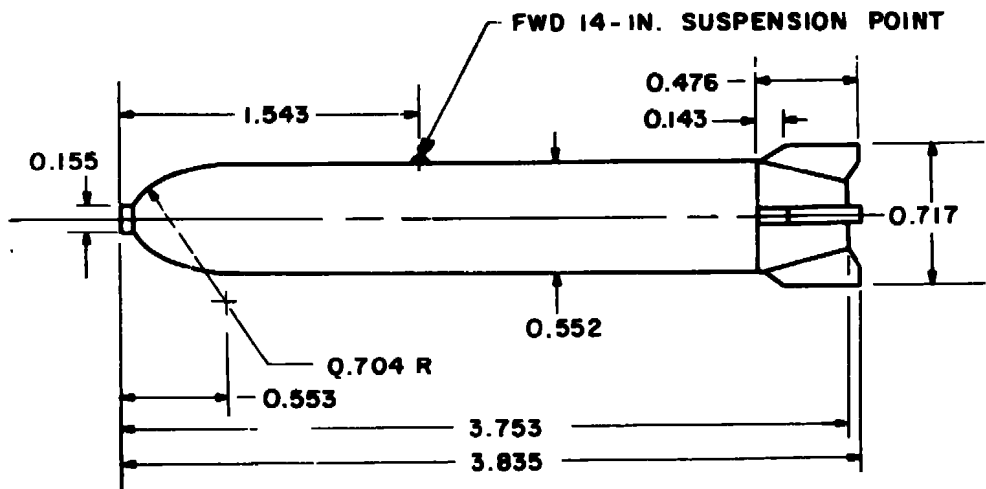
c. Extended Pave Tack pod
Figure 4. Continued.



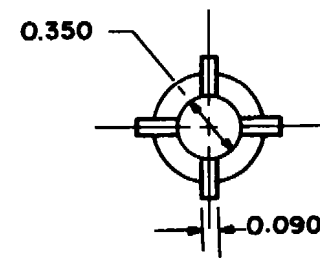
DIMENSIONS IN INCHES

d. AGM-65 Maverick
Figure 4. Continued.

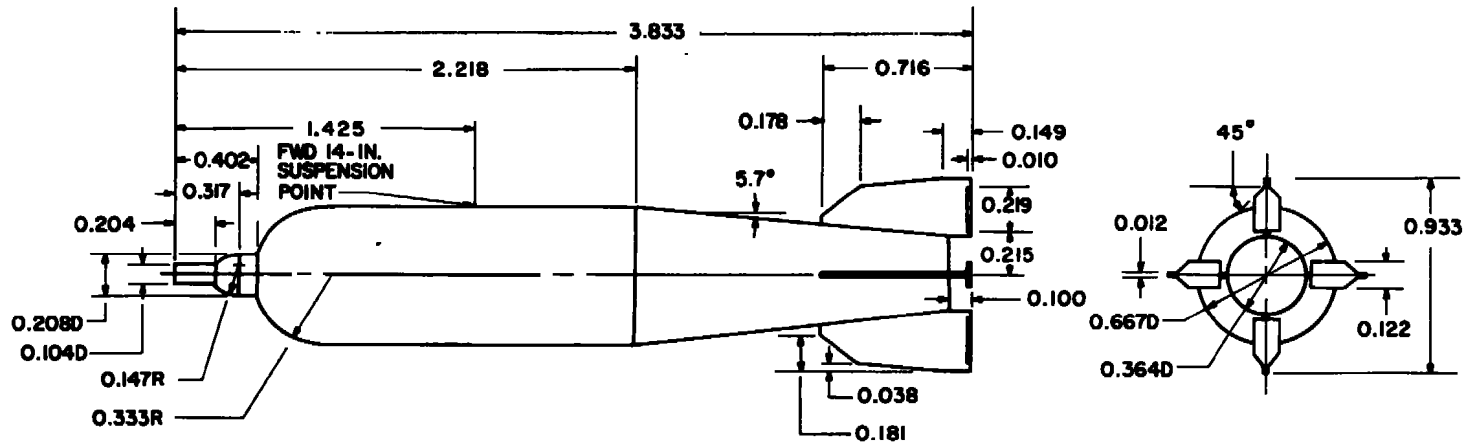




e. Rockeye
Figure 4. Continued.



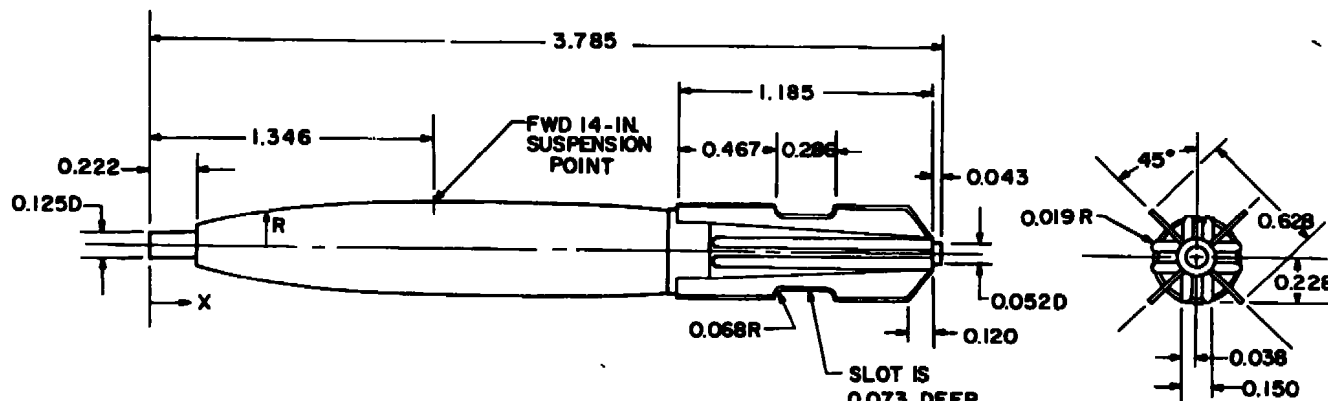
DIMENSIONS IN INCHES



DIMENSIONS IN INCHES

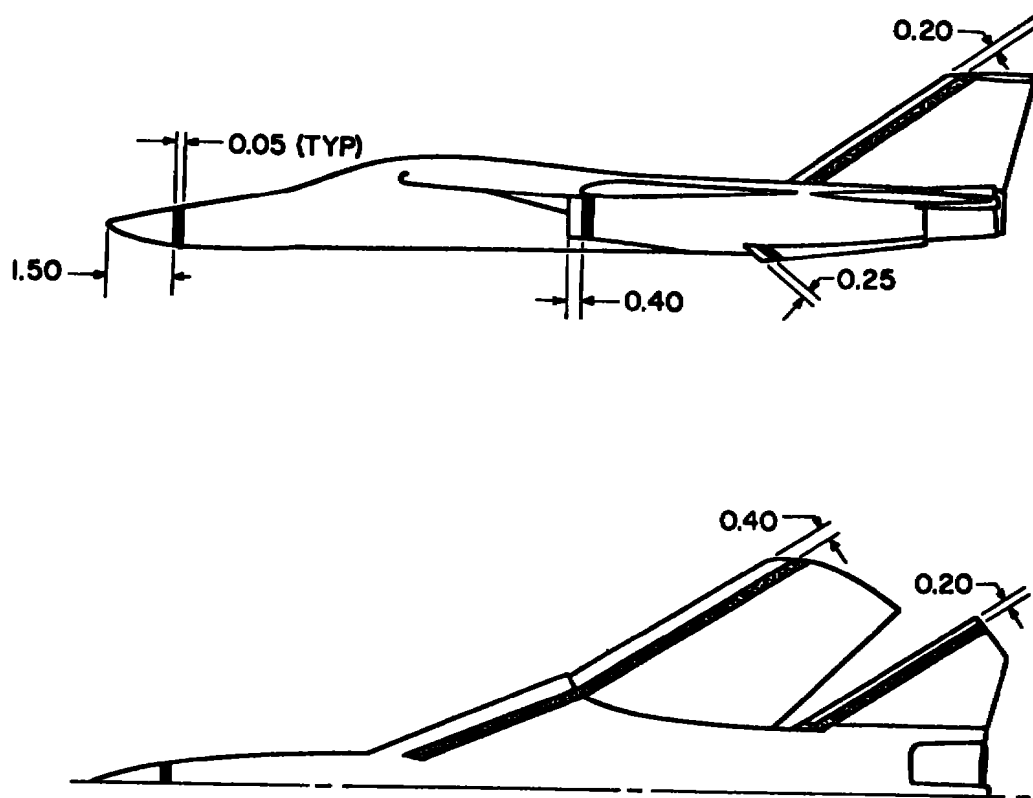
f. SUU-30H/B
Figure 4. Continued.

X, in.	R, in.
0.222	0.096
0.297	0.117
0.357	0.130
0.485	0.154
0.656	0.177
0.826	0.195
0.997	0.209
1.168	0.220
1.338	0.224
CONST DIAM	
1.893	0.224
2.063	0.222
2.234	0.216
2.404	0.206
2.479	0.201
2.479	0.209
CONST SLOPE	
2.675	0.210
CONST SLOPE	
3.440	0.088
CONST DIAM	
3.742	0.088



DIMENSIONS IN INCHES

g. MK-82SE
Figure 4. Concluded.

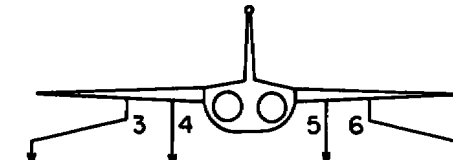


DIMENSIONS IN INCHES
#150 TRANSITION GRIT

NOTE:

TRANSITION GRIT USED ONLY
FOR LIMITED TESTING TO
EVALUATE TRANSITION GRIT
EFFECTS

Figure 5. Boundary-layer transition grit pattern.



STORES	BRU-3A/A RACK	LEFT OUTBOARD	LEFT INBOARD	RIGHT INBOARD	RIGHT OUTBOARD
CLEAN					
PYLONS ALONE	N/A	□	□	□	□
4 GBU-10	N/A	○	○	○	○
4 GBU-15 CCW	N/A	○	○	○	○
4 GBU-15 CCW AND CENTERLINE PAVE TACK POD	N/A	○	○	○	○
12 AGM-65 ON LAU-88 RACKS	N/A	○ + ○	○ + ○	○ + ○	○ + ○
16 ROCKEYE (Slant 4 Loading)	FORWARD AFT	○ + ○ ○	○ + ○ ○	○ + ○ ○	○ + ○ ○
12 ROCKEYE	FORWARD AFT	○ + ○ ○	□	□	○ + ○ ○
12 SUU-30 H/B	FORWARD AFT	○ + ○ ○	□	□	○ + ○ ○
12 MK-82SE	FORWARD AFT	○ + ○ ○	□	□	○ + ○ ○
22 MK-82SE	FORWARD AFT	○ + ○ ○	○ + ○ ○	○ + ○ ○	○ + ○ ○

Figure 6. Pylon/store configuration identification.

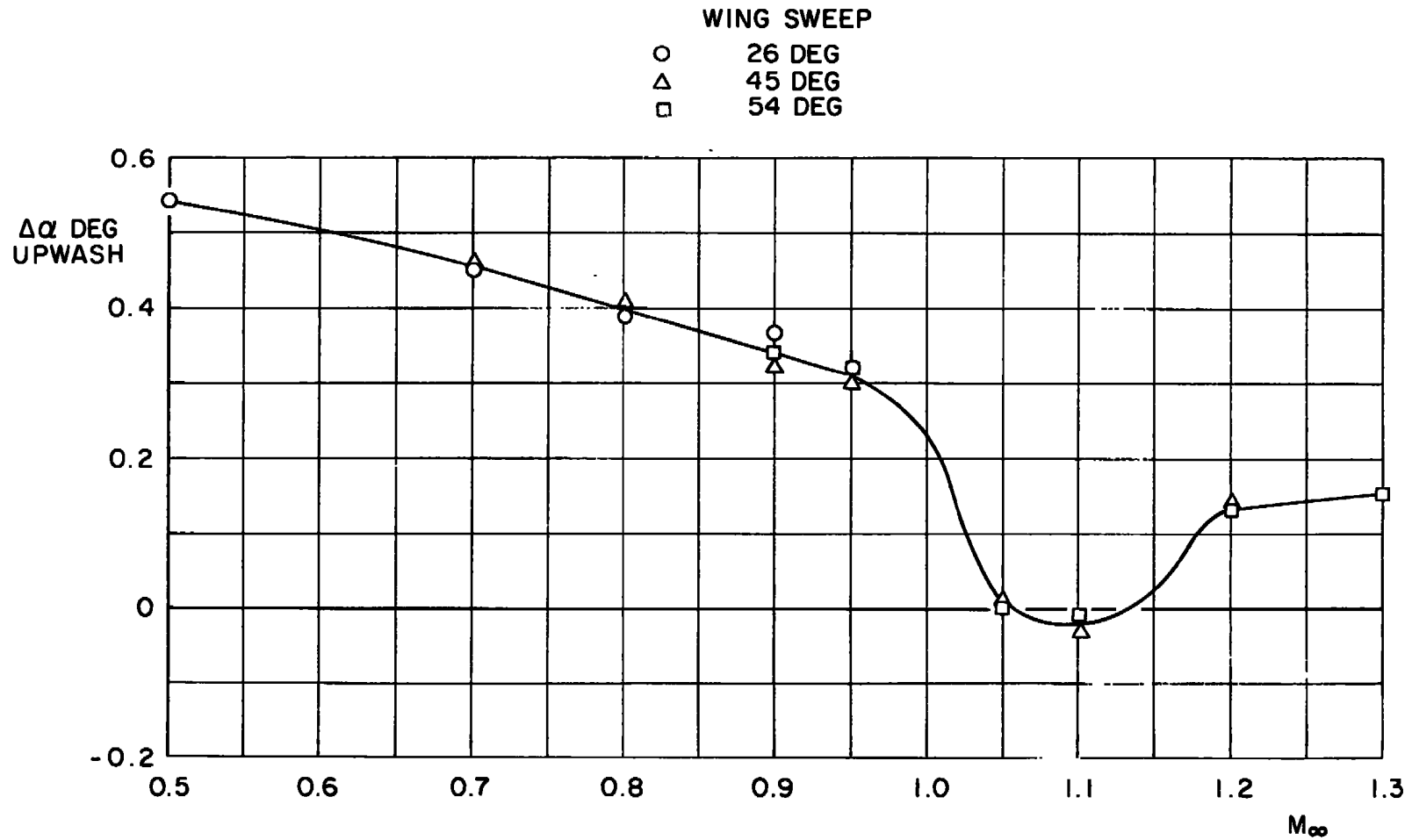
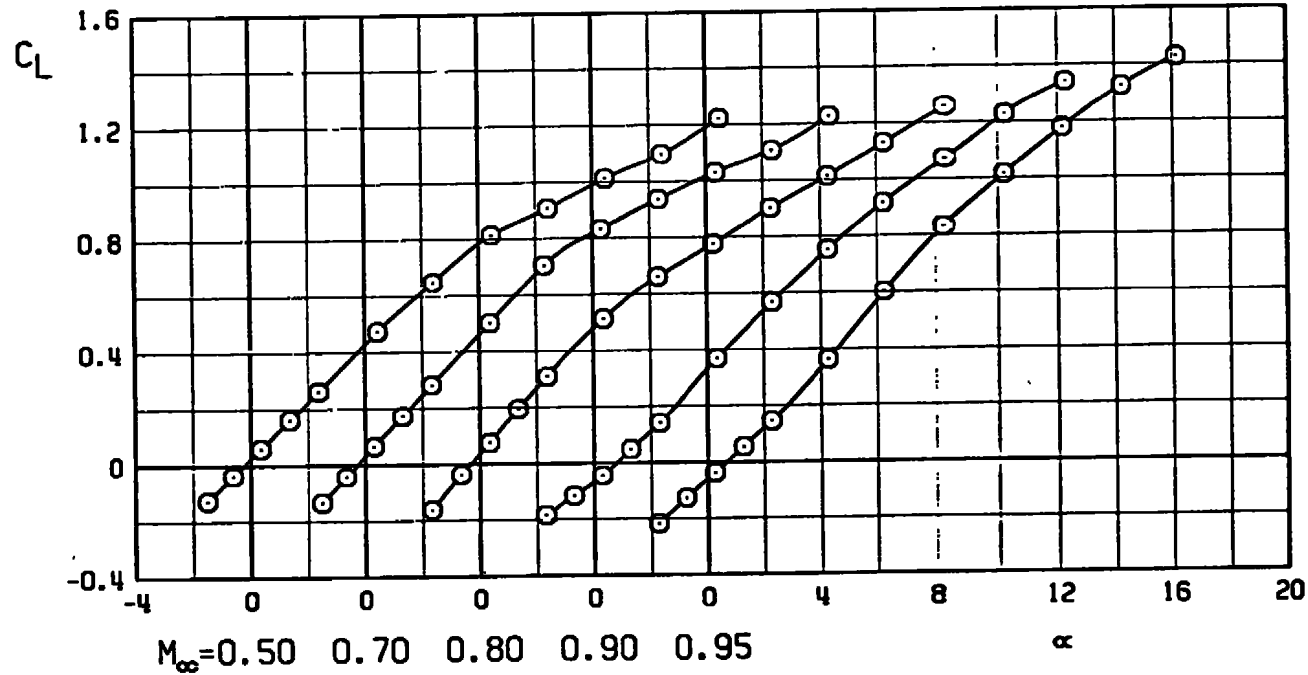
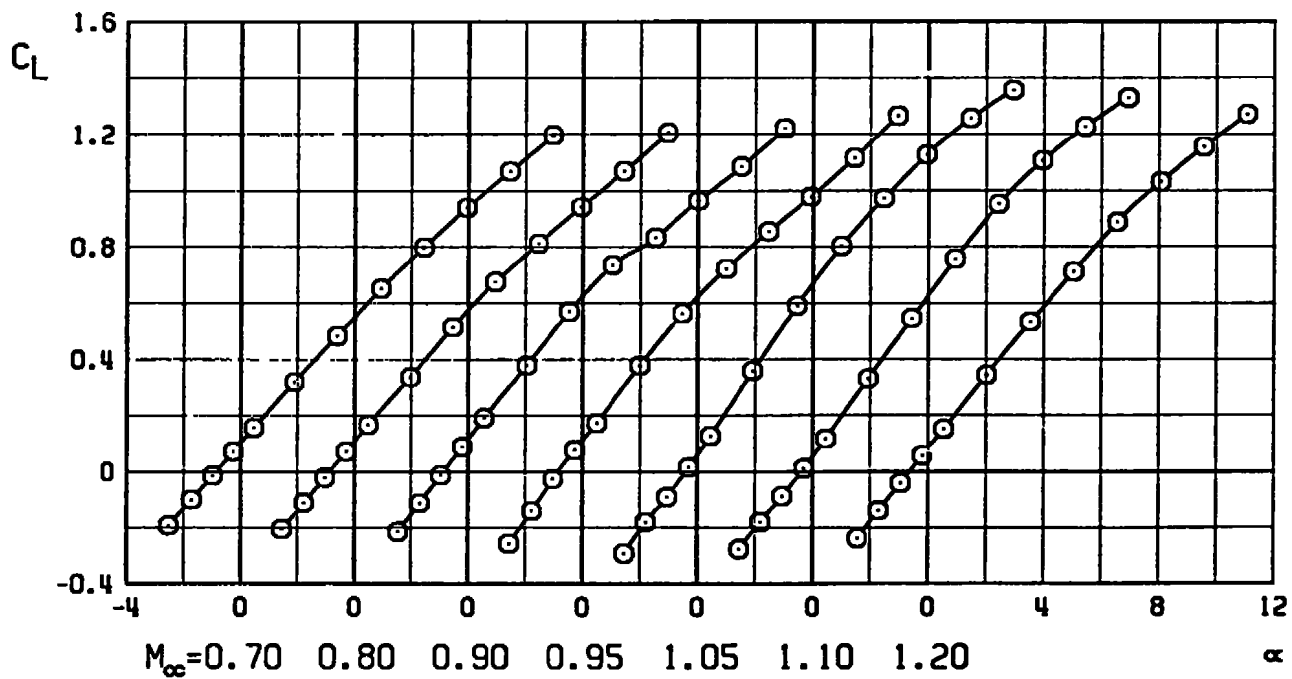


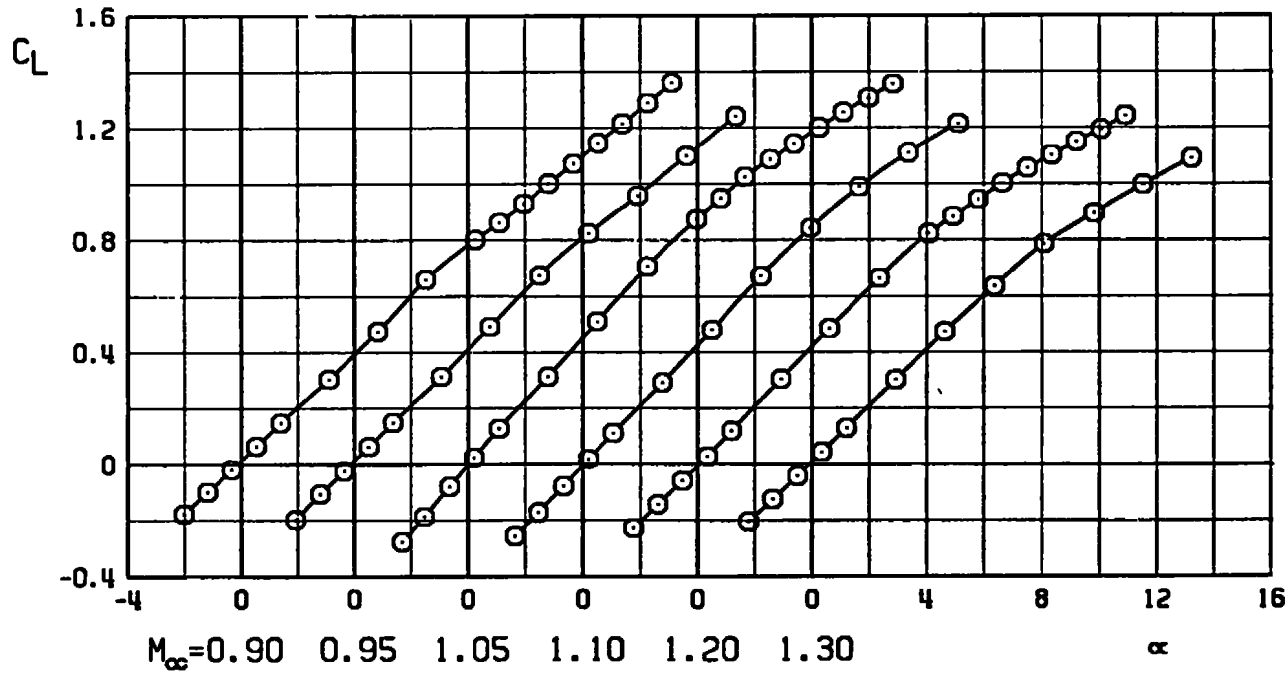
Figure 7. Tunnel flow angularity.



a. Lift coefficient, $\Lambda = 26$ deg
Figure 8. Aerodynamic characteristics of the F-111 aircraft,
clean configuration.

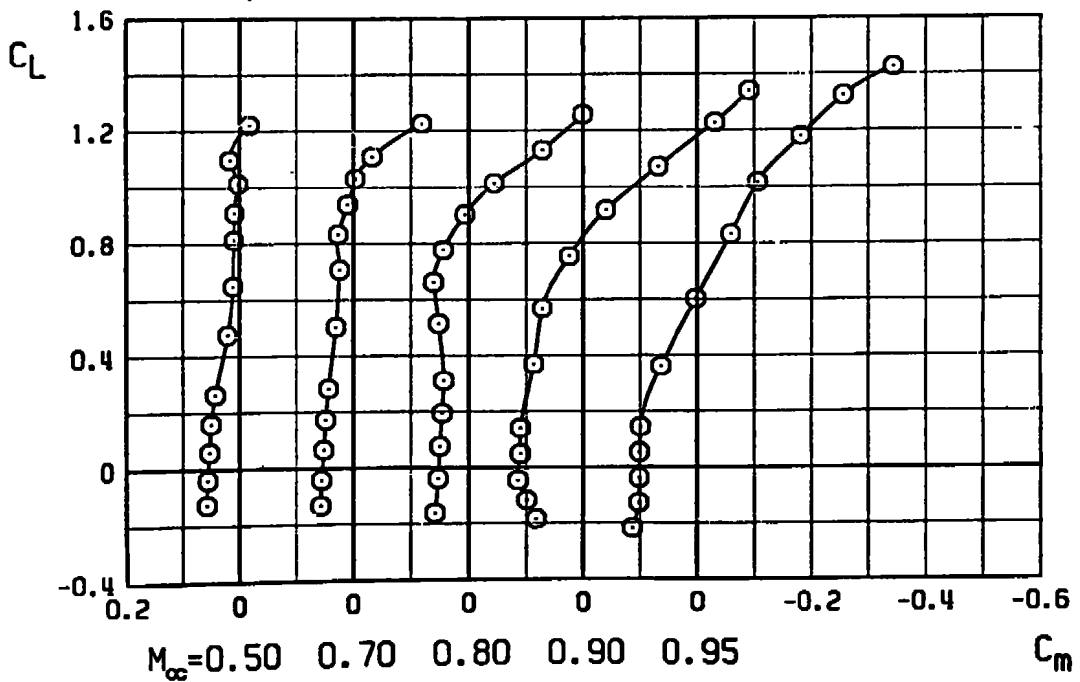


a. Continued, $\Lambda = 45$ deg
Figure 8. Continued.



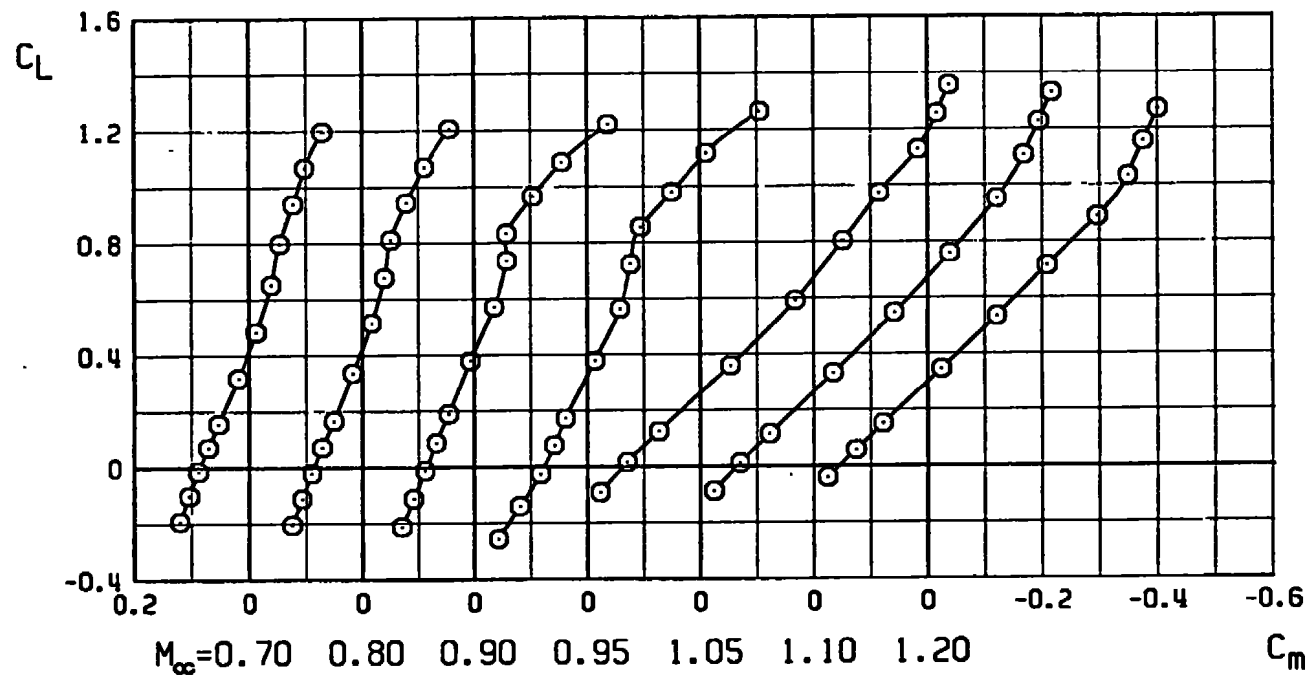
a. Concluded, $\Lambda = 54$ deg

Figure 8. Continued.



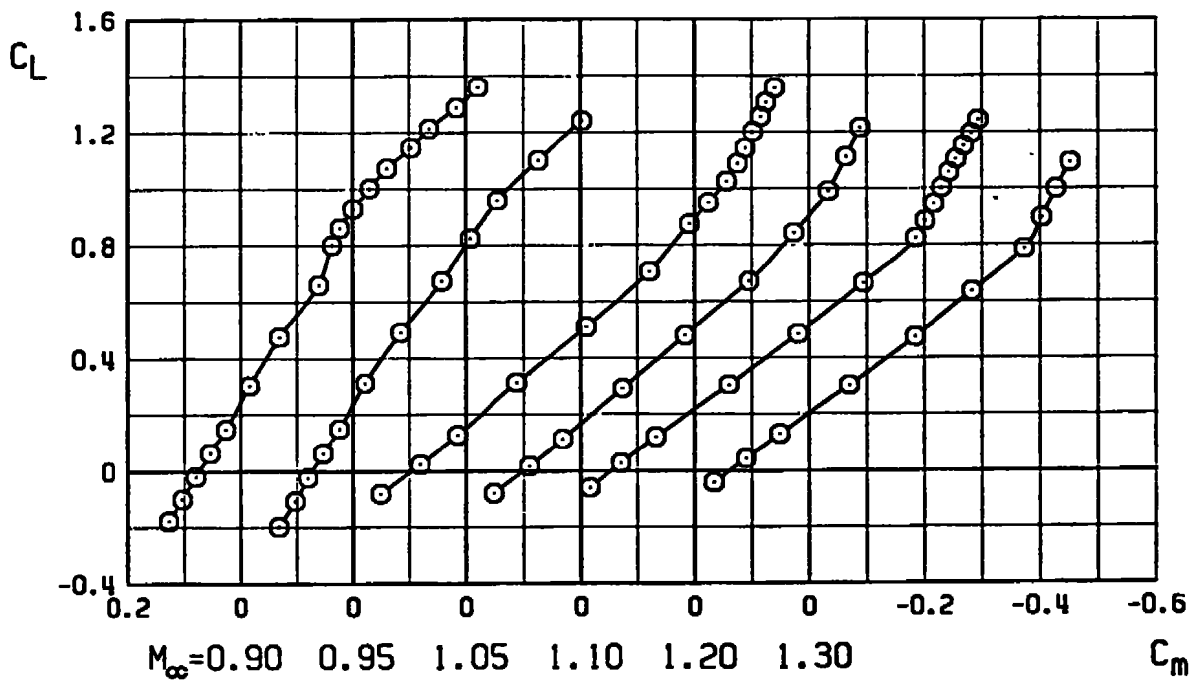
b. Pitching-moment coefficient, $\Lambda = 26$ deg

Figure 8. Continued.

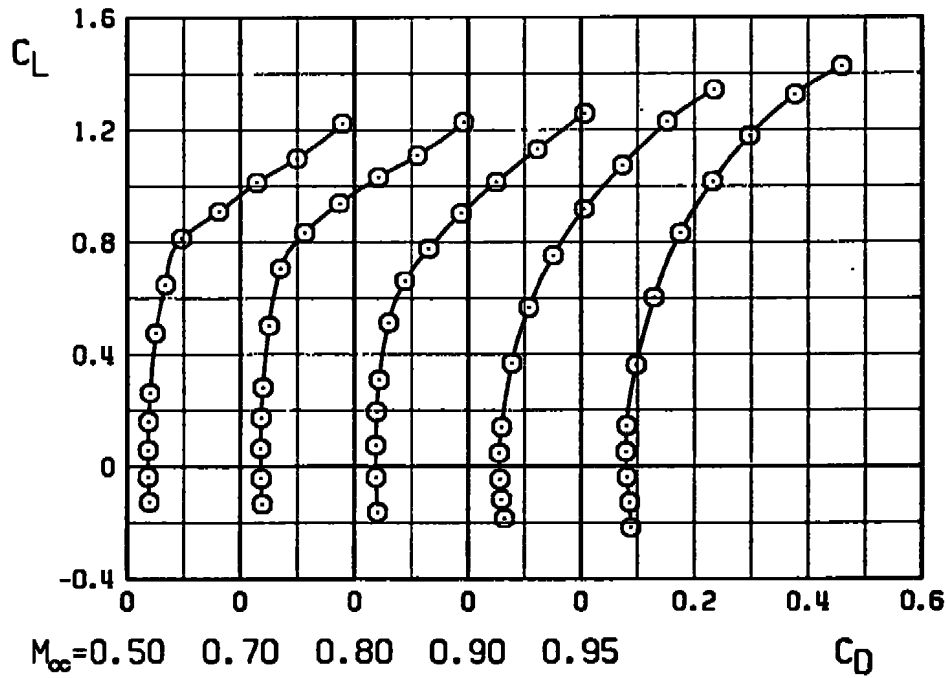


b. Continued, $\Lambda = 45$ deg

Figure 8. Continued.

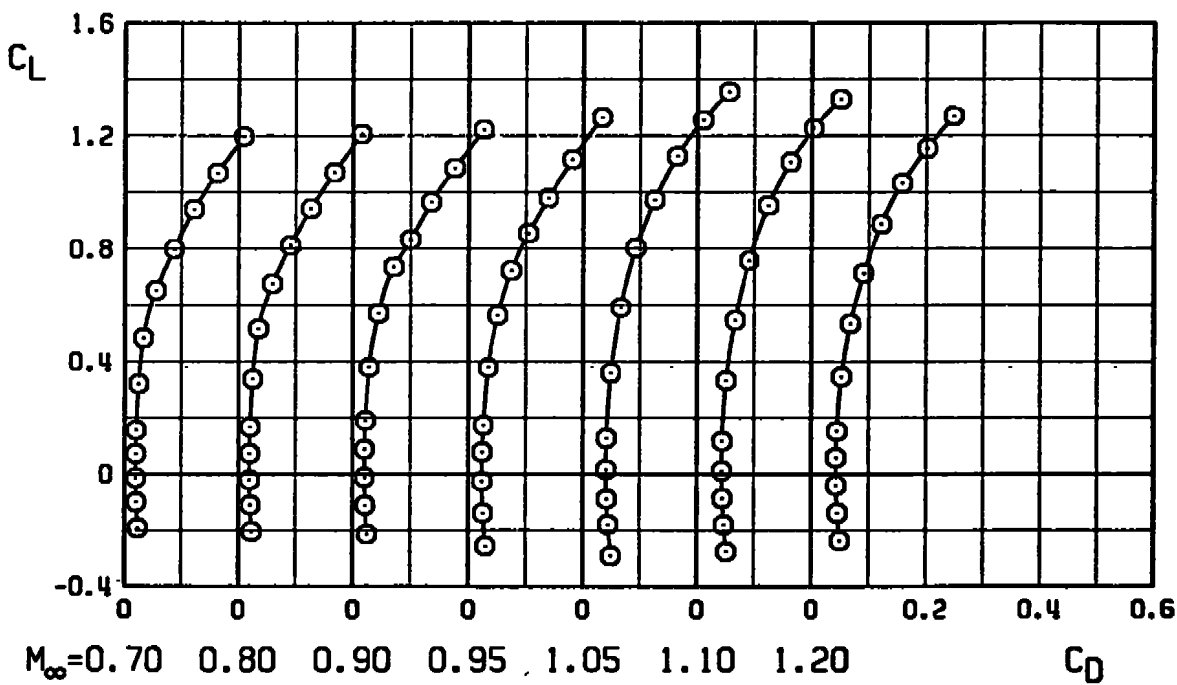


b. Concluded, $\Lambda = 54$ deg
Figure 8. Continued.

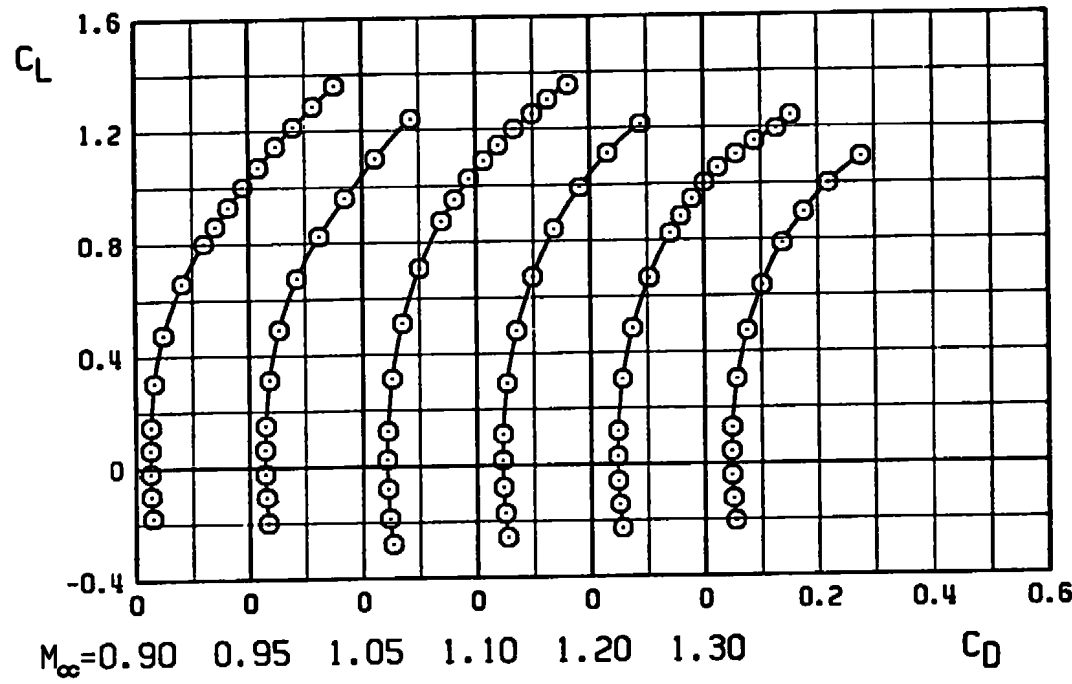


c. Drag coefficient, $\Lambda = 26$ deg
Figure 8. Continued.

40

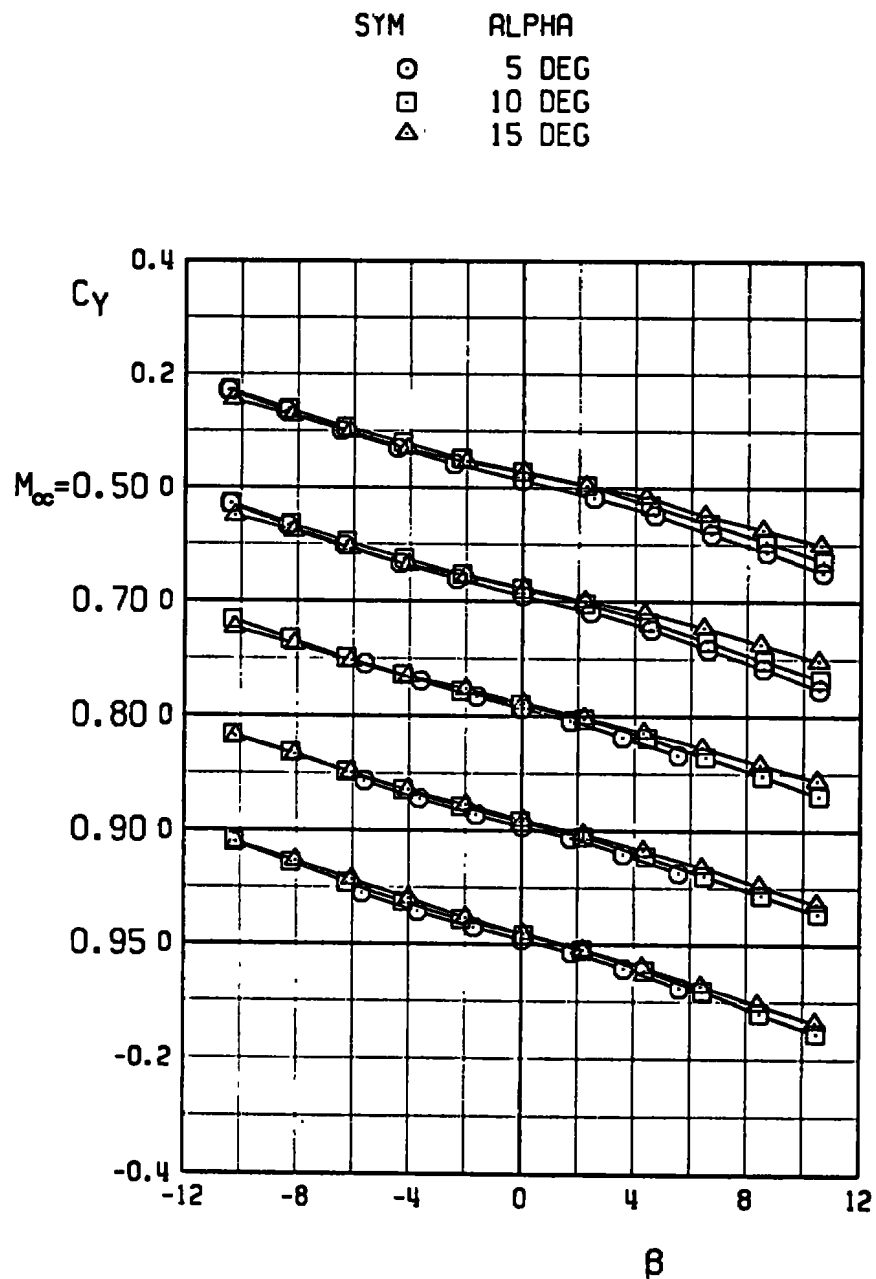


c. Continued, $\Lambda = 45$ deg
Figure 8. Continued.

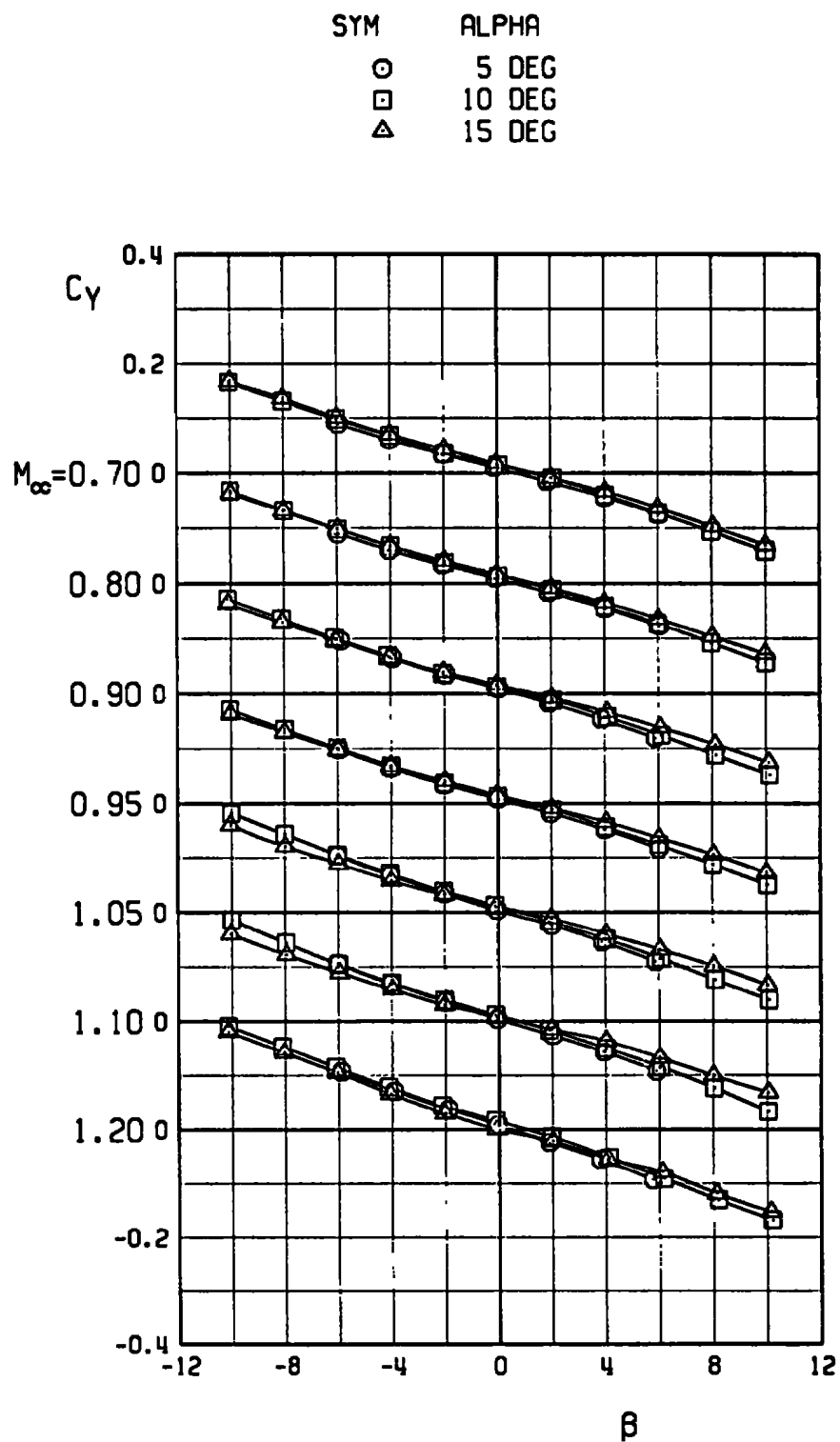


c. Concluded, $\Lambda = 54 \text{ deg}$

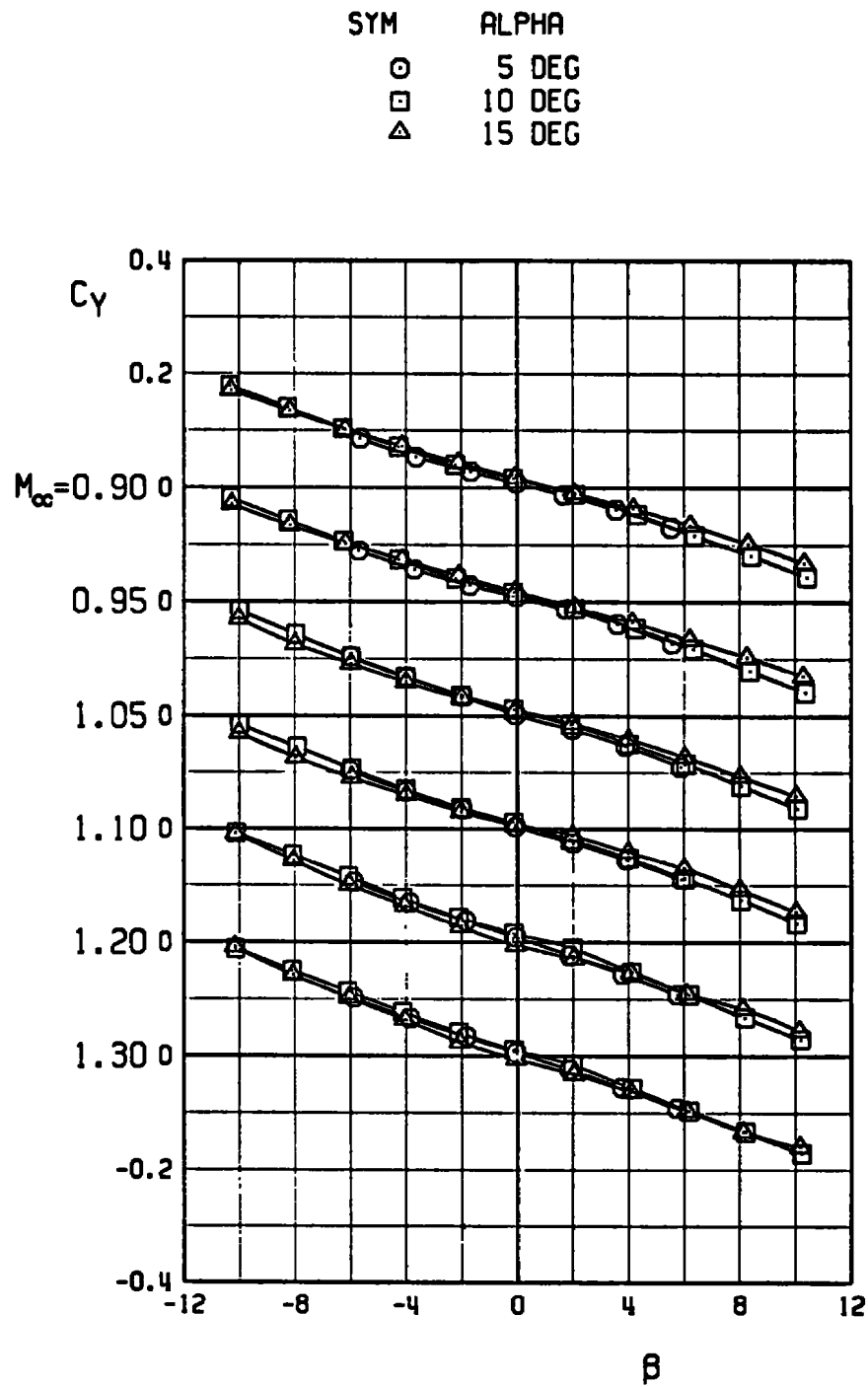
Figure 8. Continued.



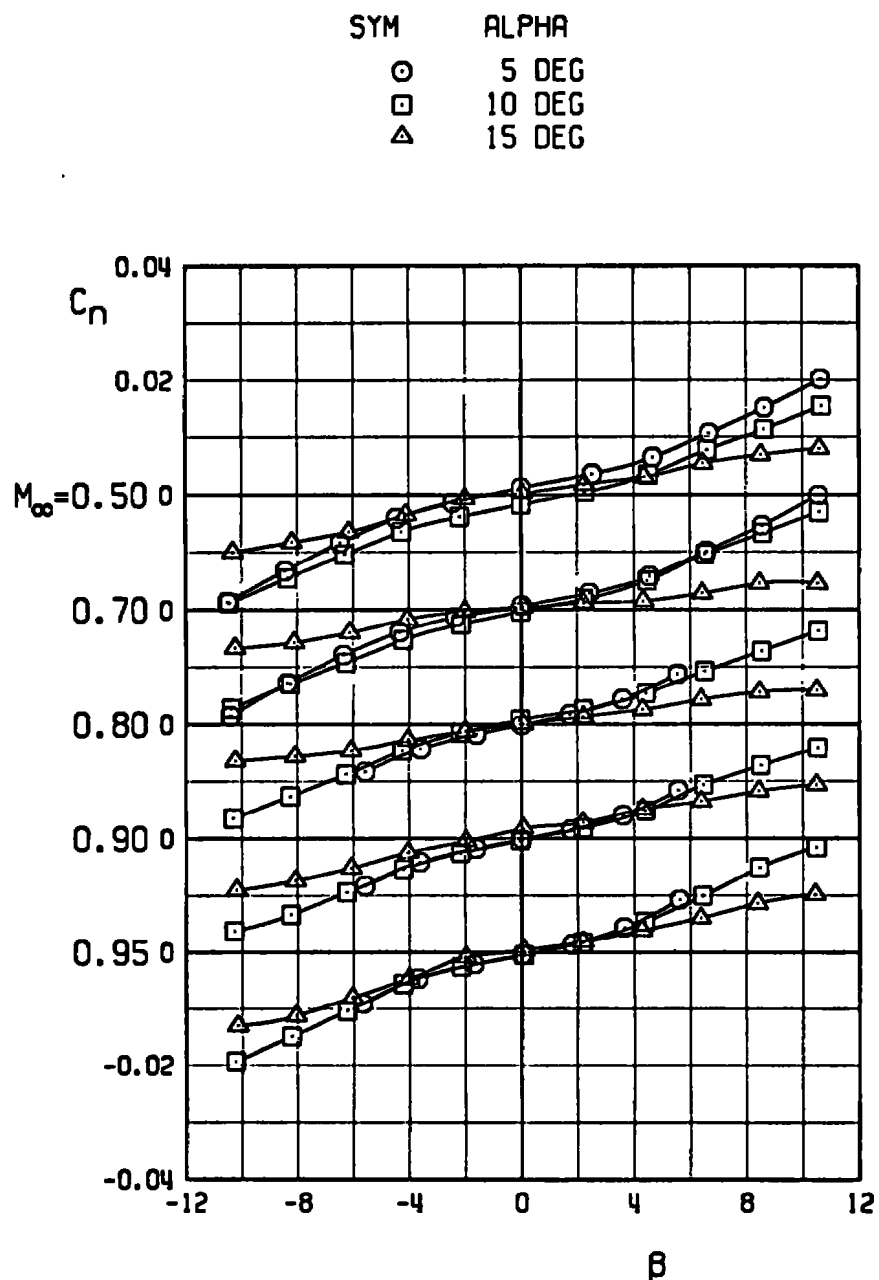
d. Side-force coefficient, $\Lambda = 26$ deg
 Figure 8. Continued.



d. Continued, $\Lambda = 45$ deg
Figure 8. Continued.



d. Concluded, $\Lambda = 54$ deg
 Figure 8. Continued.



e. Yawing-moment coefficient, $\Lambda = 26$ deg
Figure 8. Continued.

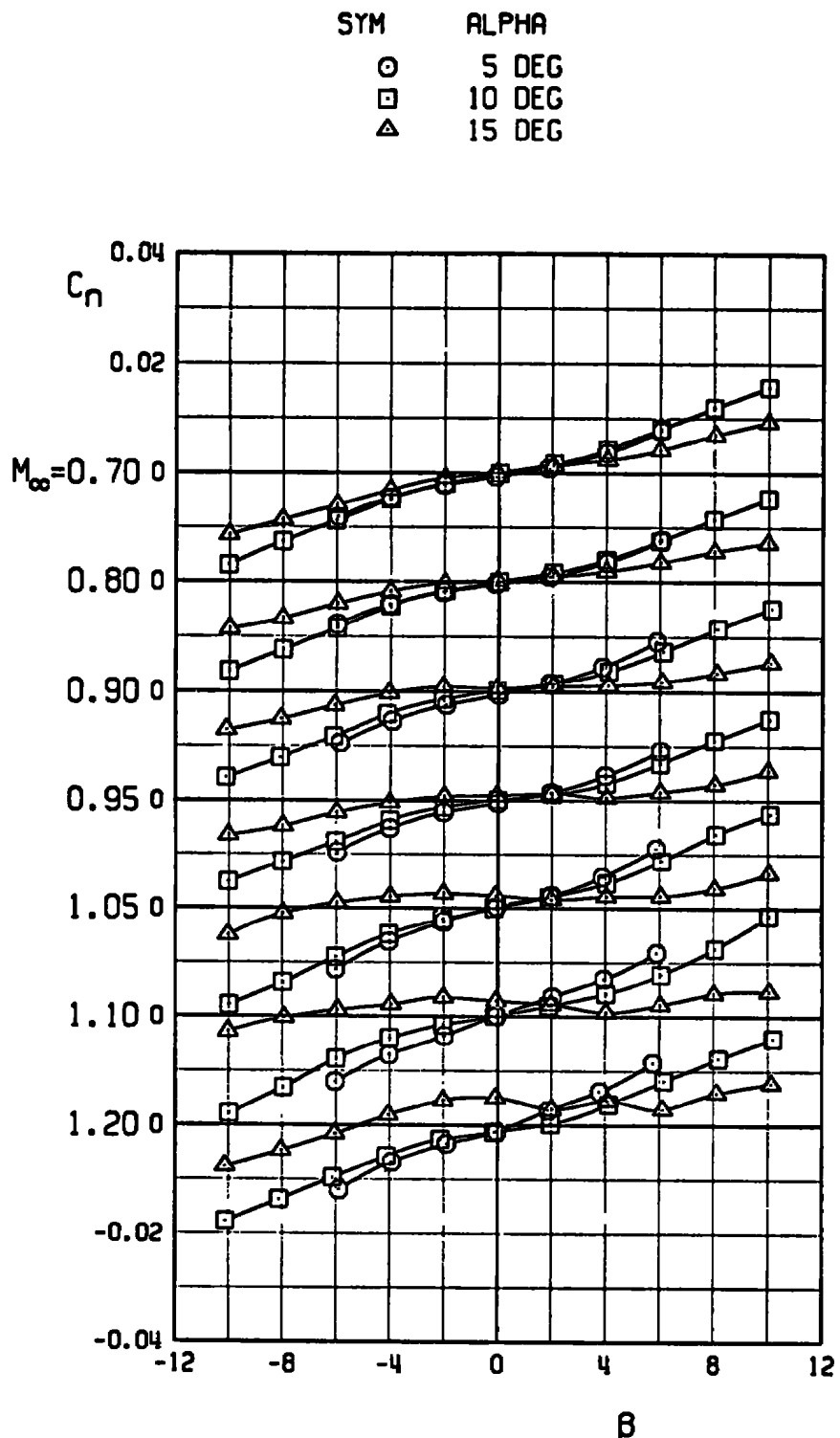
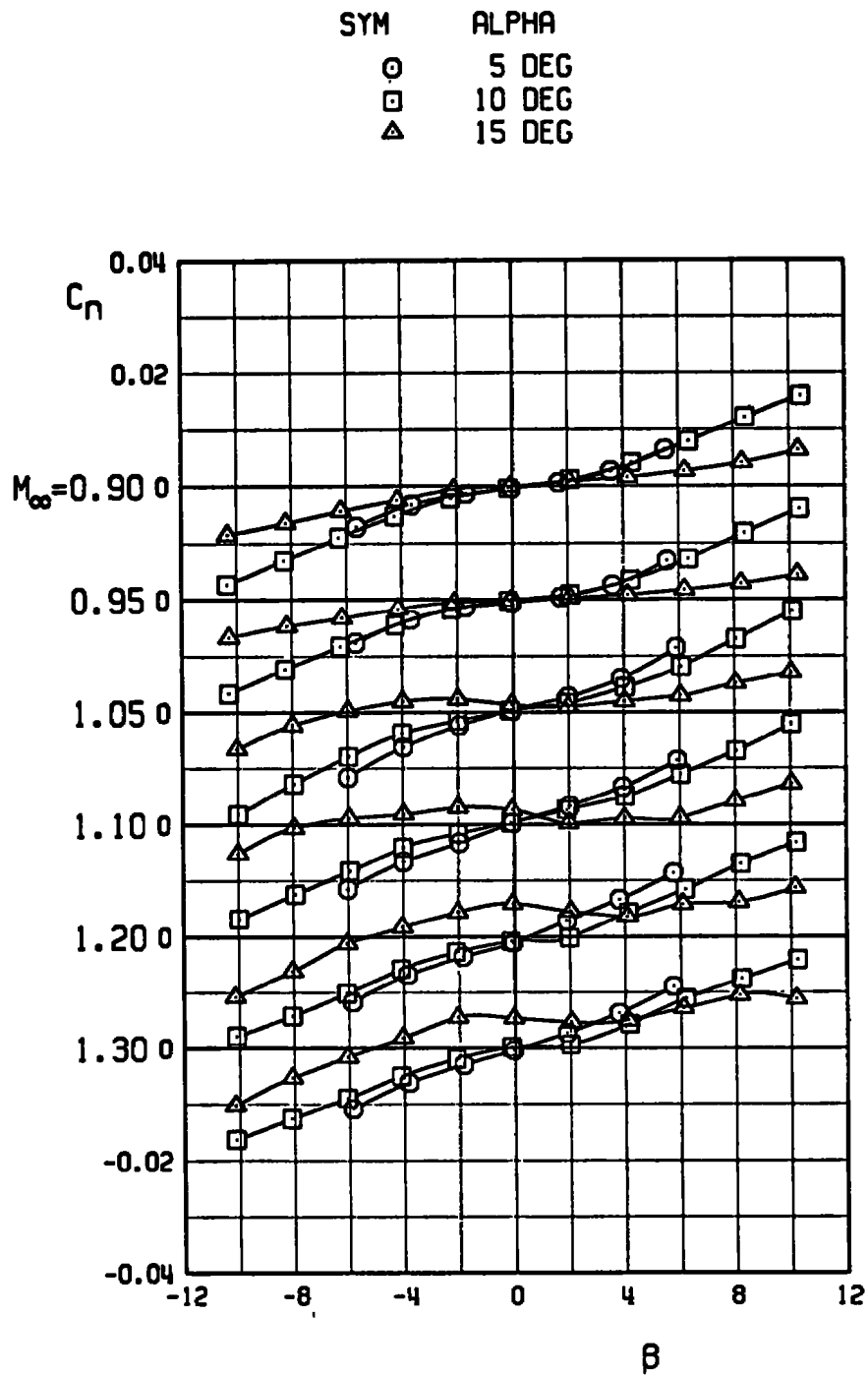
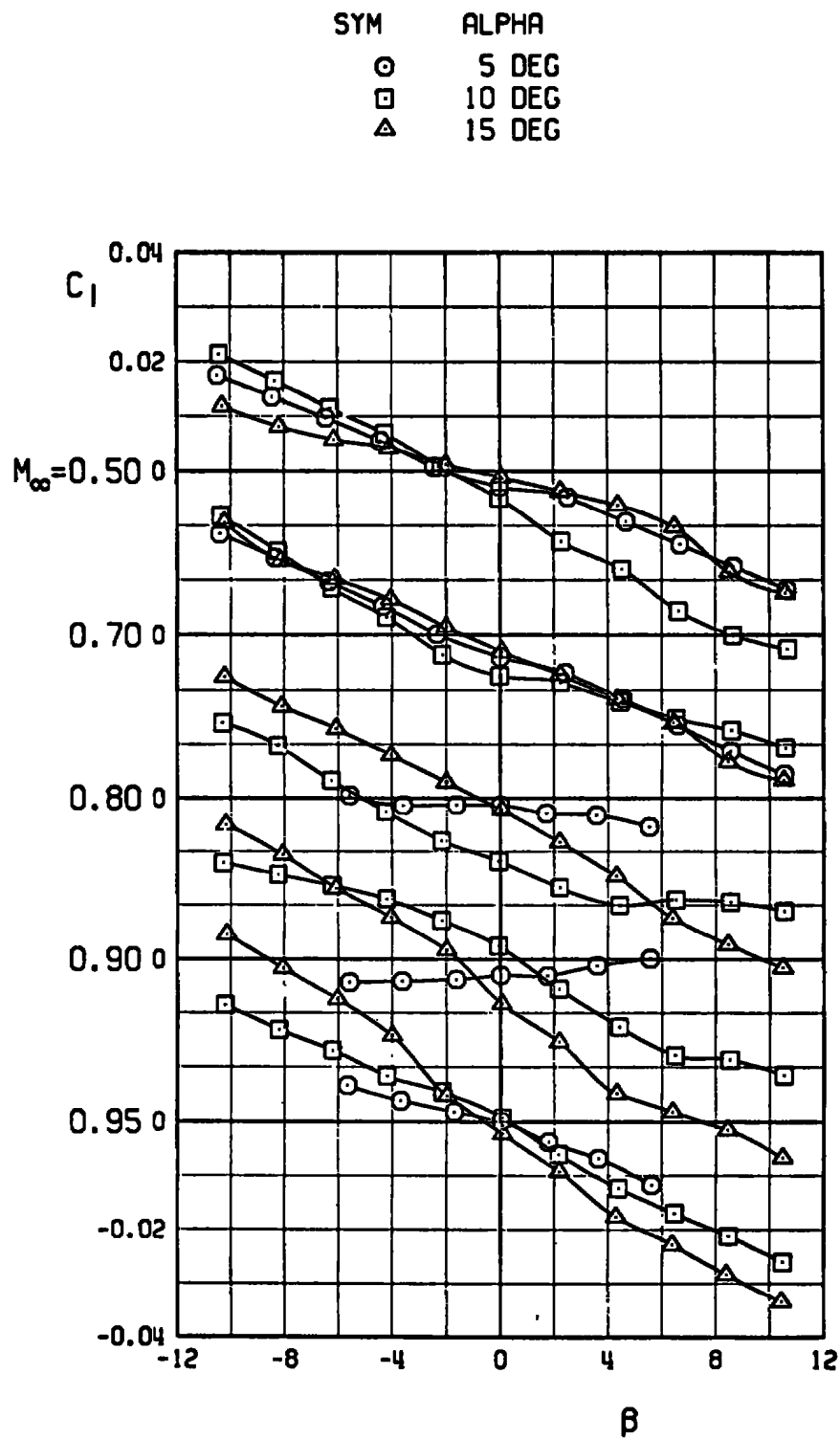
e. Continued, $\Lambda = 45$ deg

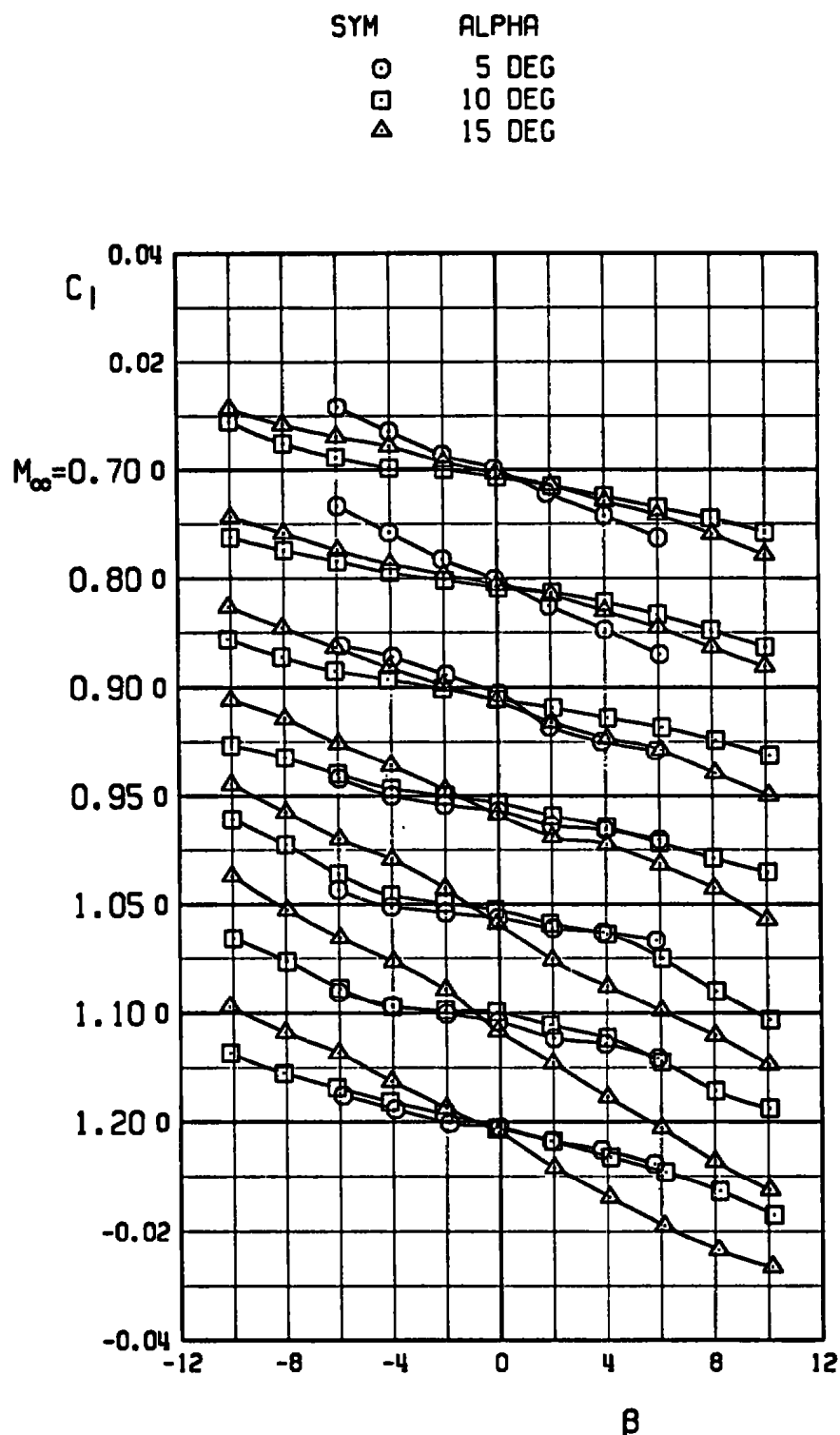
Figure 8. Continued.



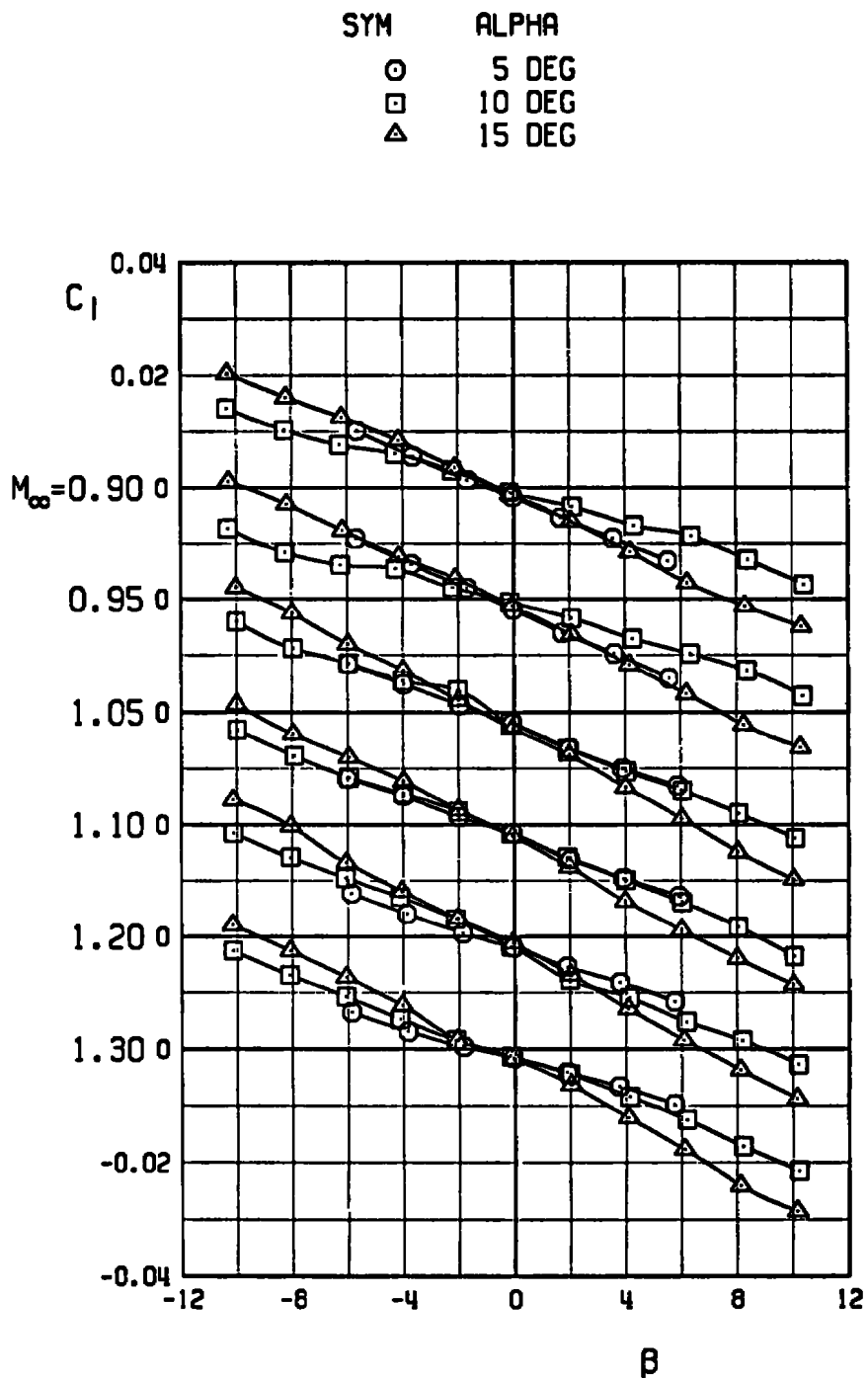
e. Concluded, $\Lambda = 54$ deg
 Figure 8. Continued.



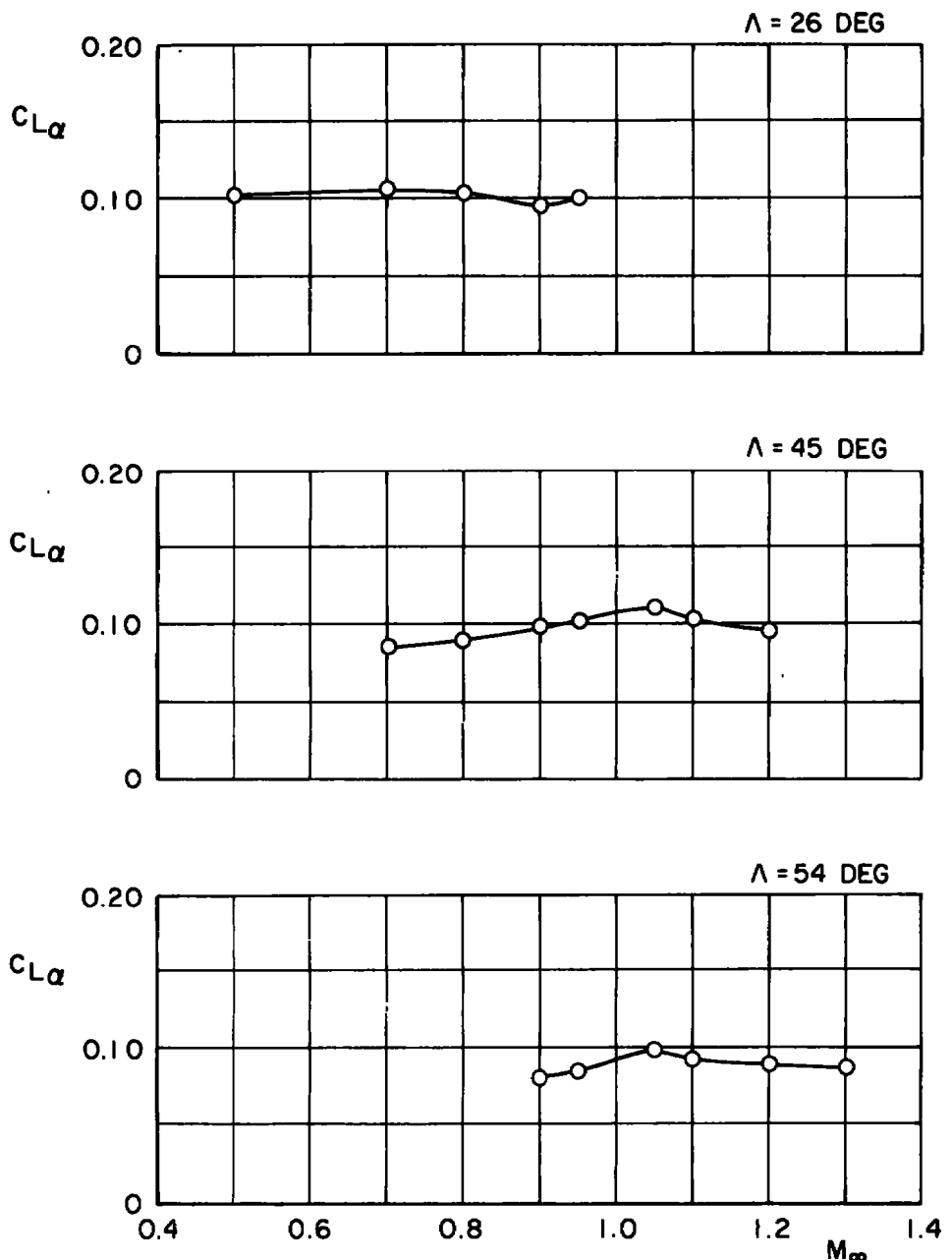
f. Rolling-moment coefficient, $\Lambda = 26$ deg
 Figure 8. Continued.



f. Continued, $\Lambda = 45$ deg
Figure 8. Continued.

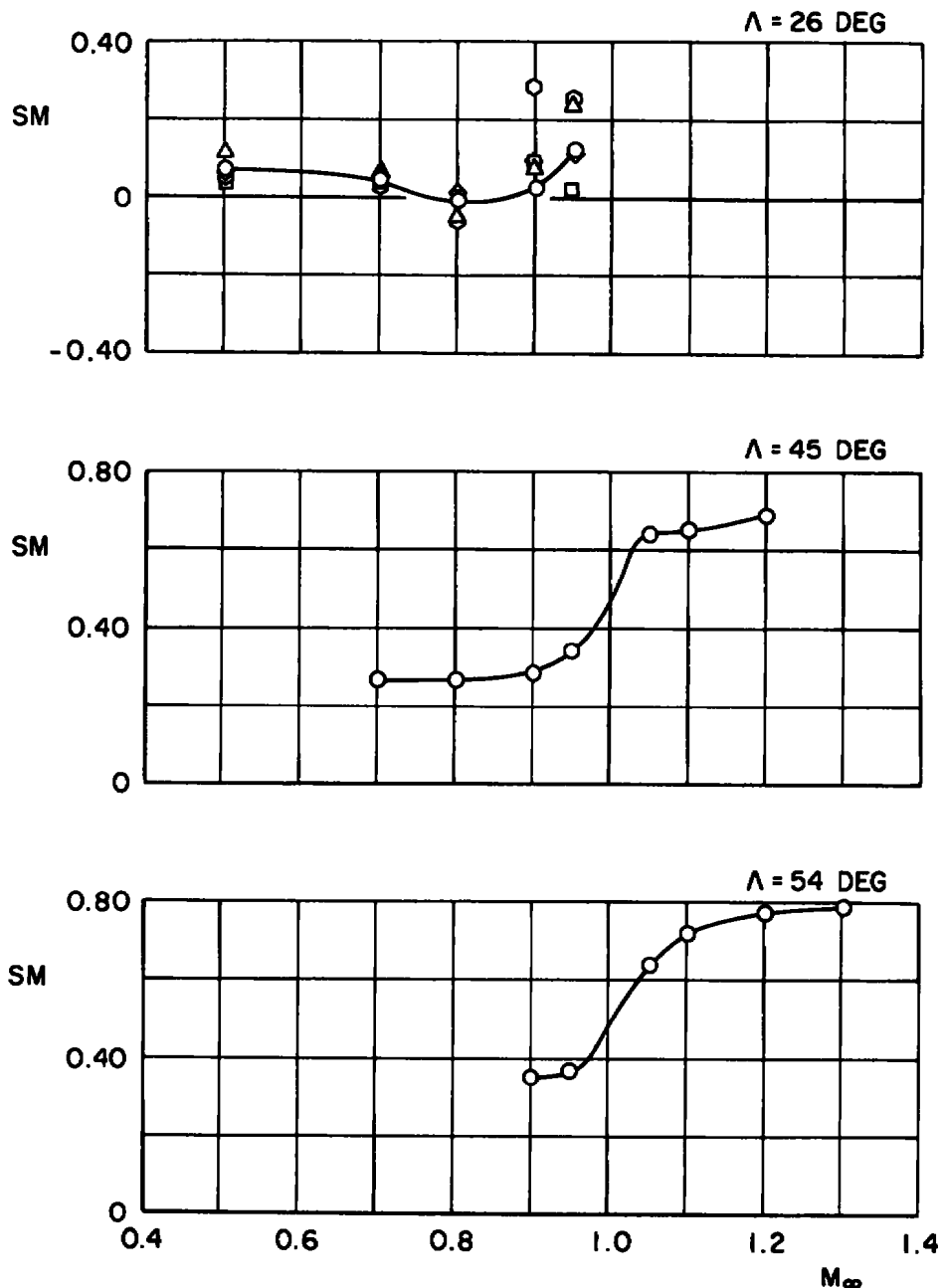


f. Concluded, $\Lambda = 54$ deg
 Figure 8. Concluded.

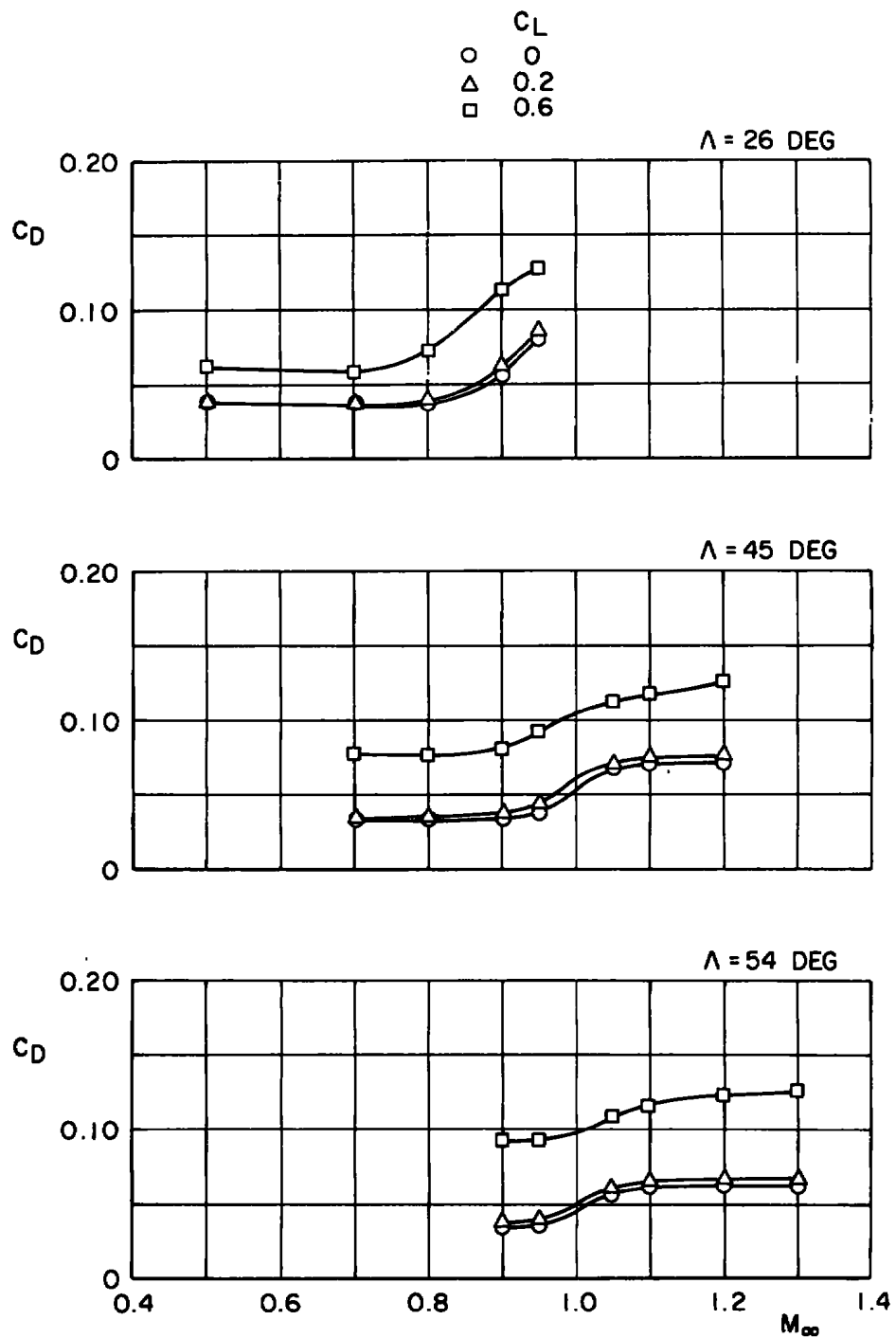


a. Lift curve slope
Figure 9. Static stability derivatives and drag coefficients of the F-111 aircraft, clean configuration.

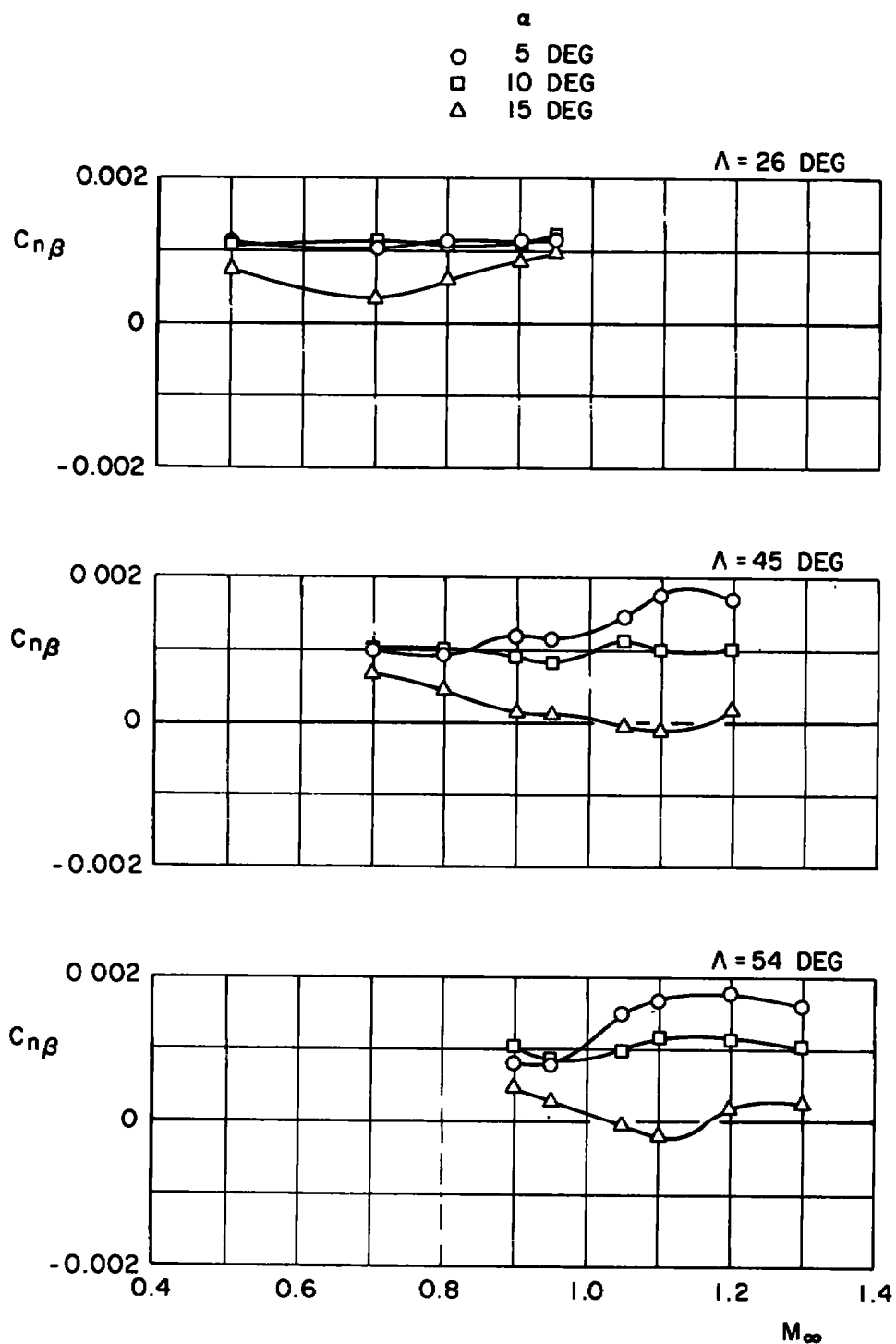
- LINEAR CURVE FIT, $-2 \leq \alpha \leq 6$ DEG
- SLOPE AT $C_L = 0$
- ◊ SLOPE AT $C_L = 0.2$
- △ SLOPE AT $C_L = 0.4$
- SLOPE AT $C_L = 0.6$



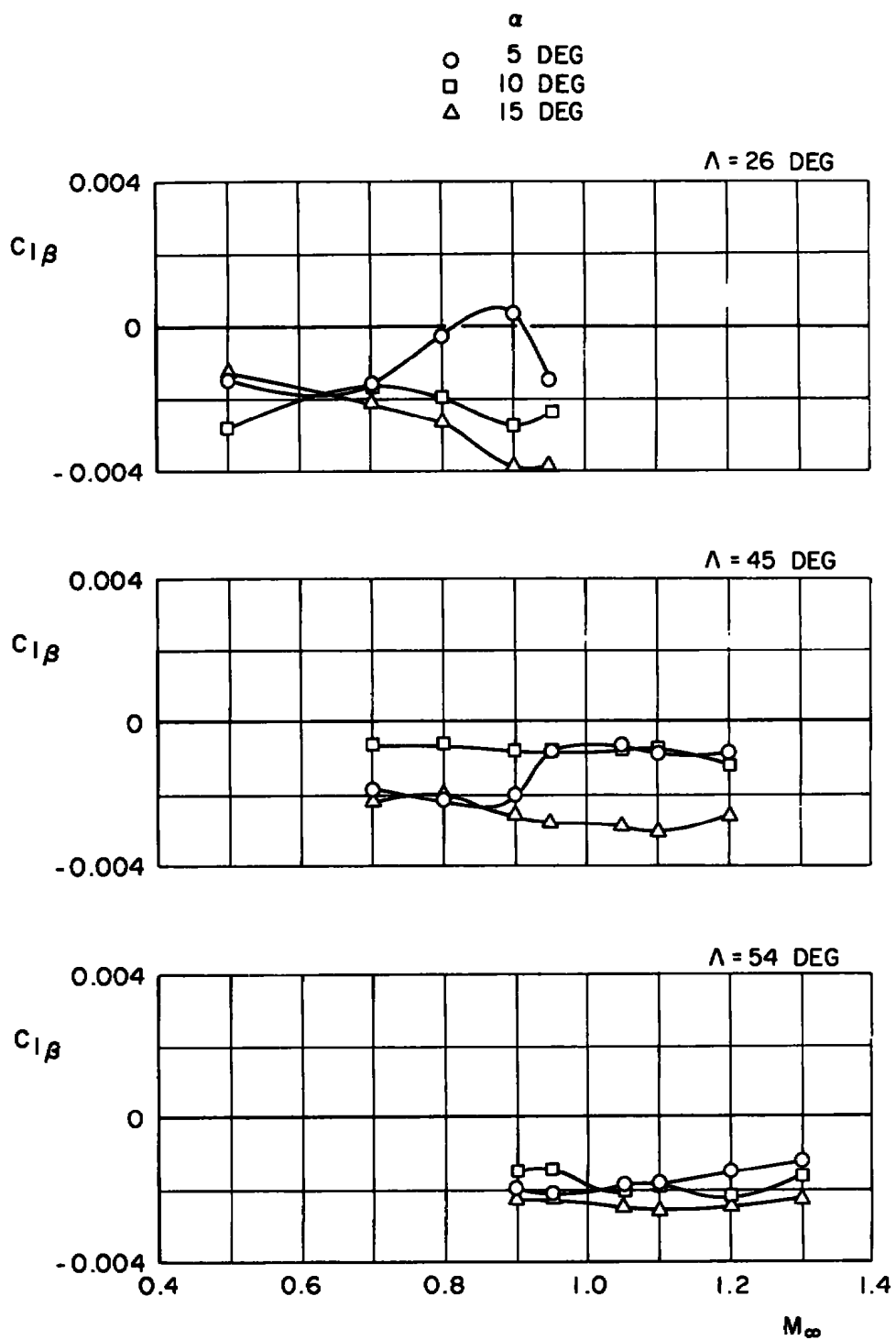
b. Static margin
Figure 9. Continued.



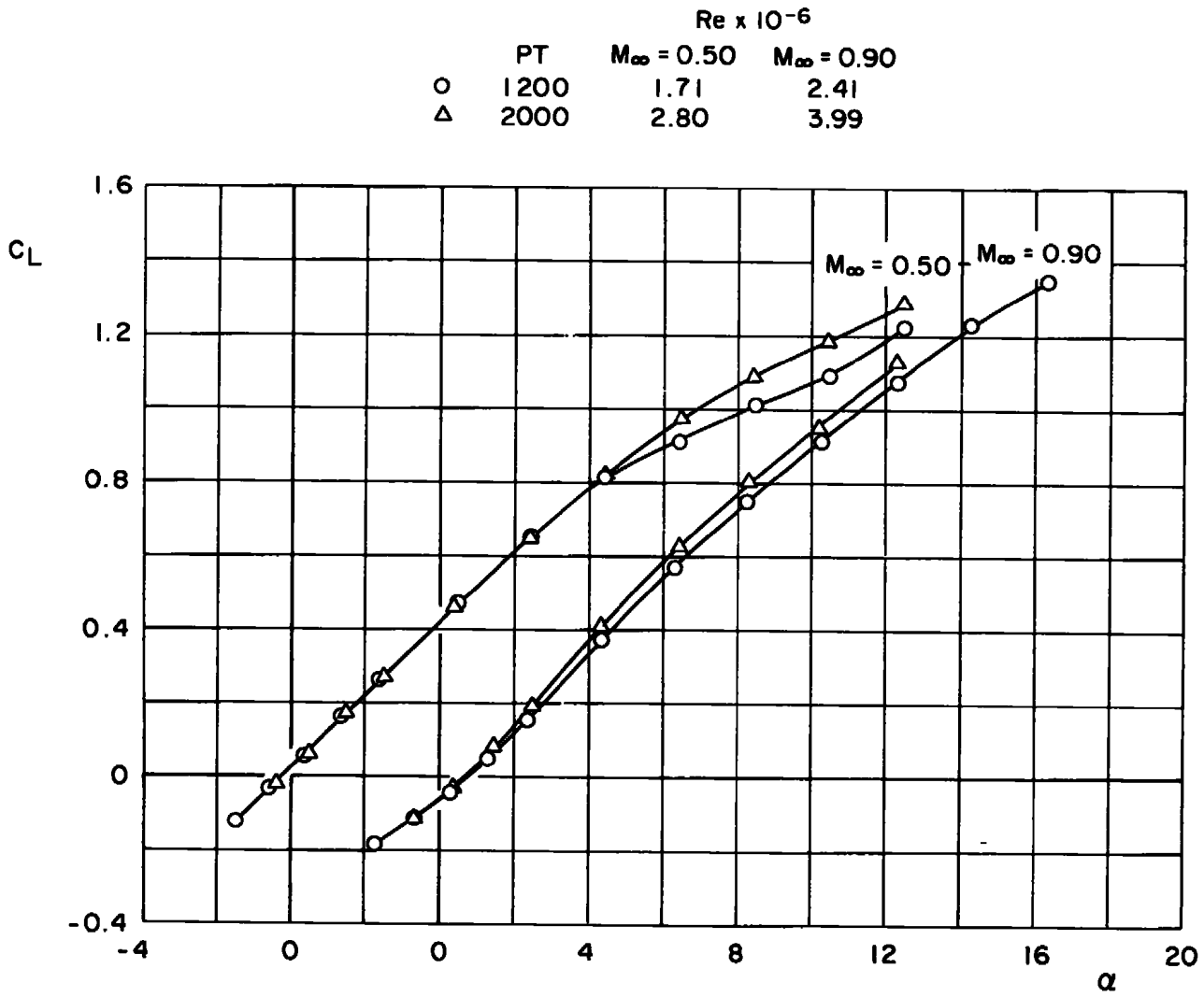
c. Drag coefficient
Figure 9. Continued.



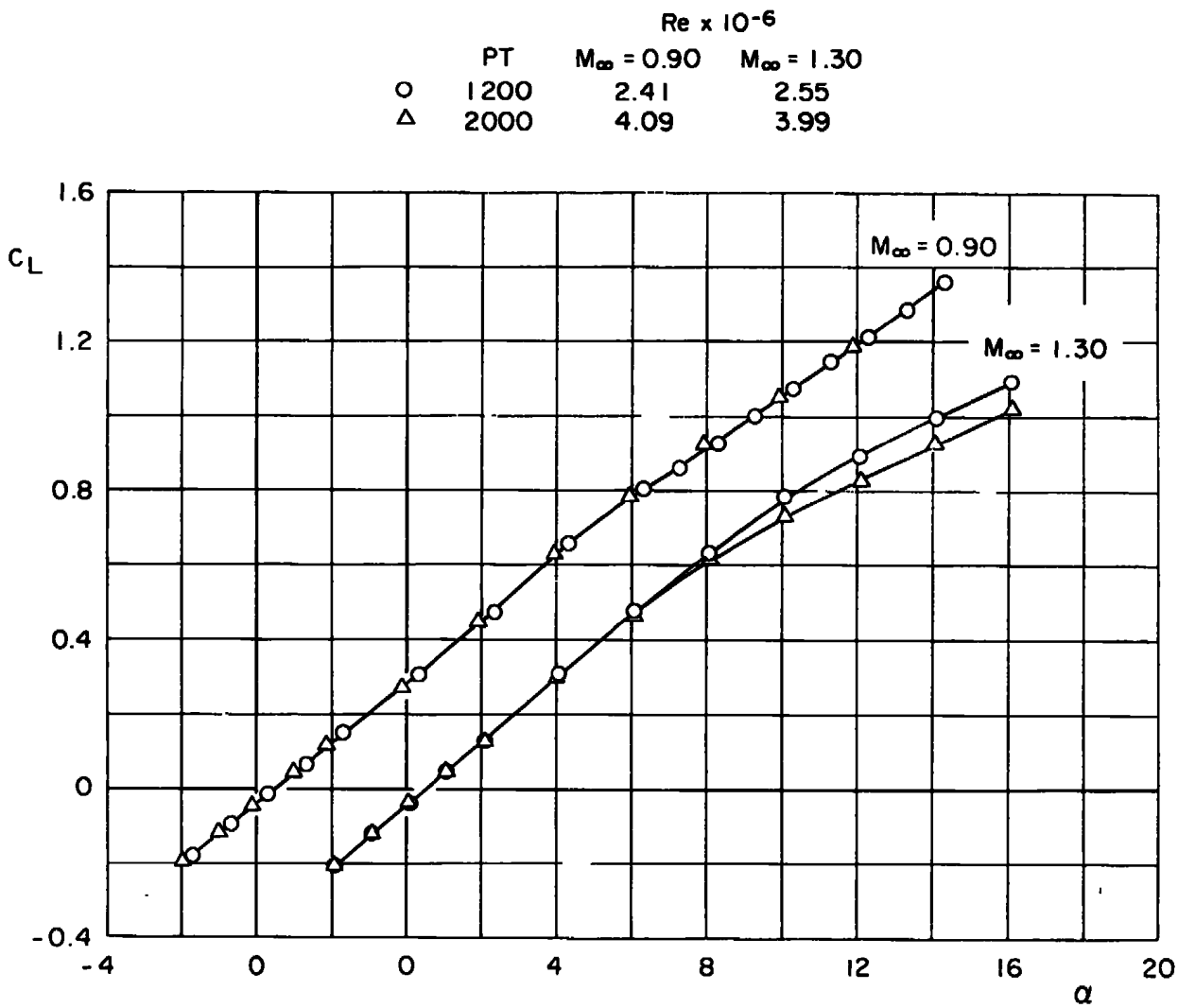
d. Static directional stability derivative
Figure 9. Continued.



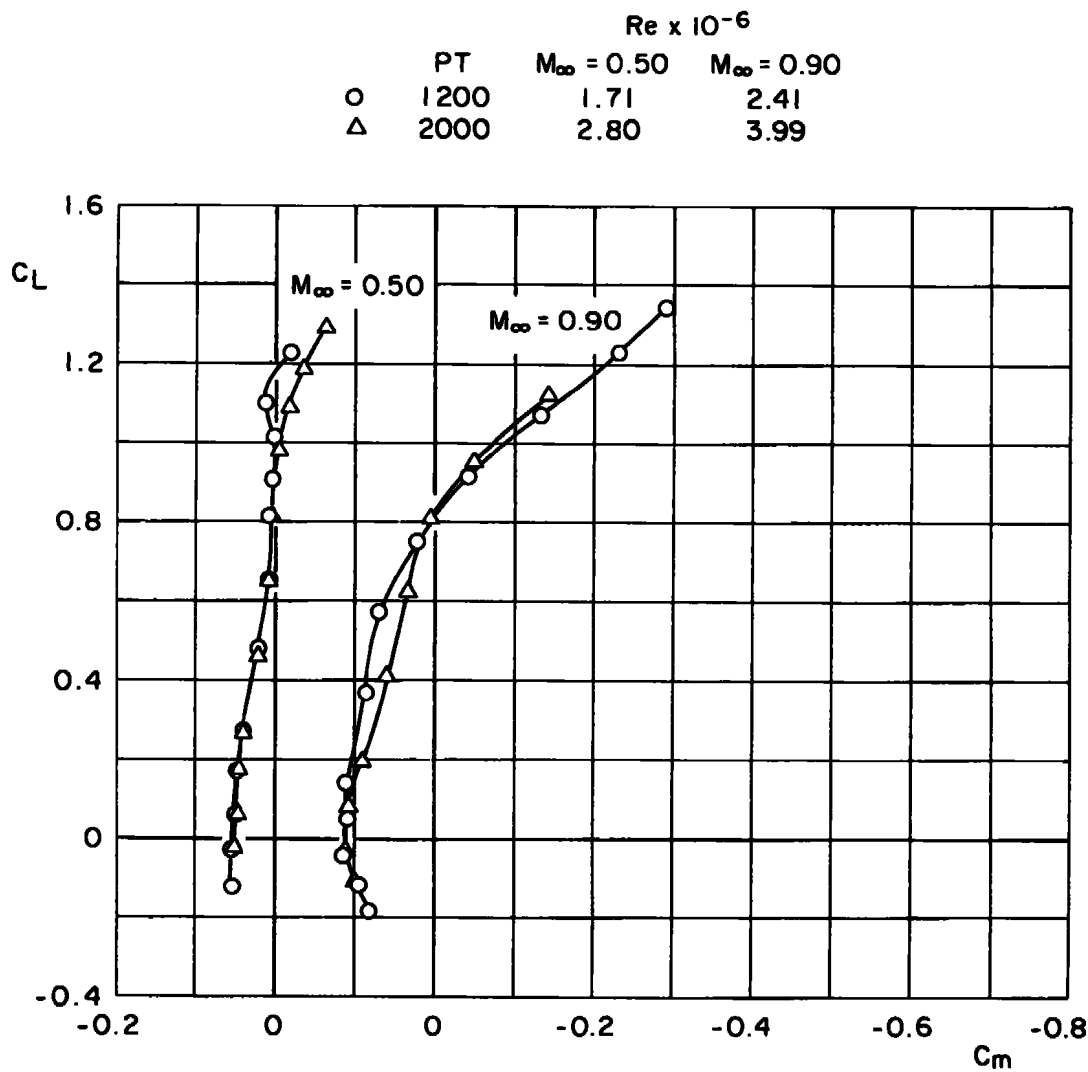
e. Effective dihedral
Figure 9. Concluded.



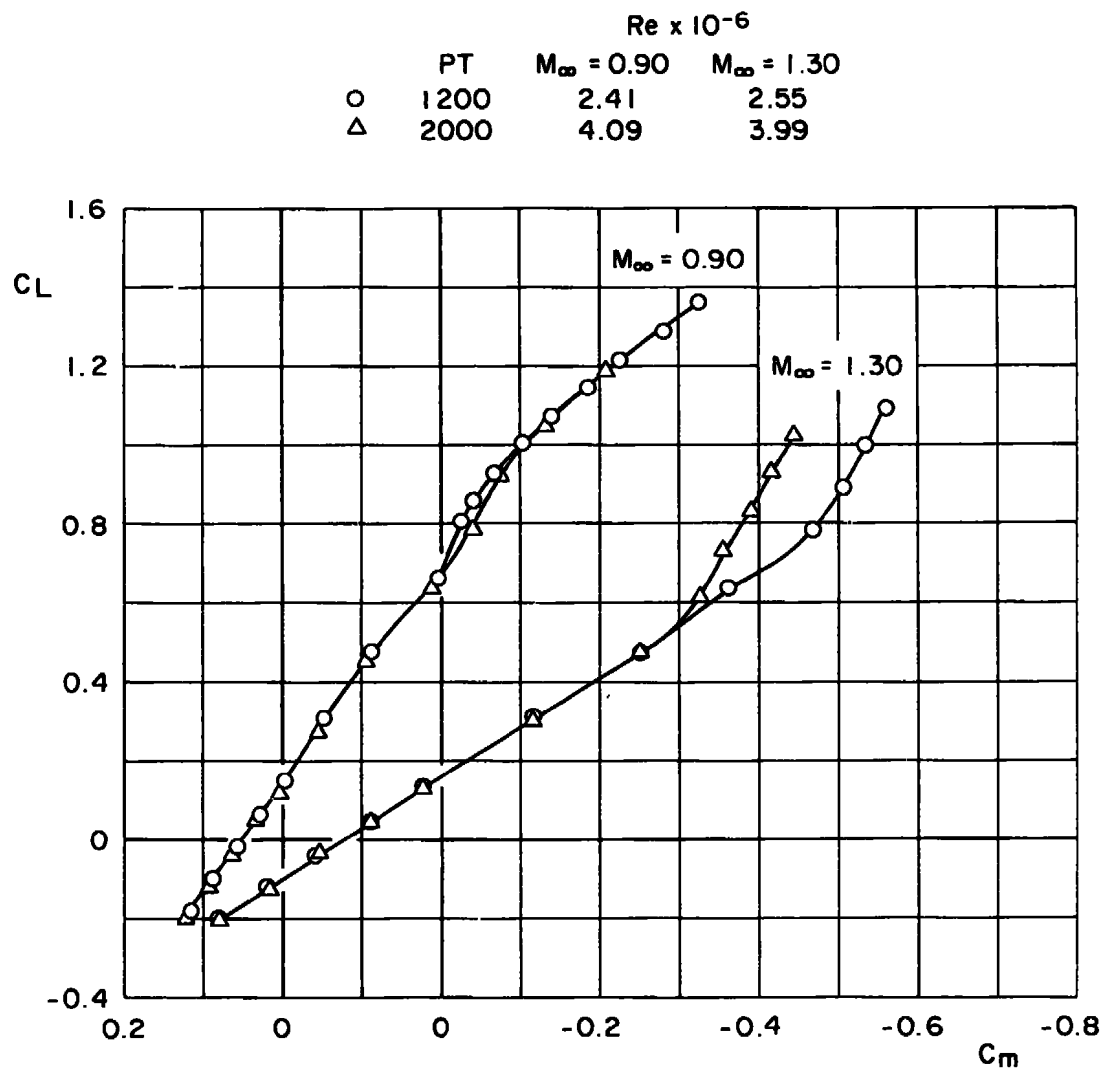
a. Lift coefficient, $\Lambda = 26$ deg
 Figure 10. Reynolds number effects.



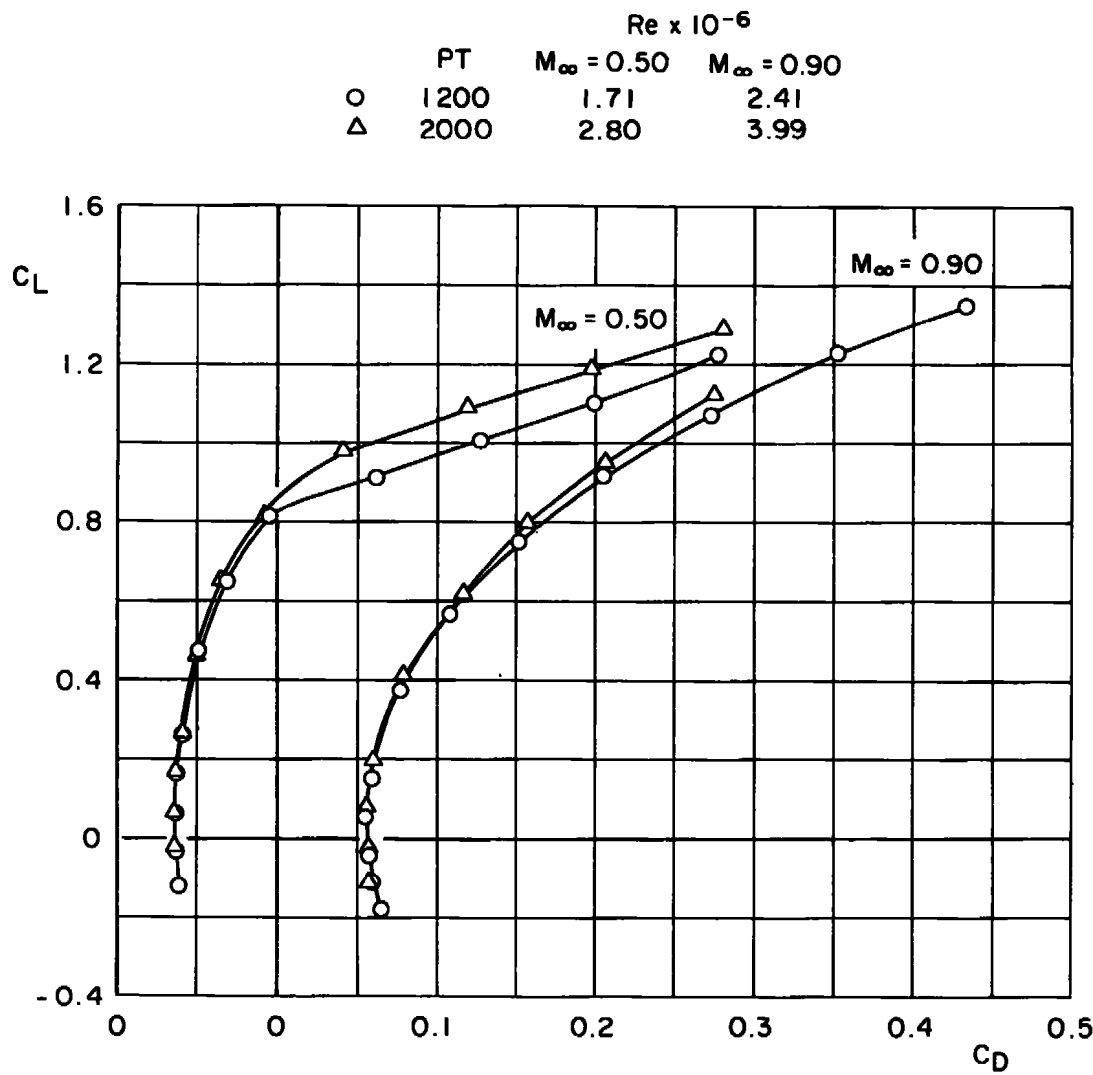
a. Concluded, $\Lambda = 54$ deg
Figure 10. Continued.



b. Pitching-moment coefficient, $\Lambda = 26$ deg
Figure 10. Continued.

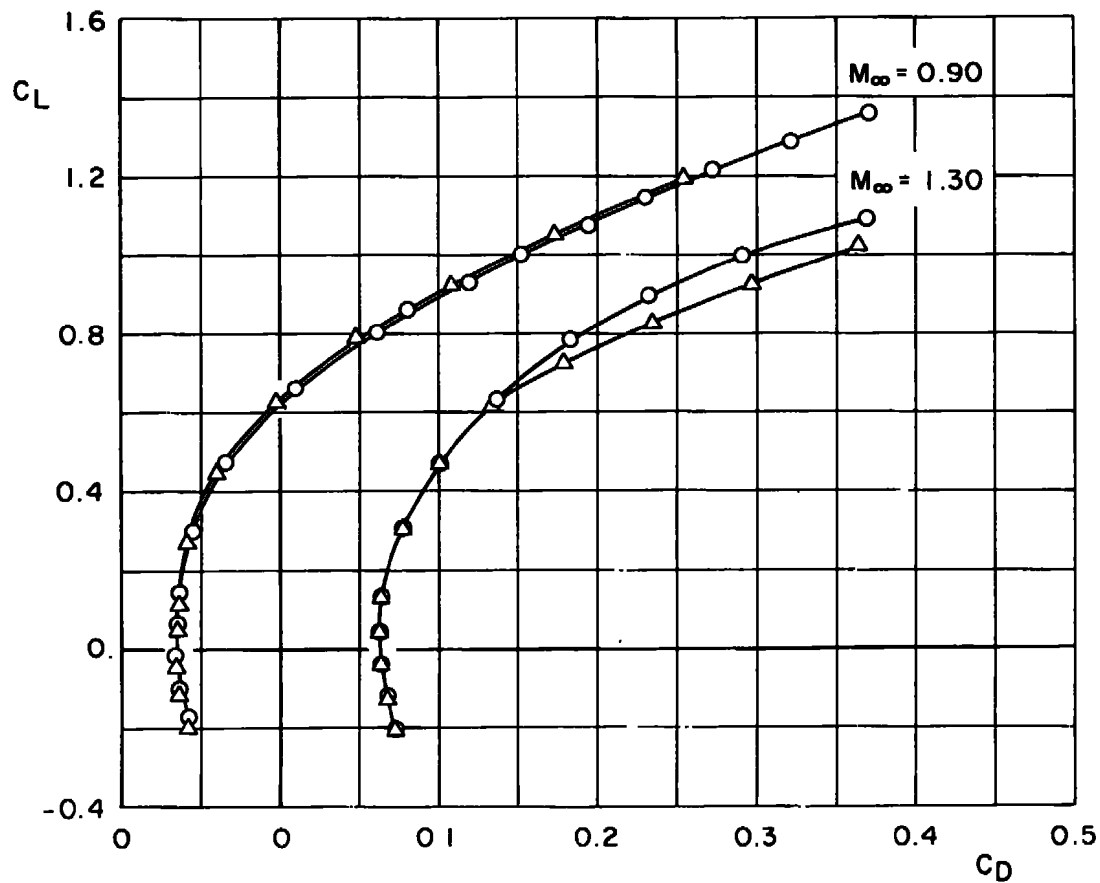


b. Continued, $\Lambda = 54$ deg
 Figure 10. Continued.



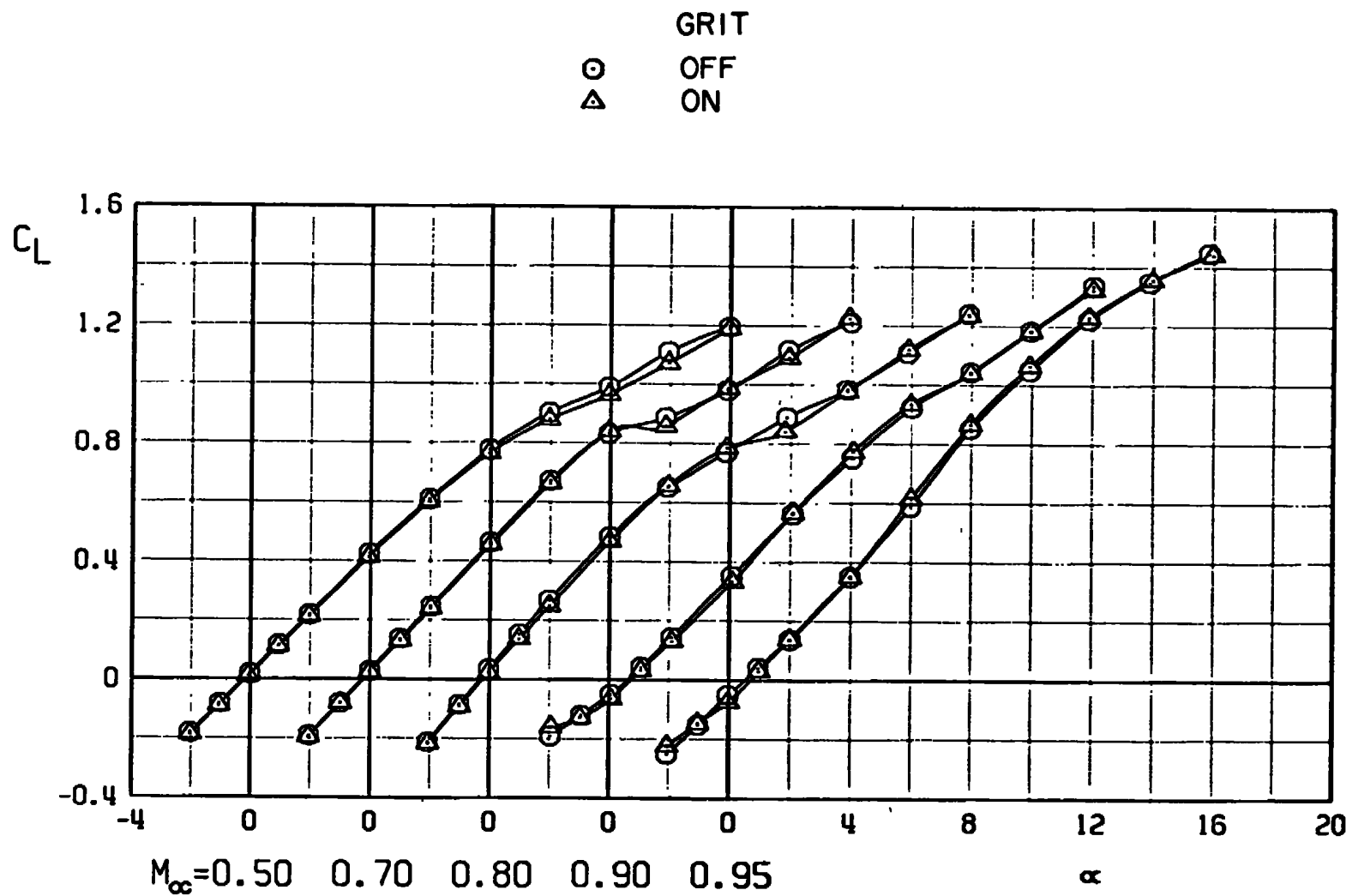
c. Drag coefficient, $\Lambda = 26$ deg
 Figure 10. Continued.

$\text{Re} \times 10^{-6}$
 PT $M_\infty = 0.90$ $M_\infty = 1.30$
 ○ 1200 2.41 2.55
 △ 2000 4.09 3.99

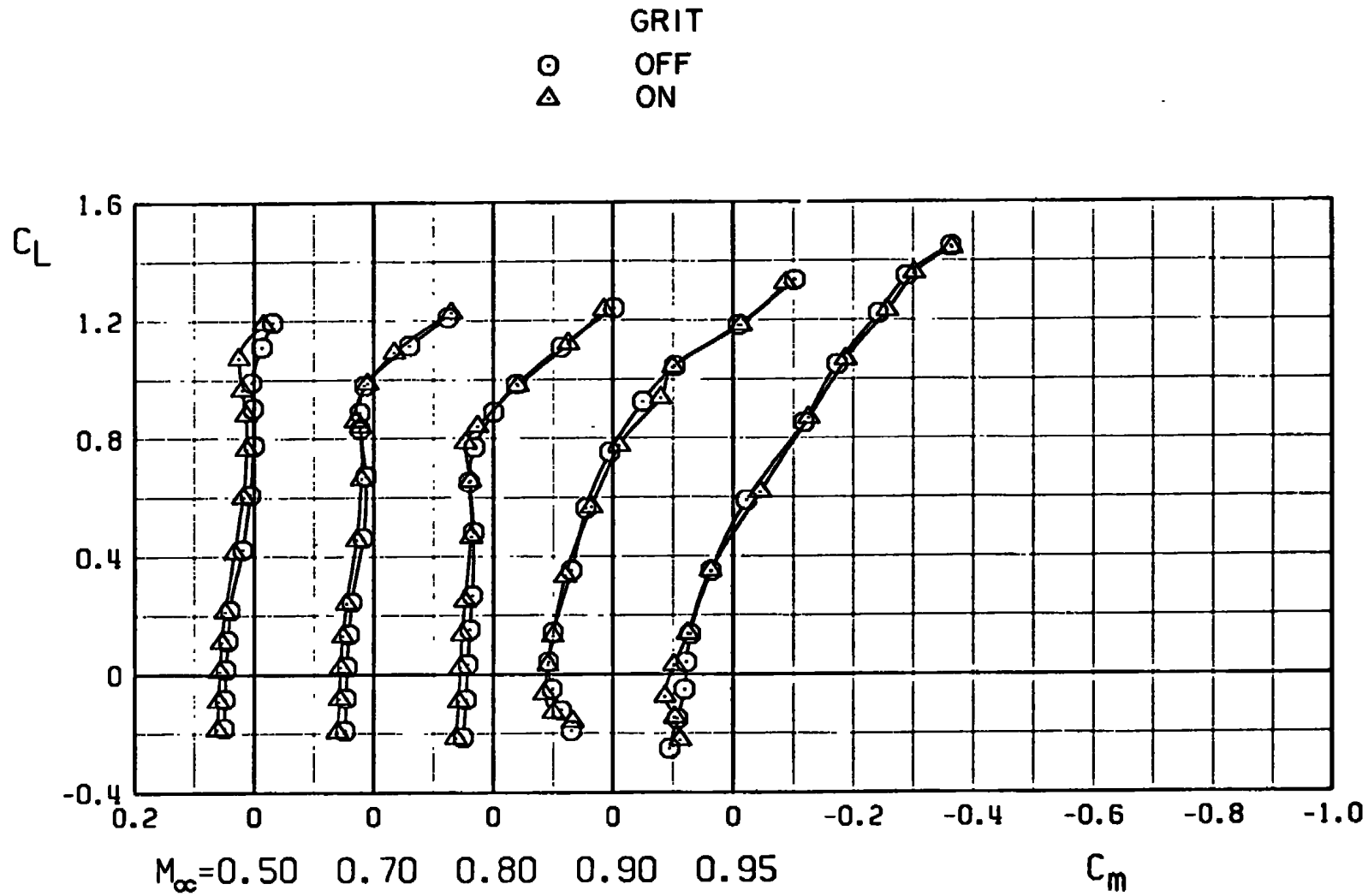


c. Concluded, $\Lambda = 54$ deg
 Figure 10. Concluded.

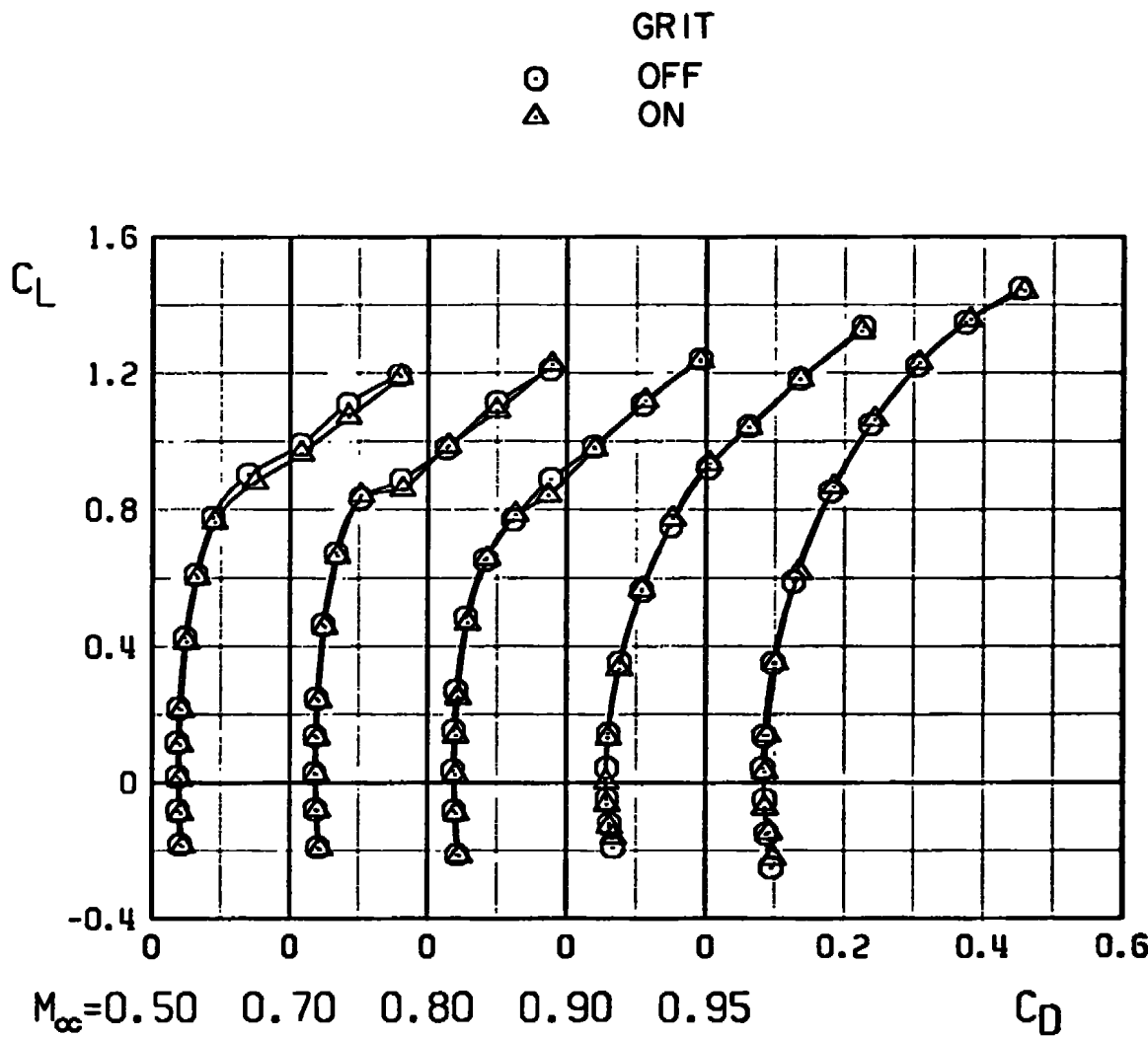
62



a. Lift coefficient
Figure 11. Transition grit effects, $\Lambda = 26$ deg.



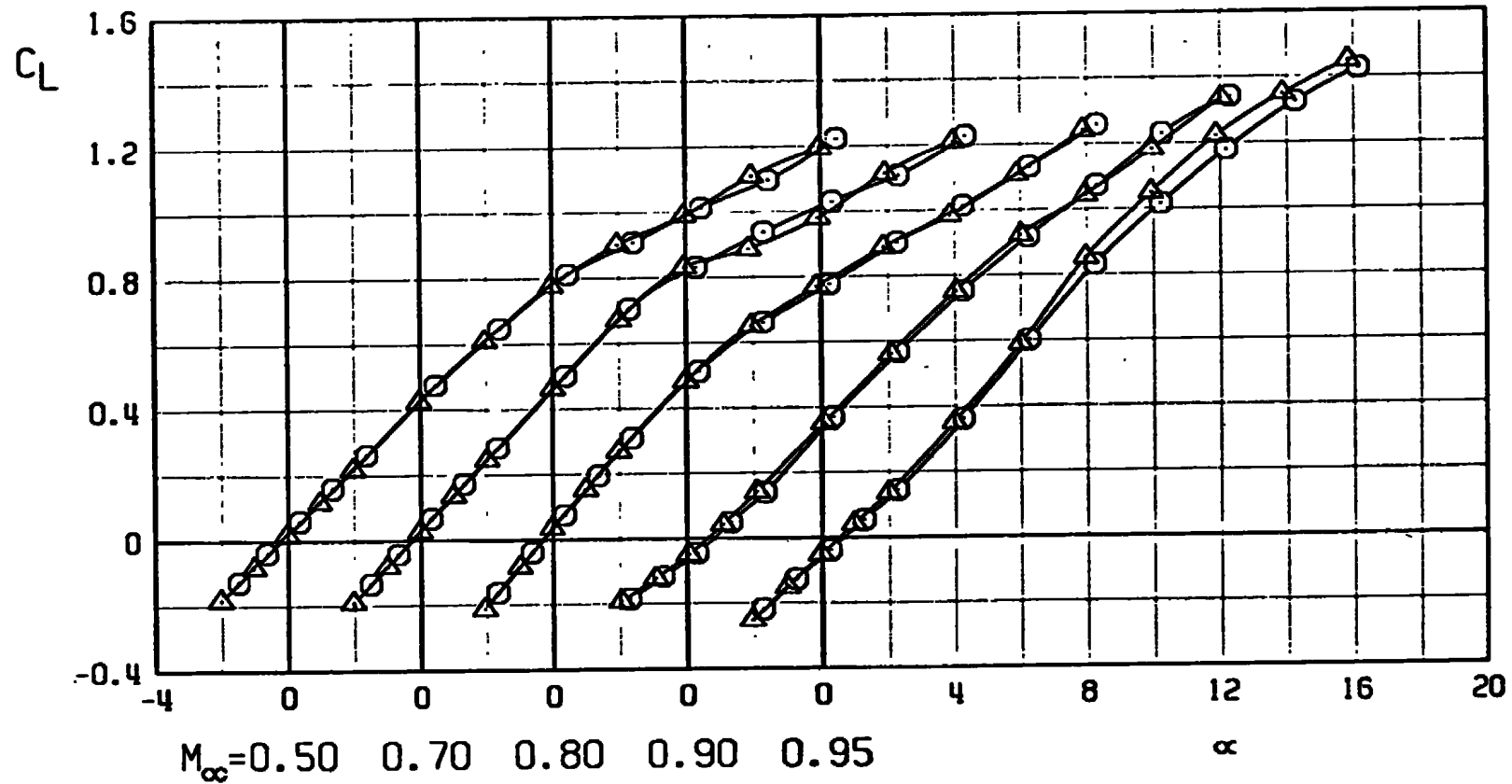
b. Pitching-moment coefficient
Figure 11. Continued.



c. Drag coefficient
Figure 11. Concluded.

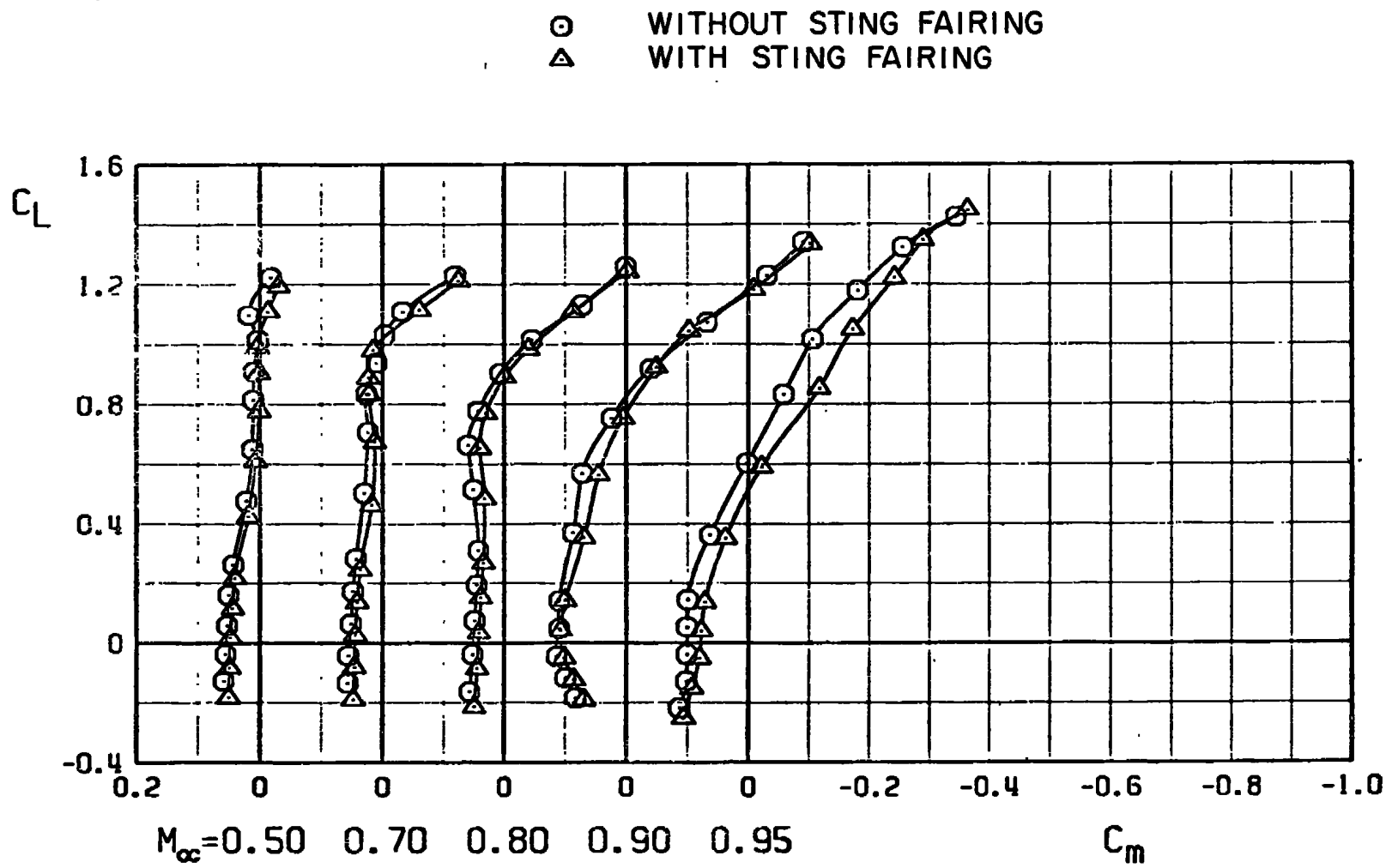
○ WITHOUT STING FAIRING
△ WITH STING FAIRING

65

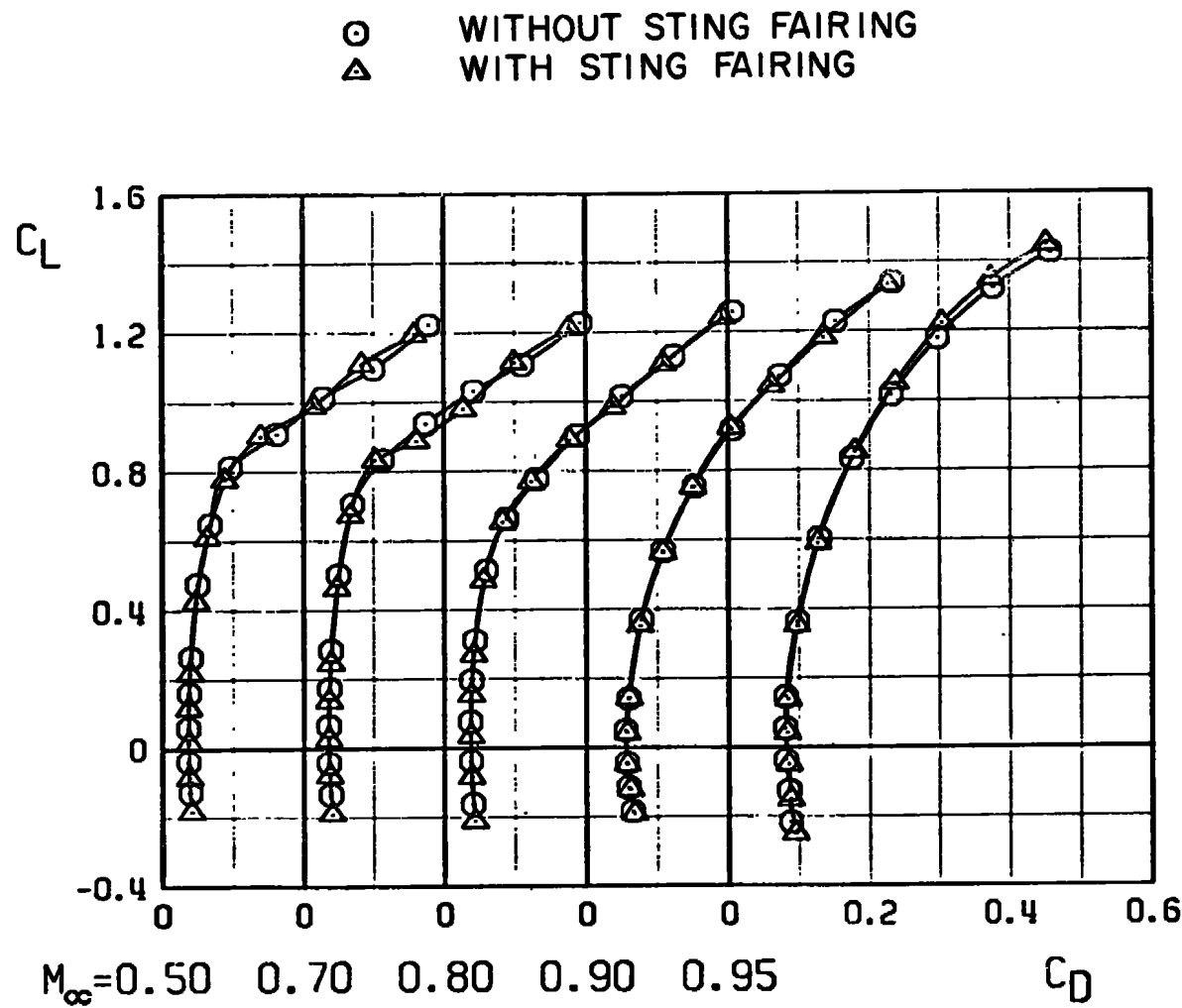


a. Lift coefficient

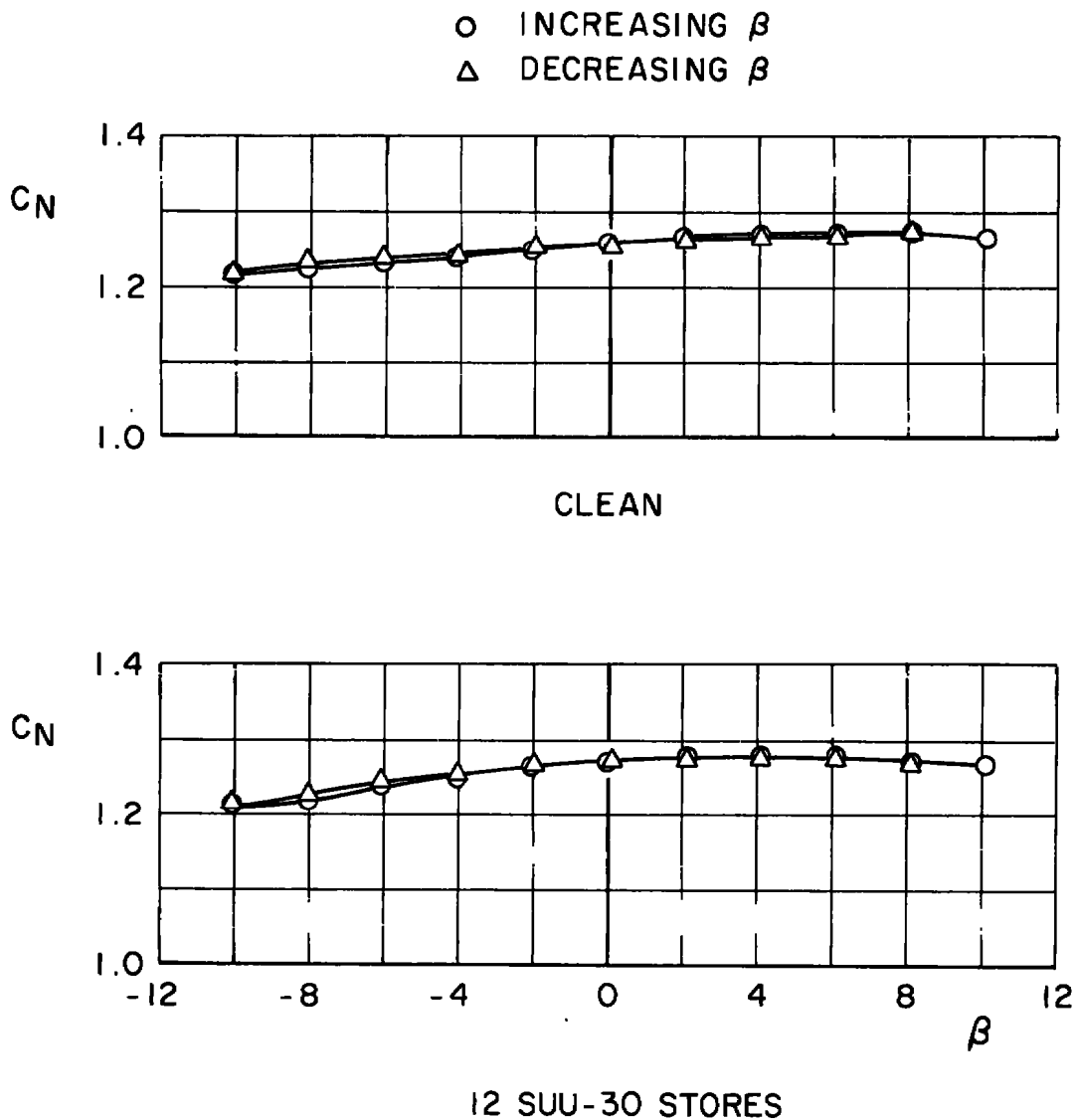
Figure 12. Sting fairing effects, $\Delta = 26 \text{ deg.}$



b. Pitching-moment coefficient
Figure 12. Continued.

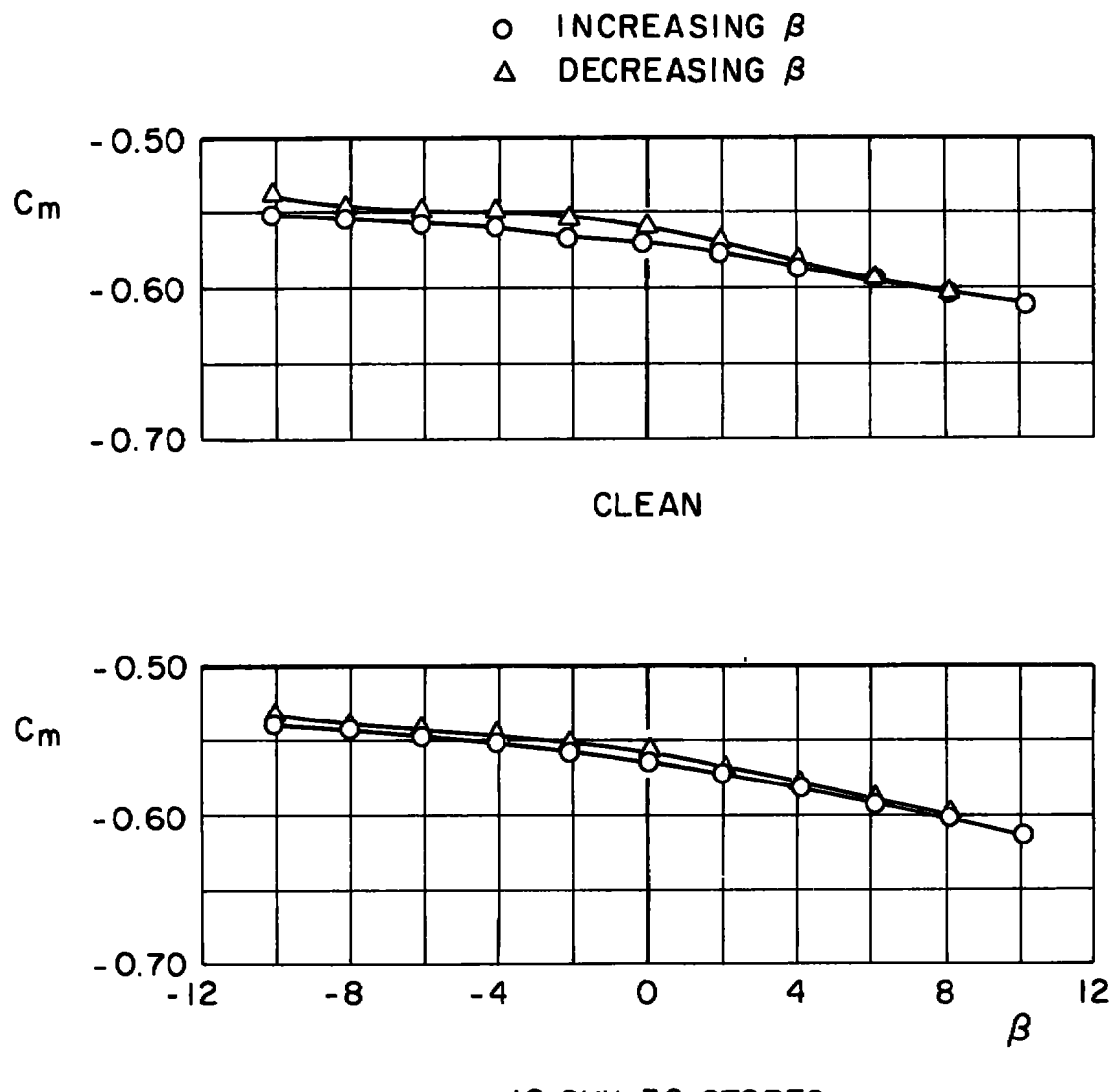


c. Drag coefficient
Figure 12. Concluded.



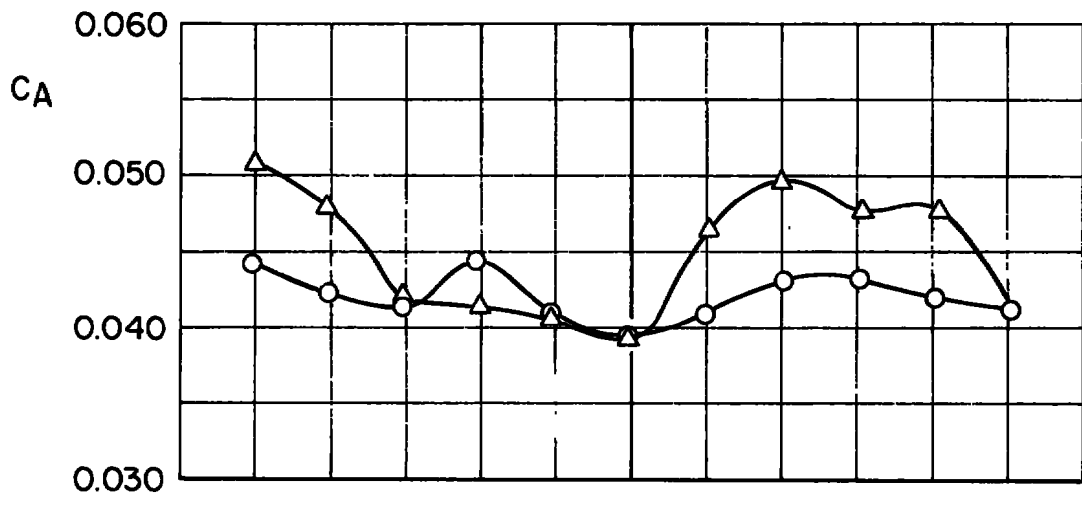
a. Normal-force coefficient

Figure 13. Typical hysteresis effects, $\alpha = 15$ deg,
 $\Lambda = 45$ deg, $M_\infty = 1.2$.

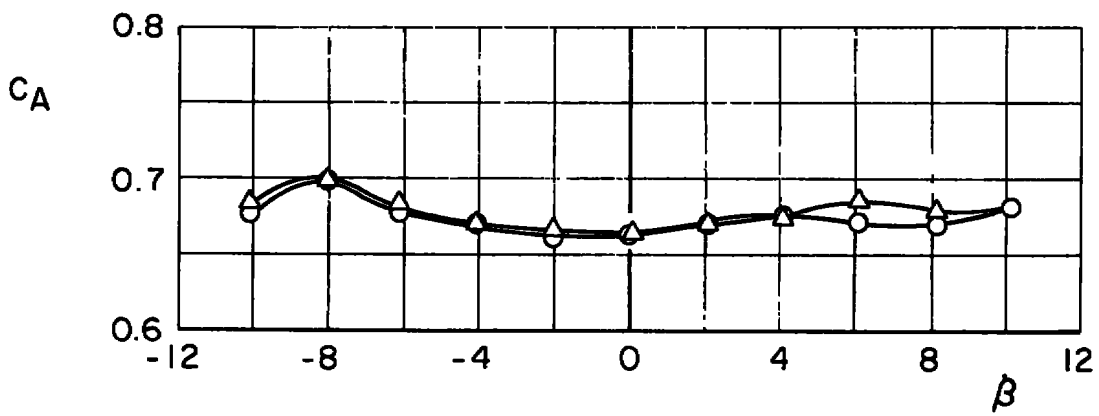


b. Pitching-moment coefficient
Figure 13. Continued.

O INCREASING β
 △ DECREASING β

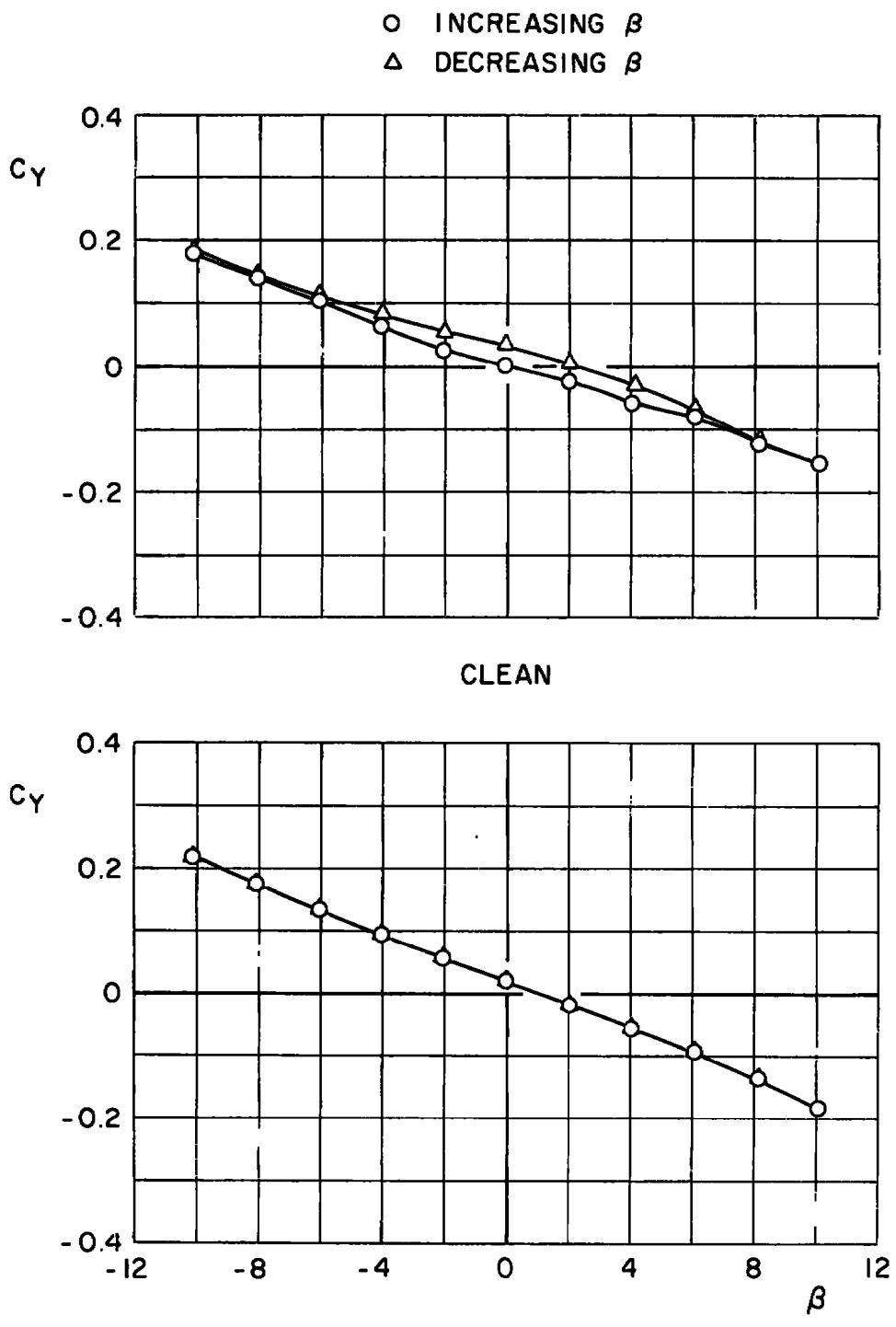


CLEAN



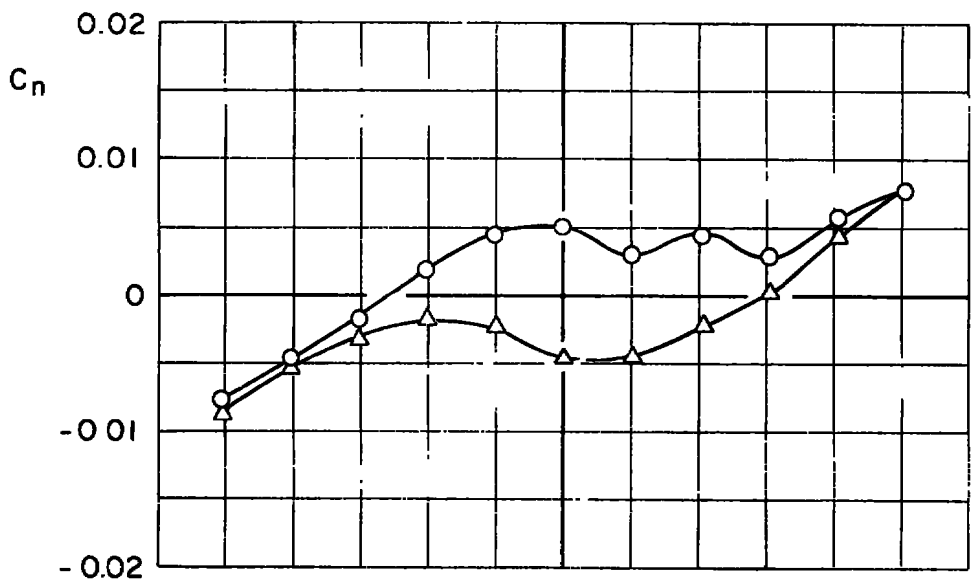
1.2 SUU-30 STORES

c. Axial-force coefficient
 Figure 13. Continued.

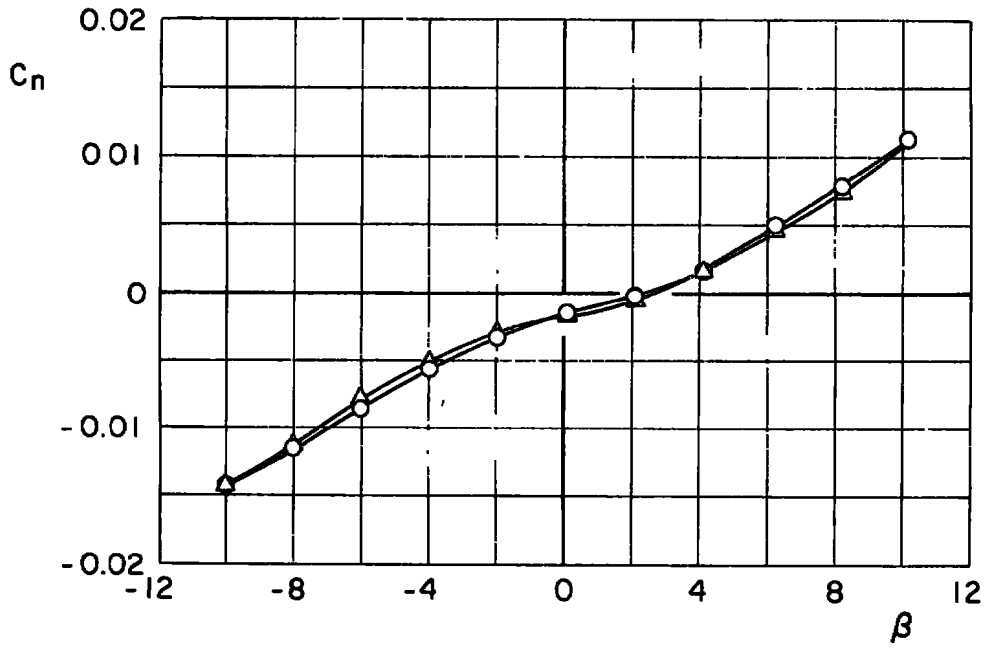


d. Side-force coefficient
 Figure 13. Continued.

○ INCREASING β
 △ DECREASING β

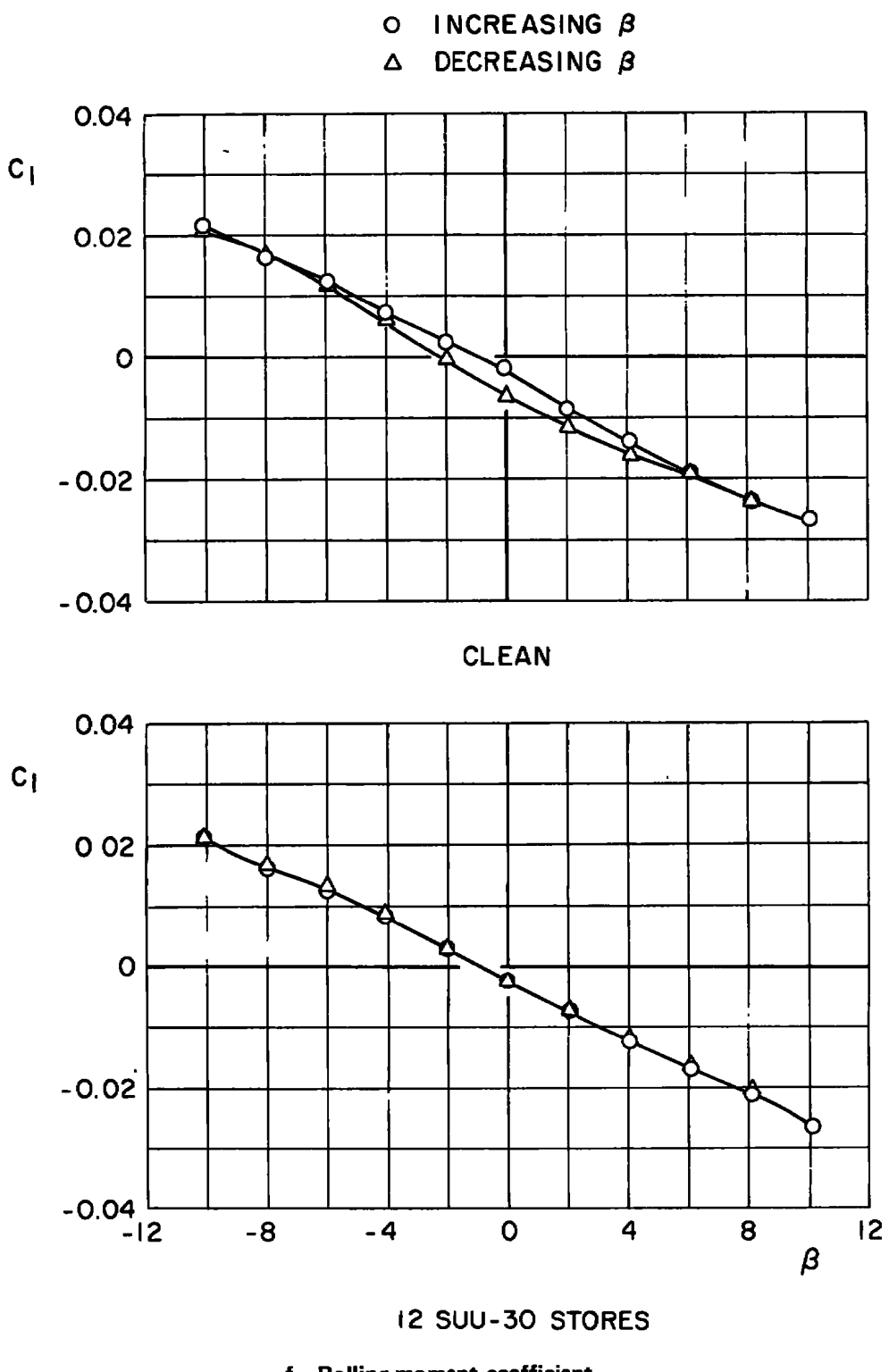


CLEAN

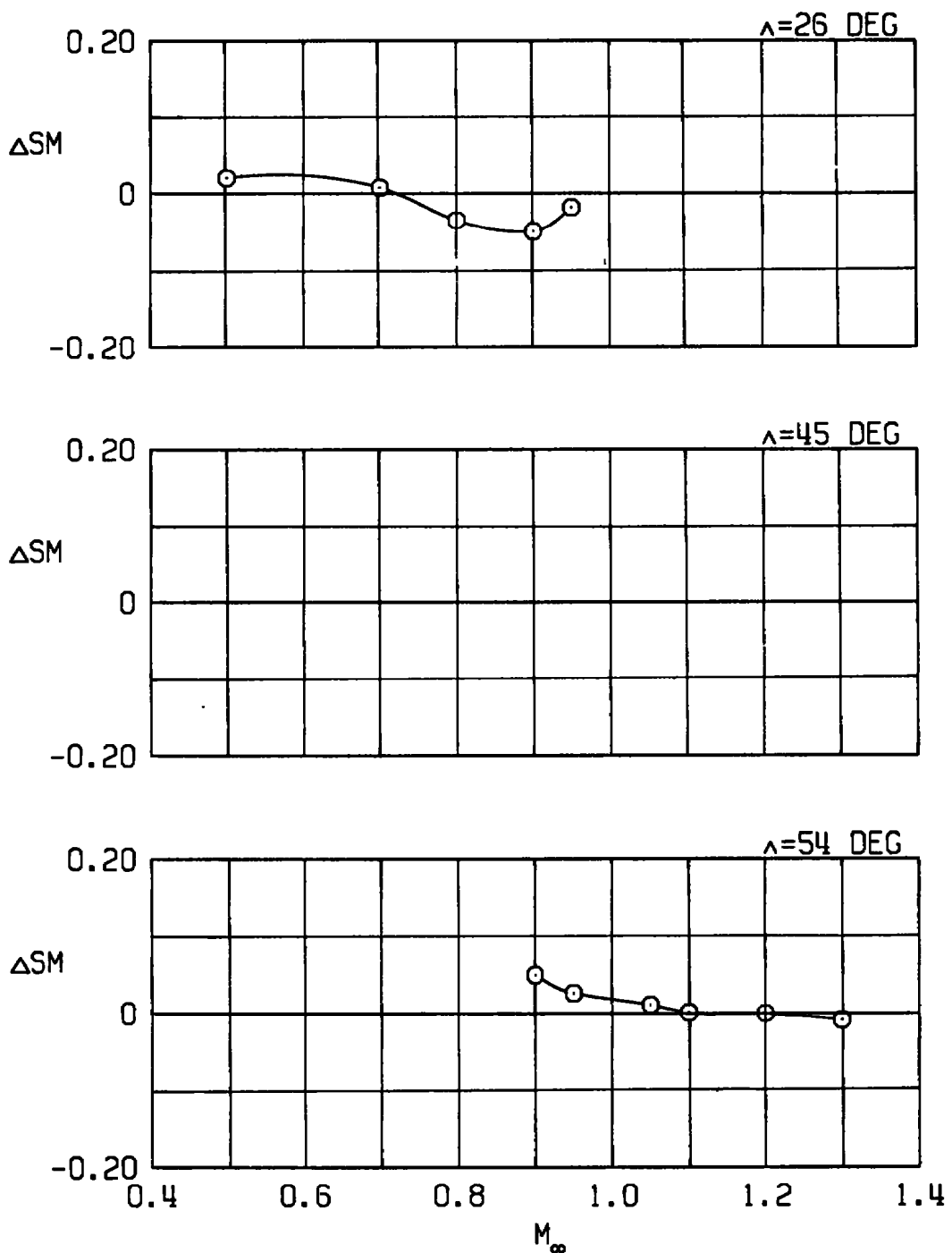


12 SUU-30 STORES

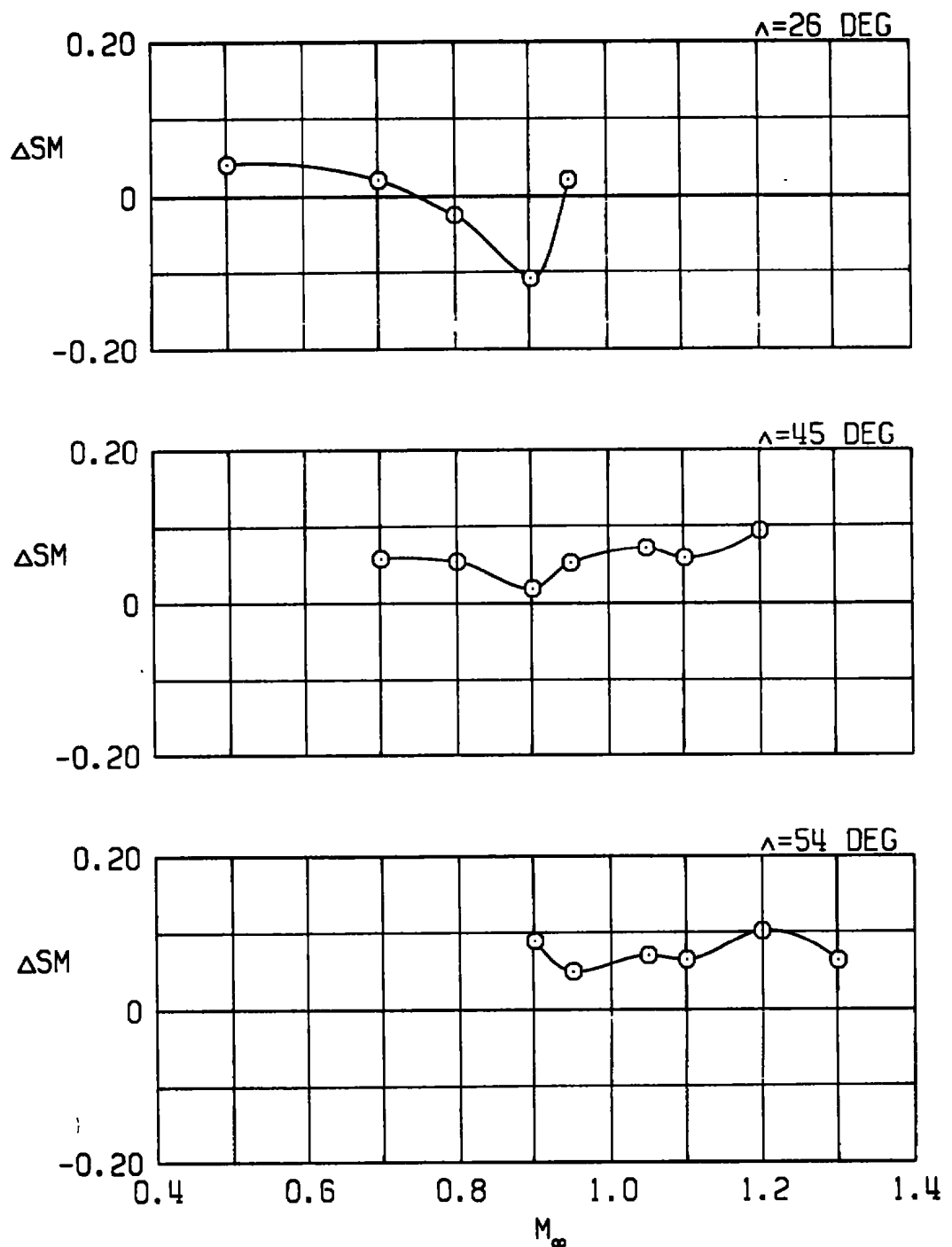
e. Yawing-moment coefficient
 Figure 13. Continued.



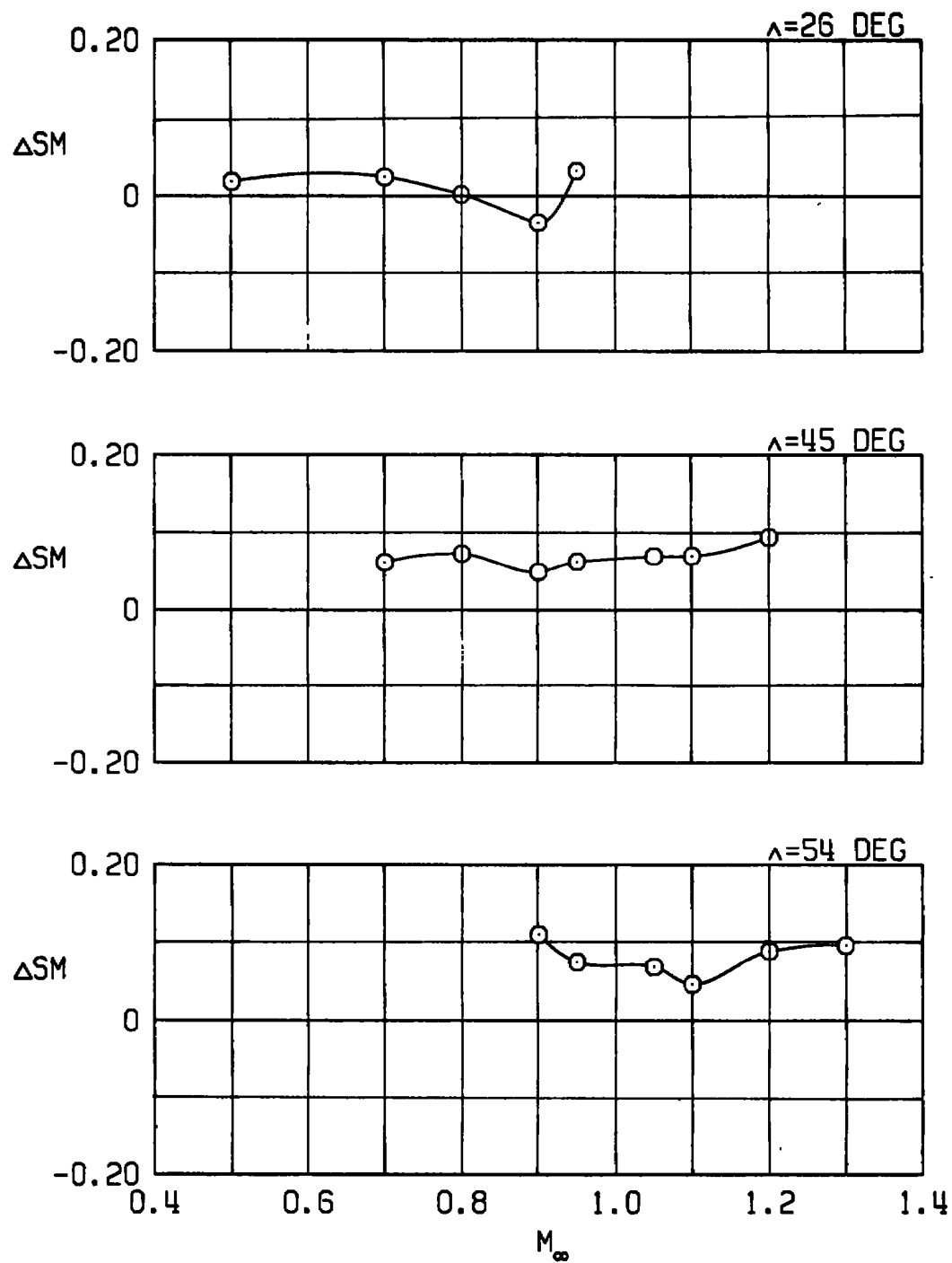
f. Rolling-moment coefficient
 Figure 13. Concluded.



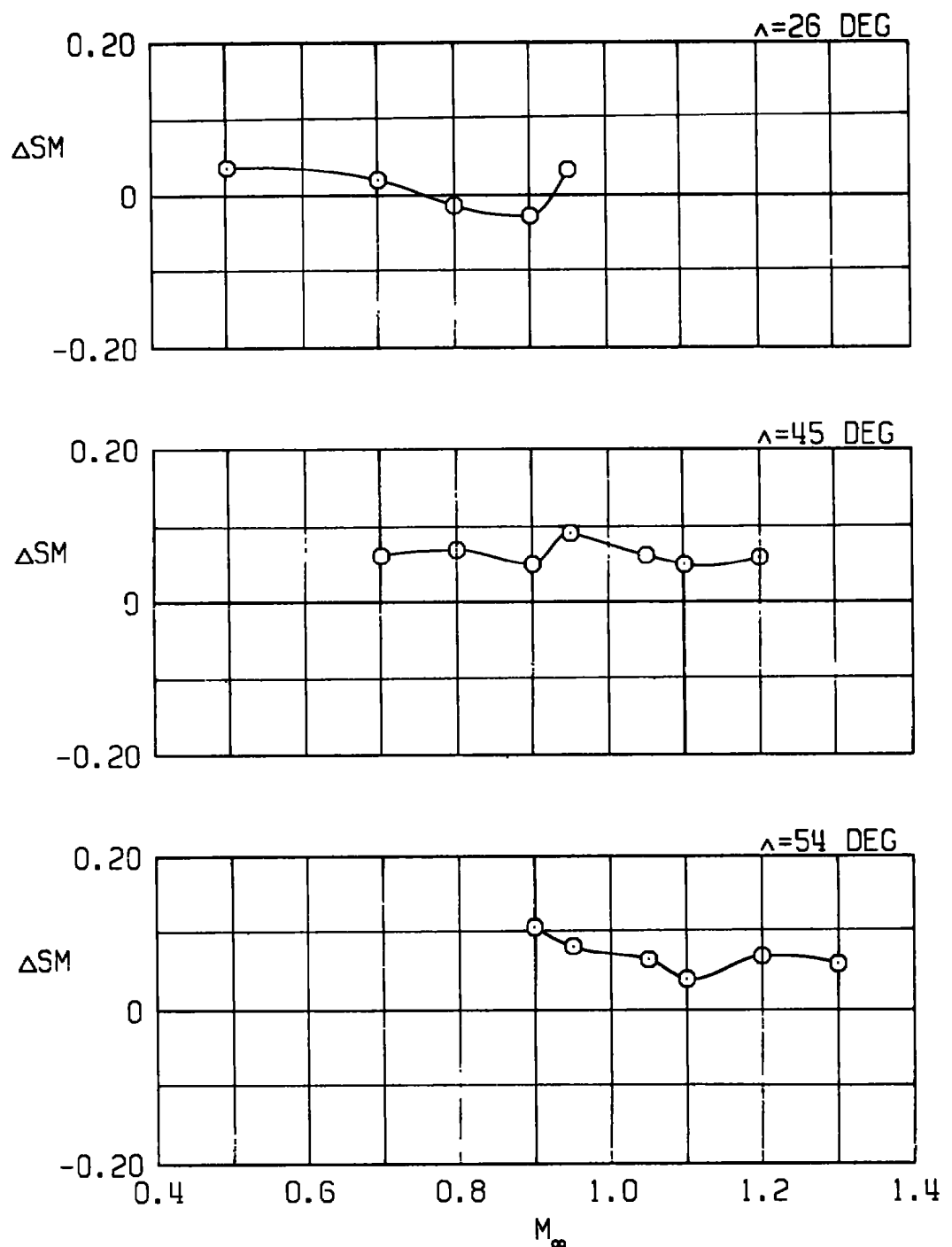
a. Pylons alone
Figure 14. Effects of external stores on the static margin.



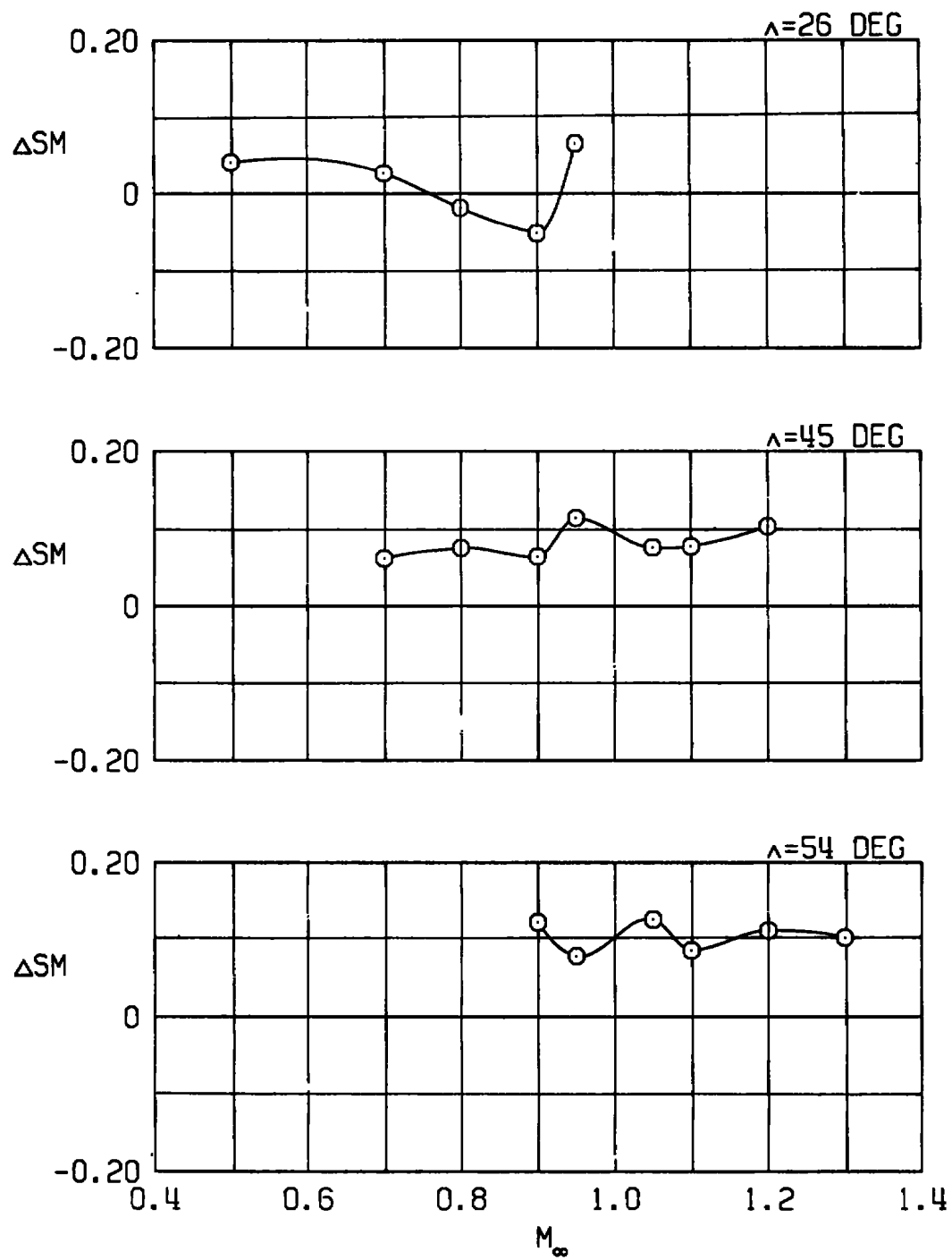
b. Four GBU-10 stores
Figure 14. Continued.



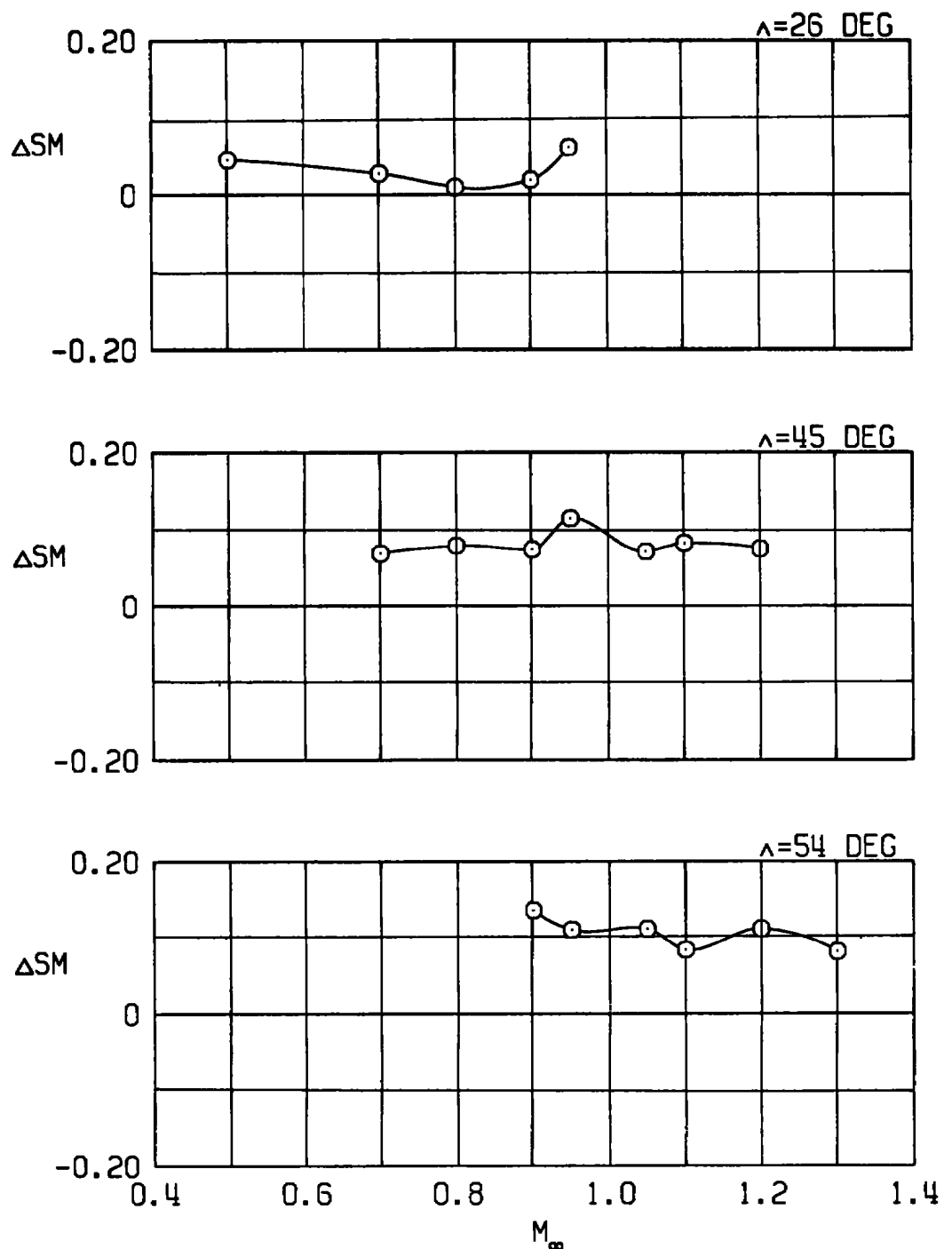
c. Four GBU-15CCW stores
Figure 14. Continued.



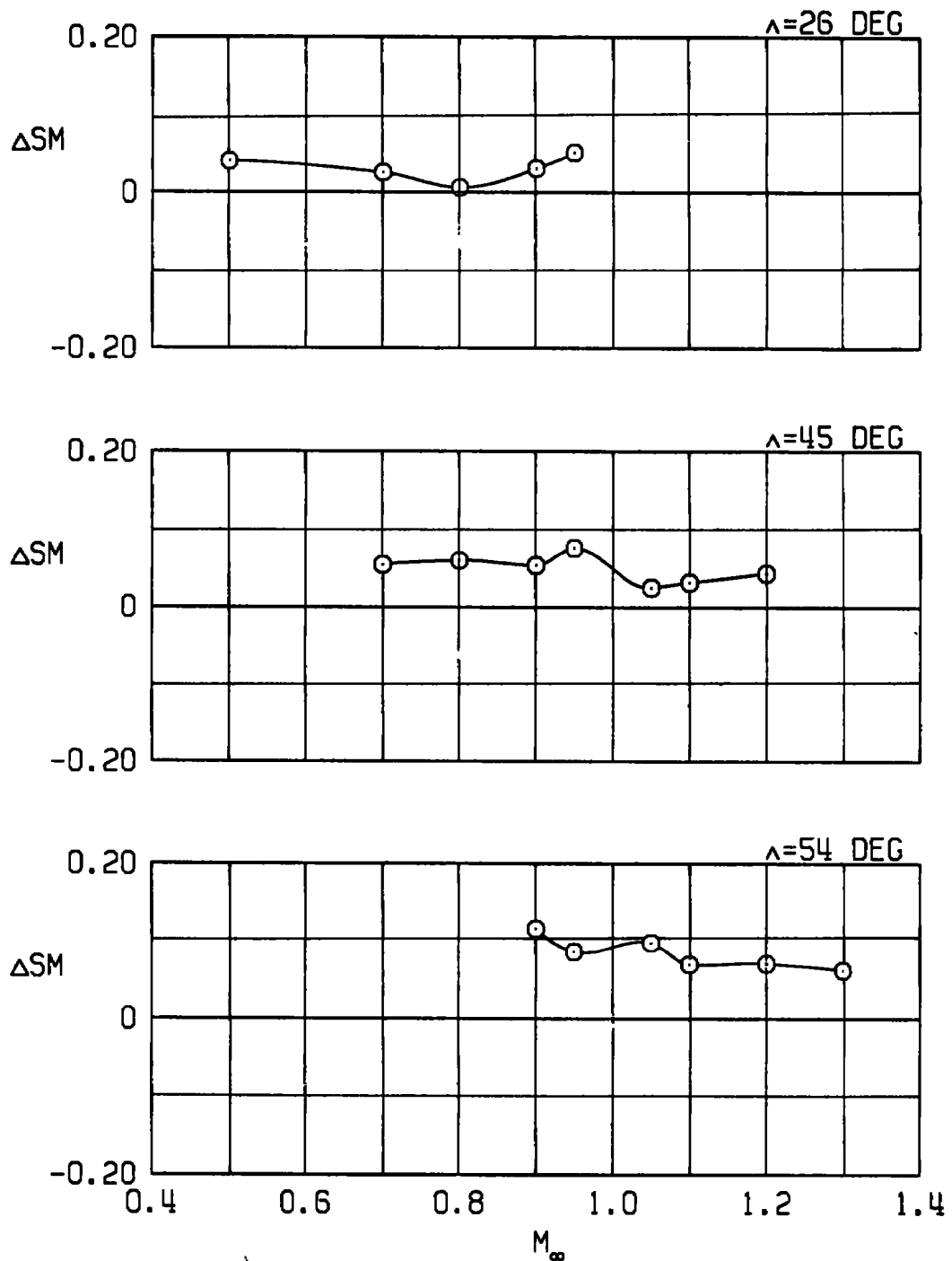
d. Four GBU-15 stores and extended
Pave Tack pod
Figure 14. Continued.



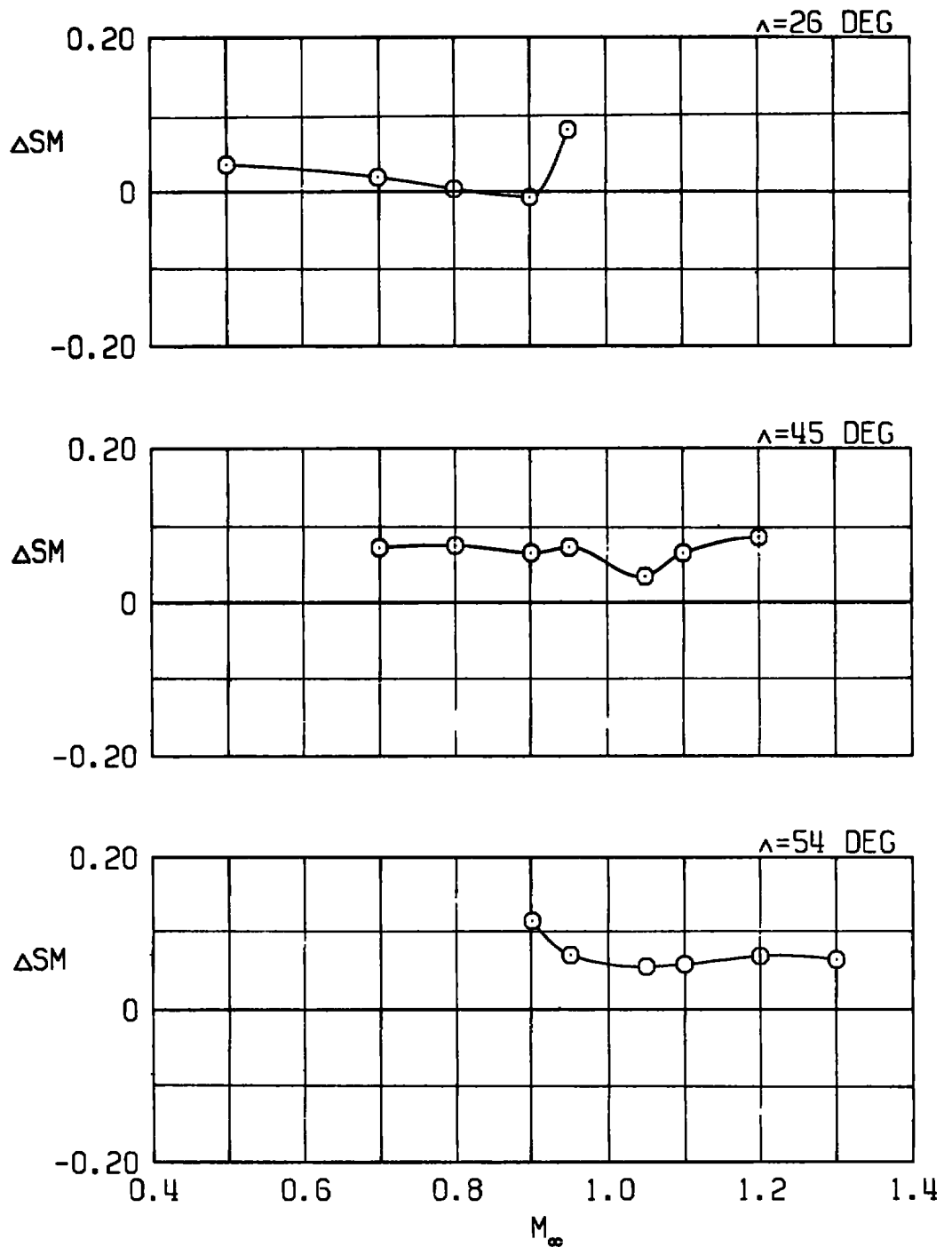
e. 12 AGM-65 stores
Figure 14. Continued.



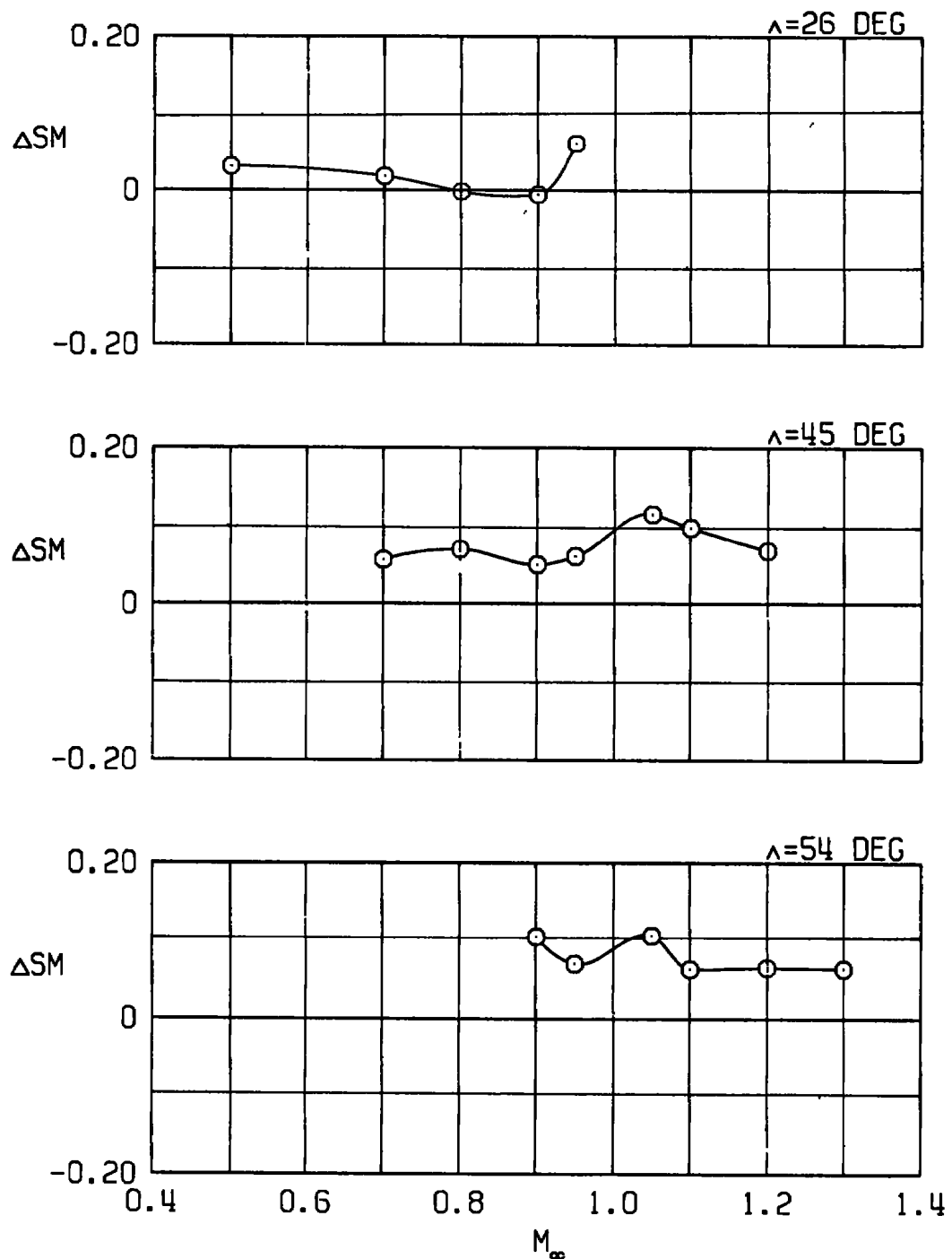
f. 16 Rockeye stores (slant 4 loading)
Figure 14. Continued.



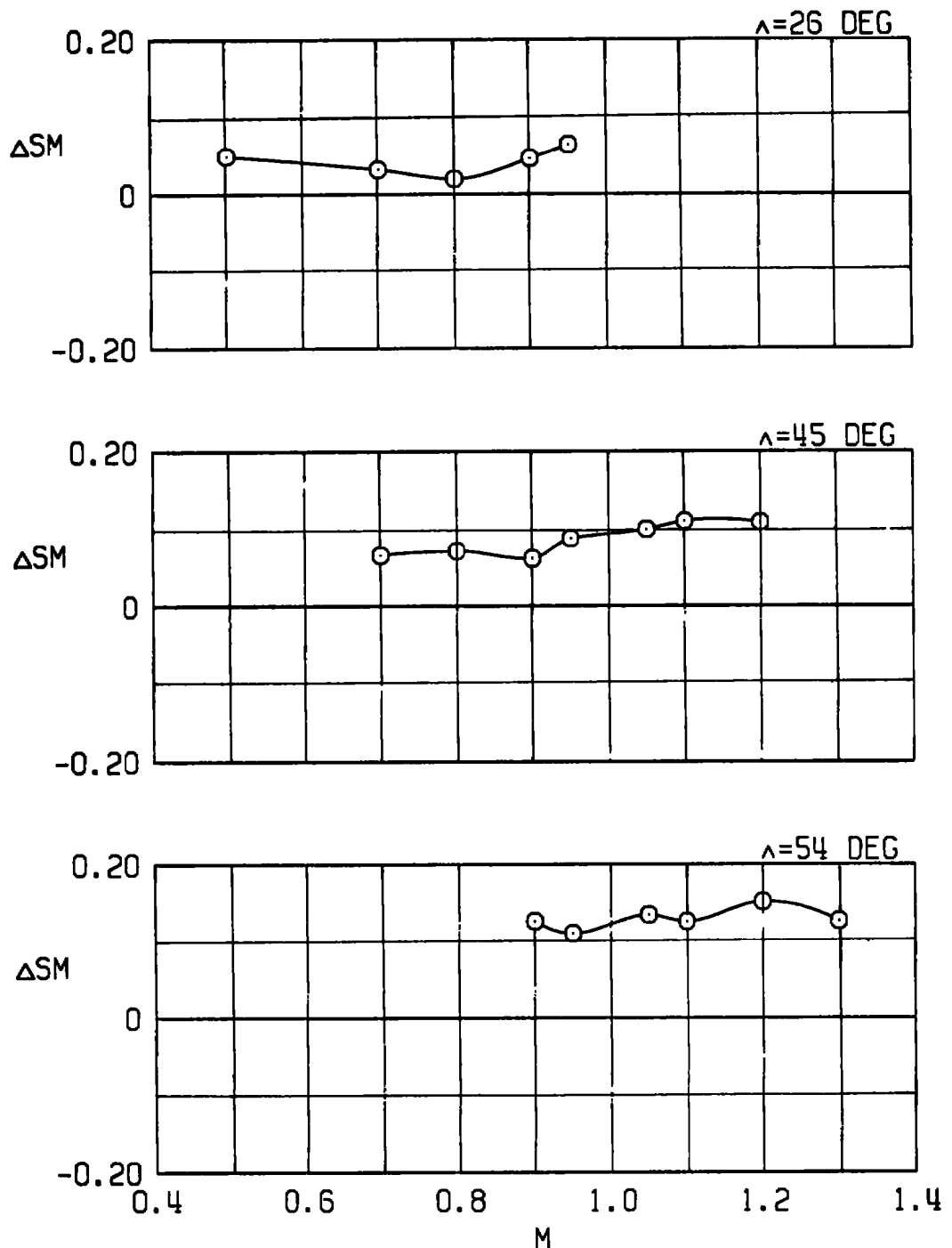
g. 12 Rockeye stores (outboard pylons)
 Figure 14. Continued.



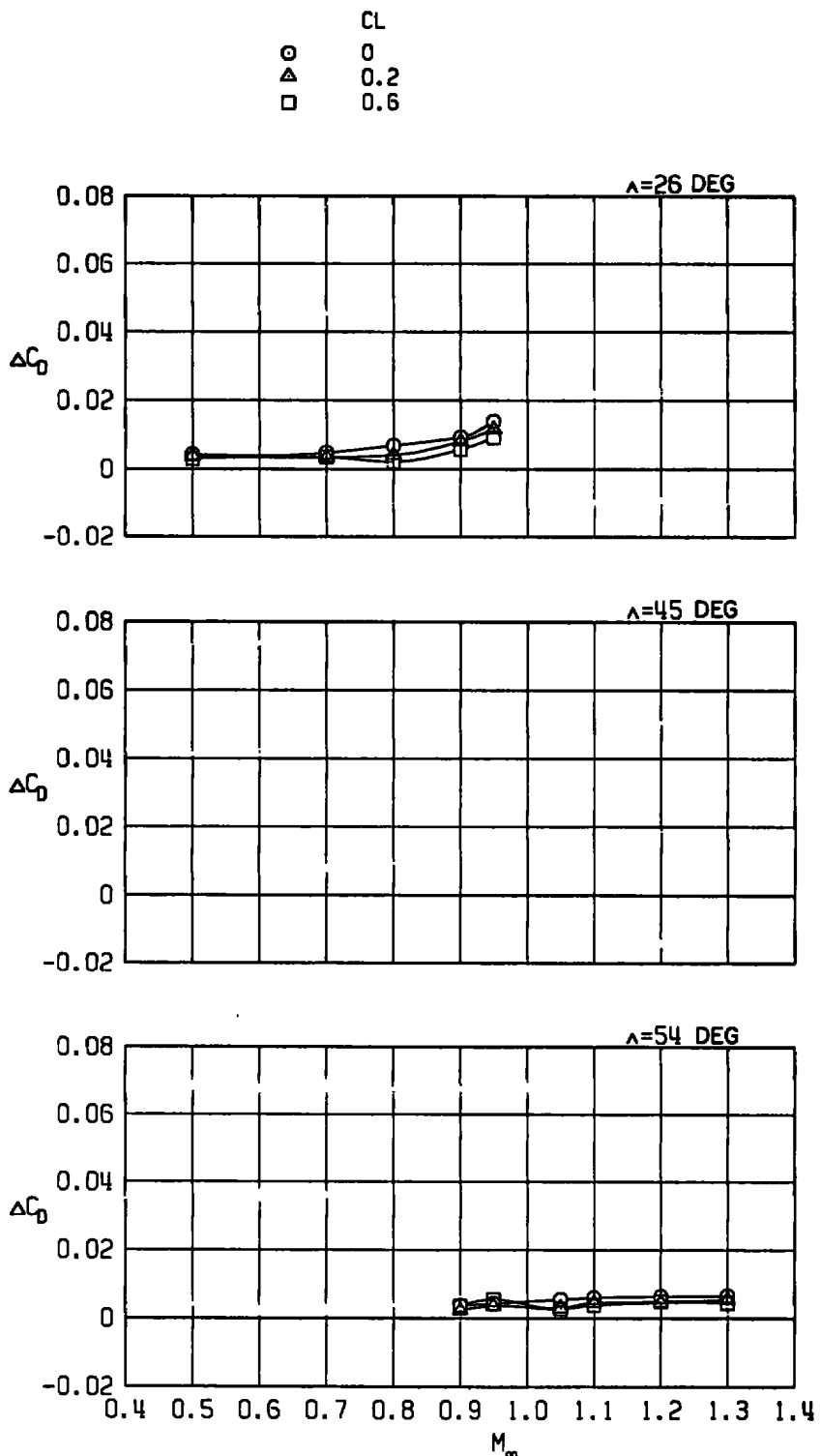
h. 12 SUU-30 stores (outboard pylons)
Figure 14. Continued.



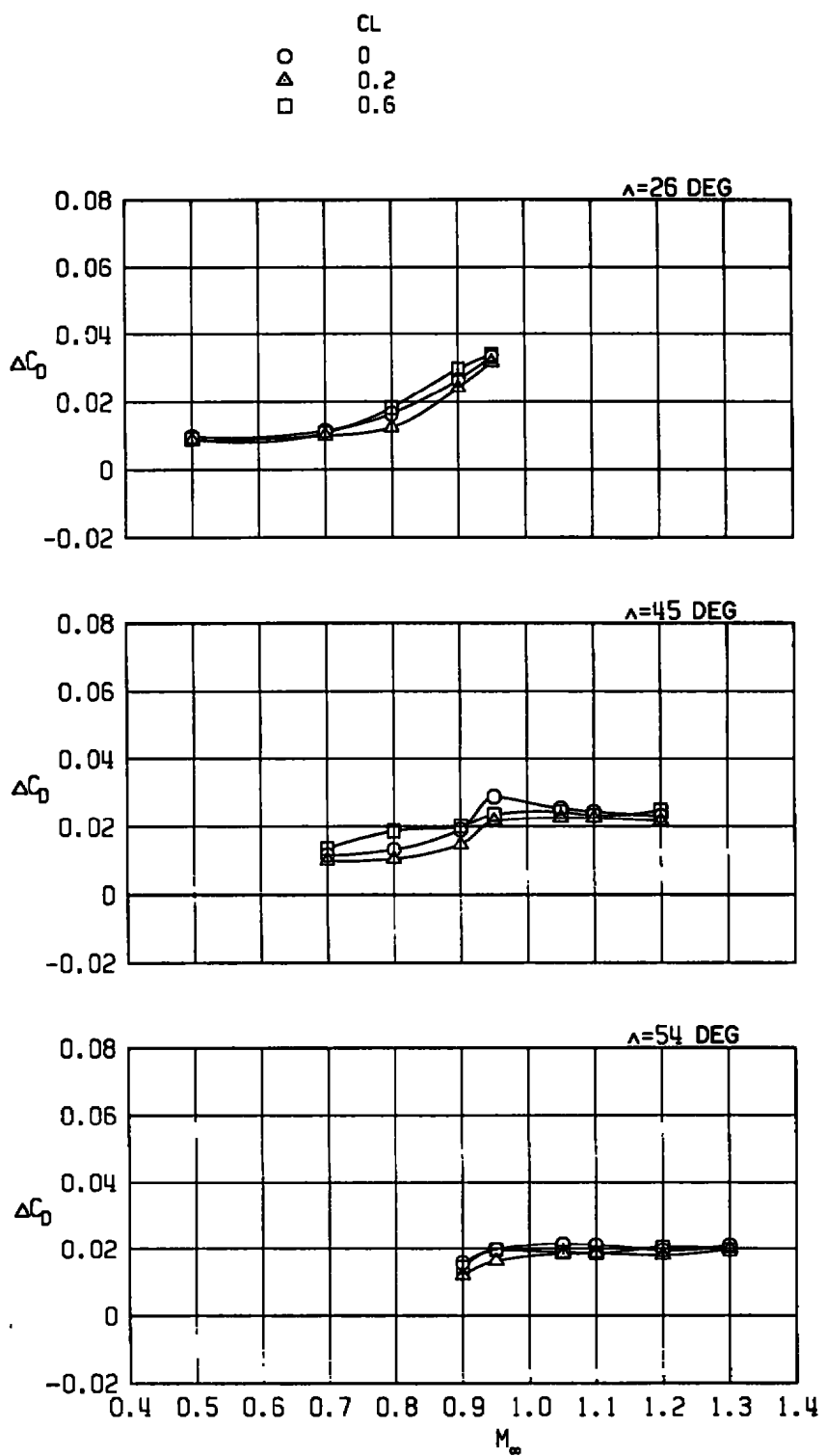
i. 12 MK-82SE stores (outboard pylons)
Figure 14. Continued.



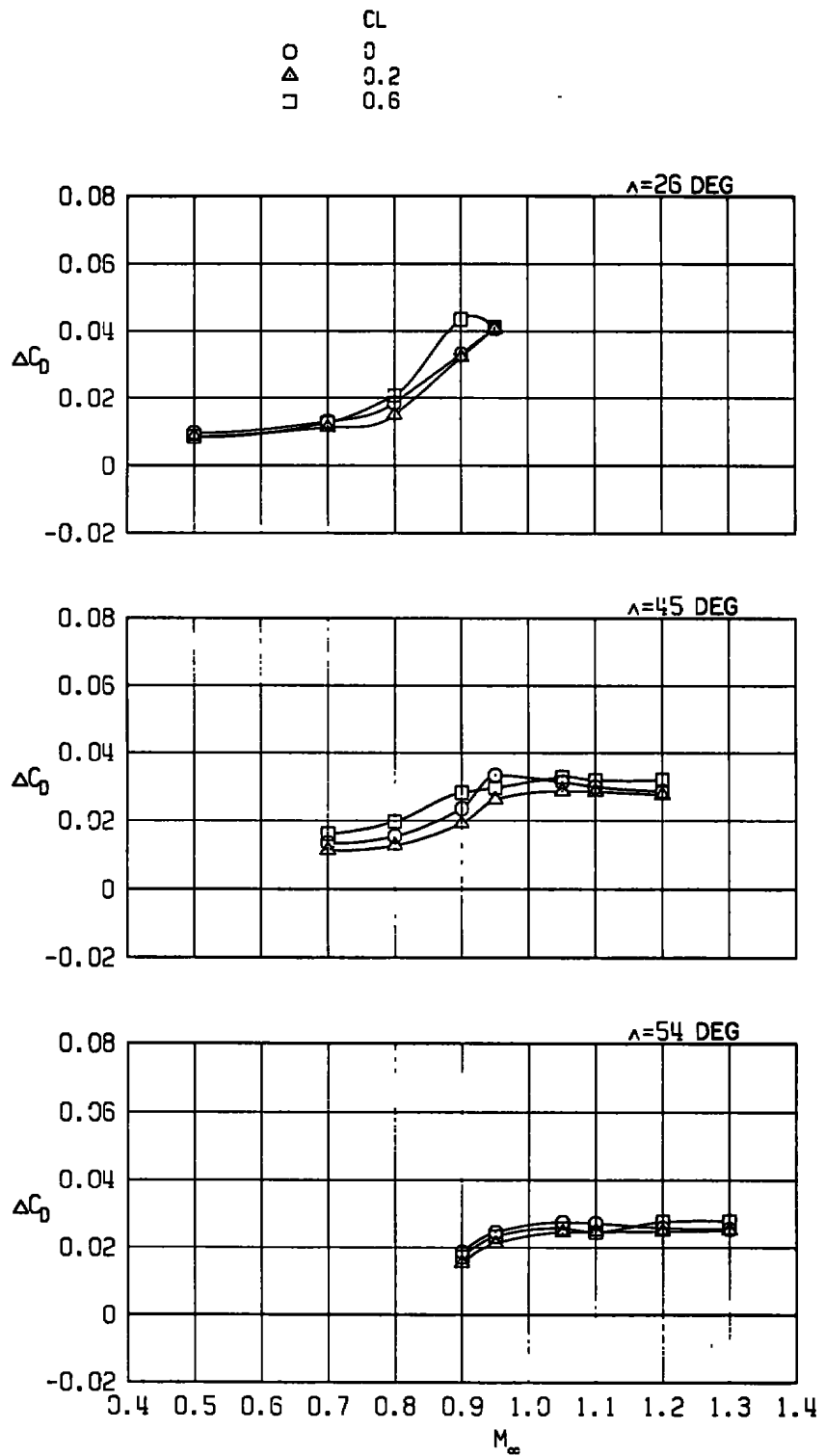
j. 22 MK-82SE stores
 Figure 14. Concluded.



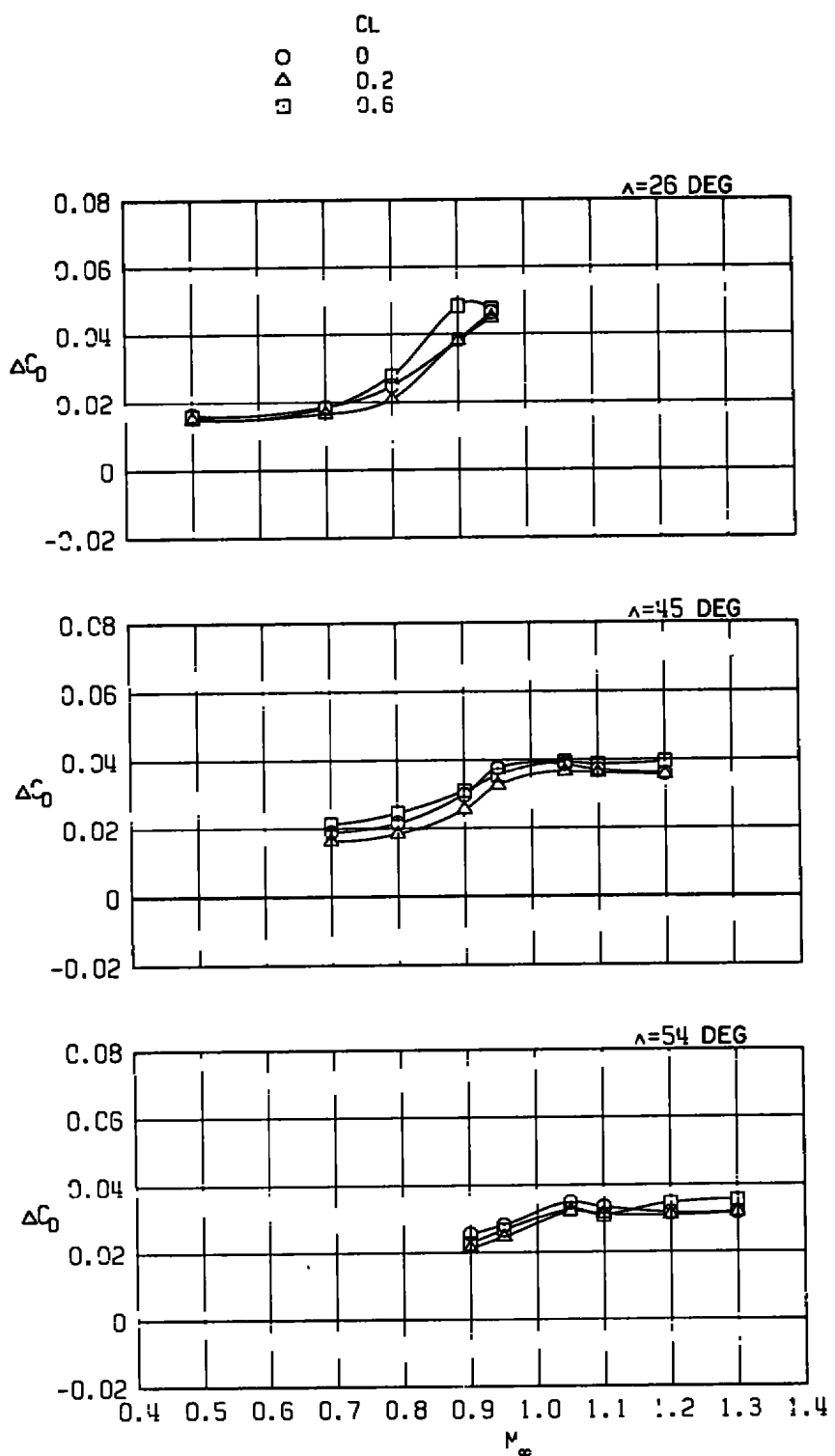
a. Pylons alone
Figure 15. Effects of external stores on the drag coefficient.



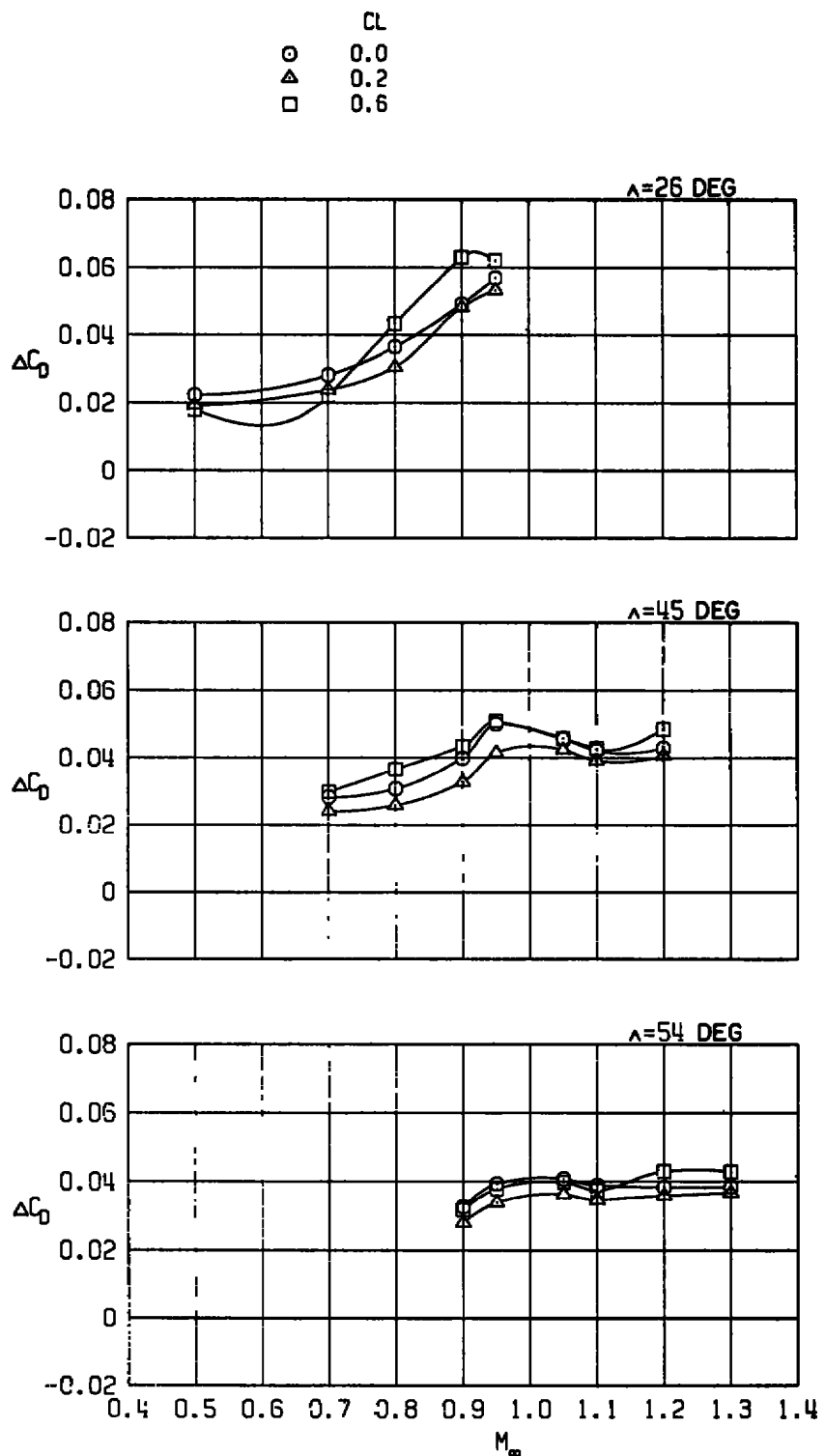
b. Four GBU-10 stores
Figure 15. Continued.



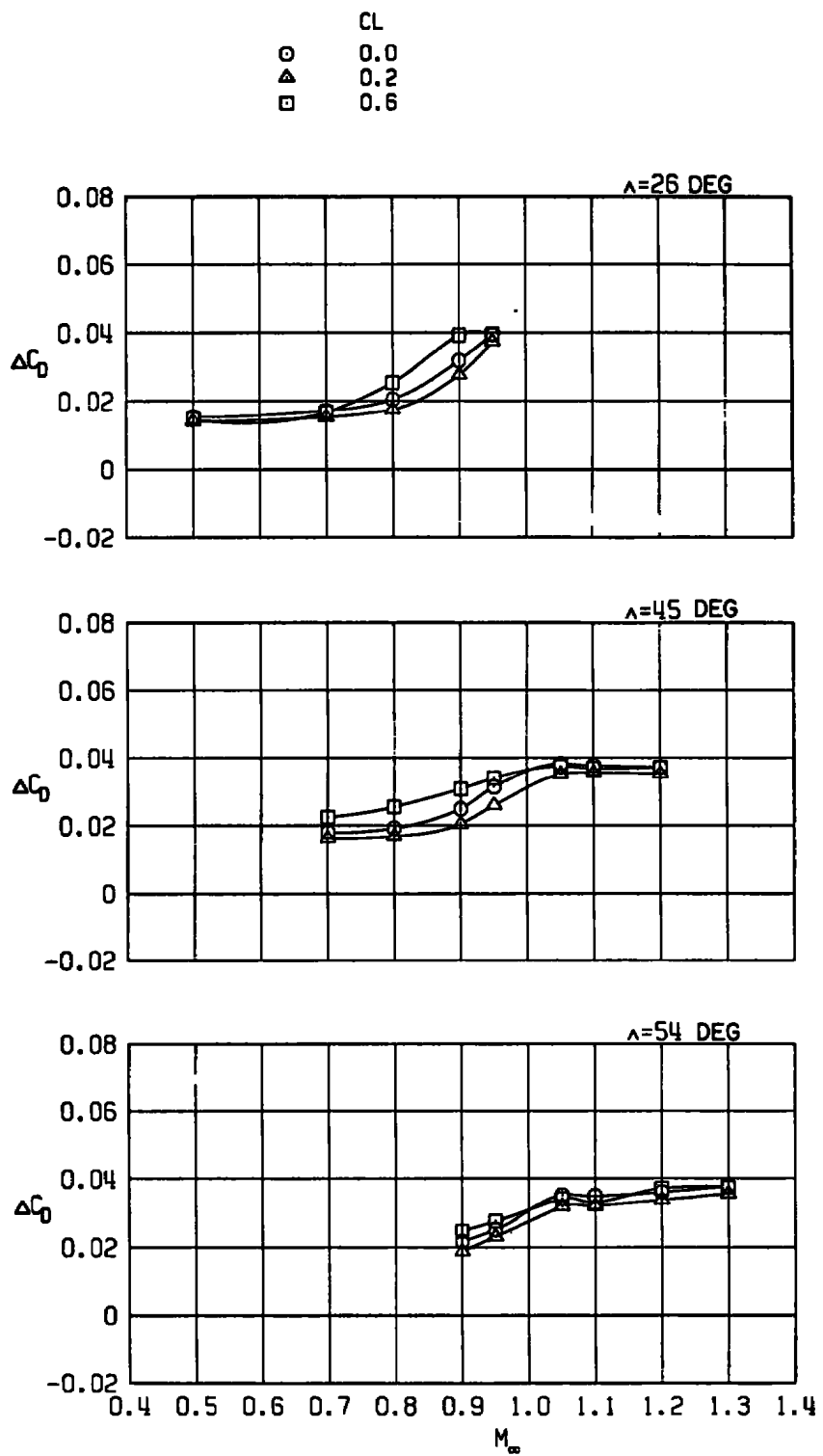
c. Four GBU-15CCW stores
Figure 15. Continued.



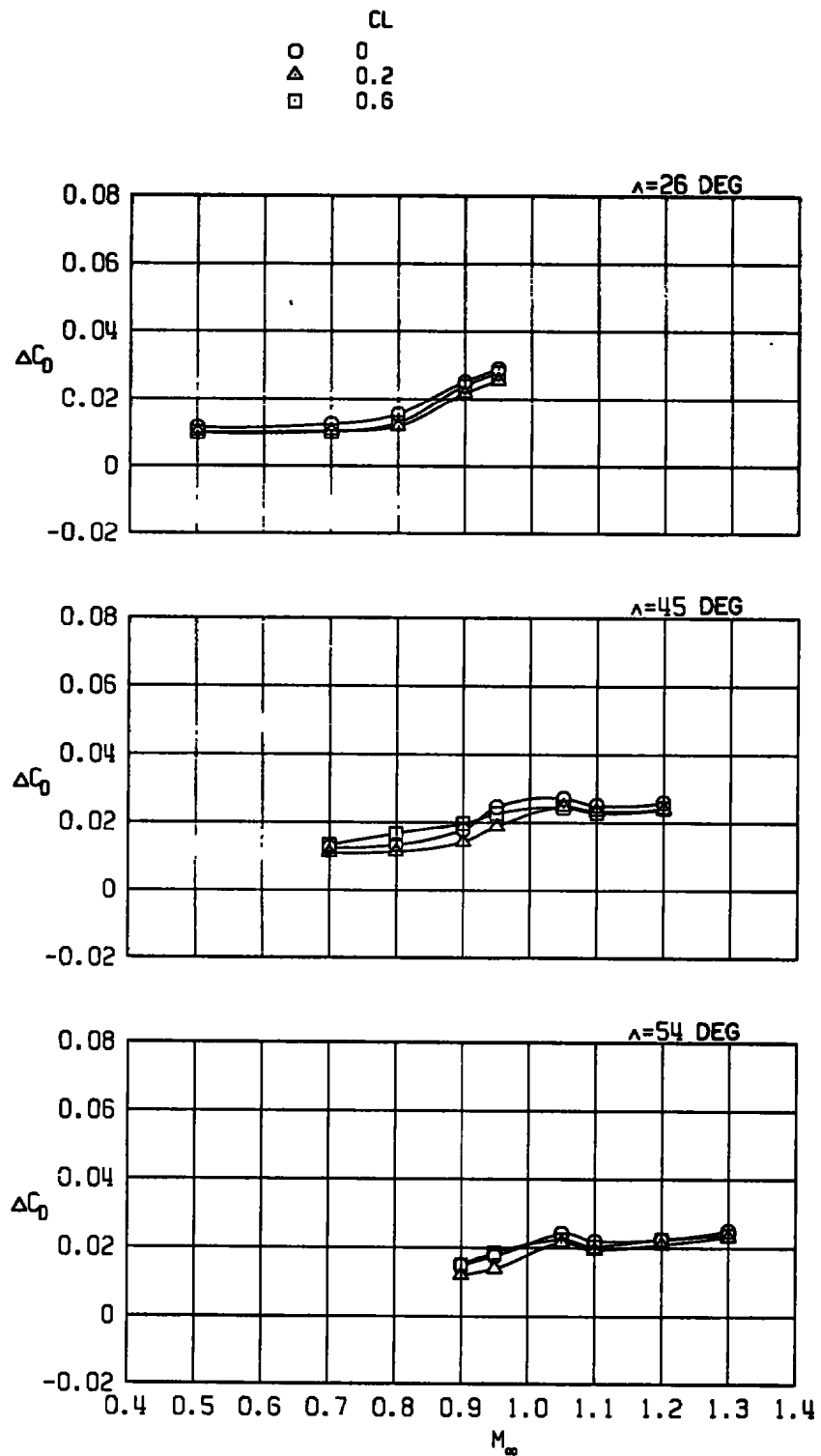
d. Four GBU-15CCW stores and extended
Pave Tack pod
Figure 15. Continued.



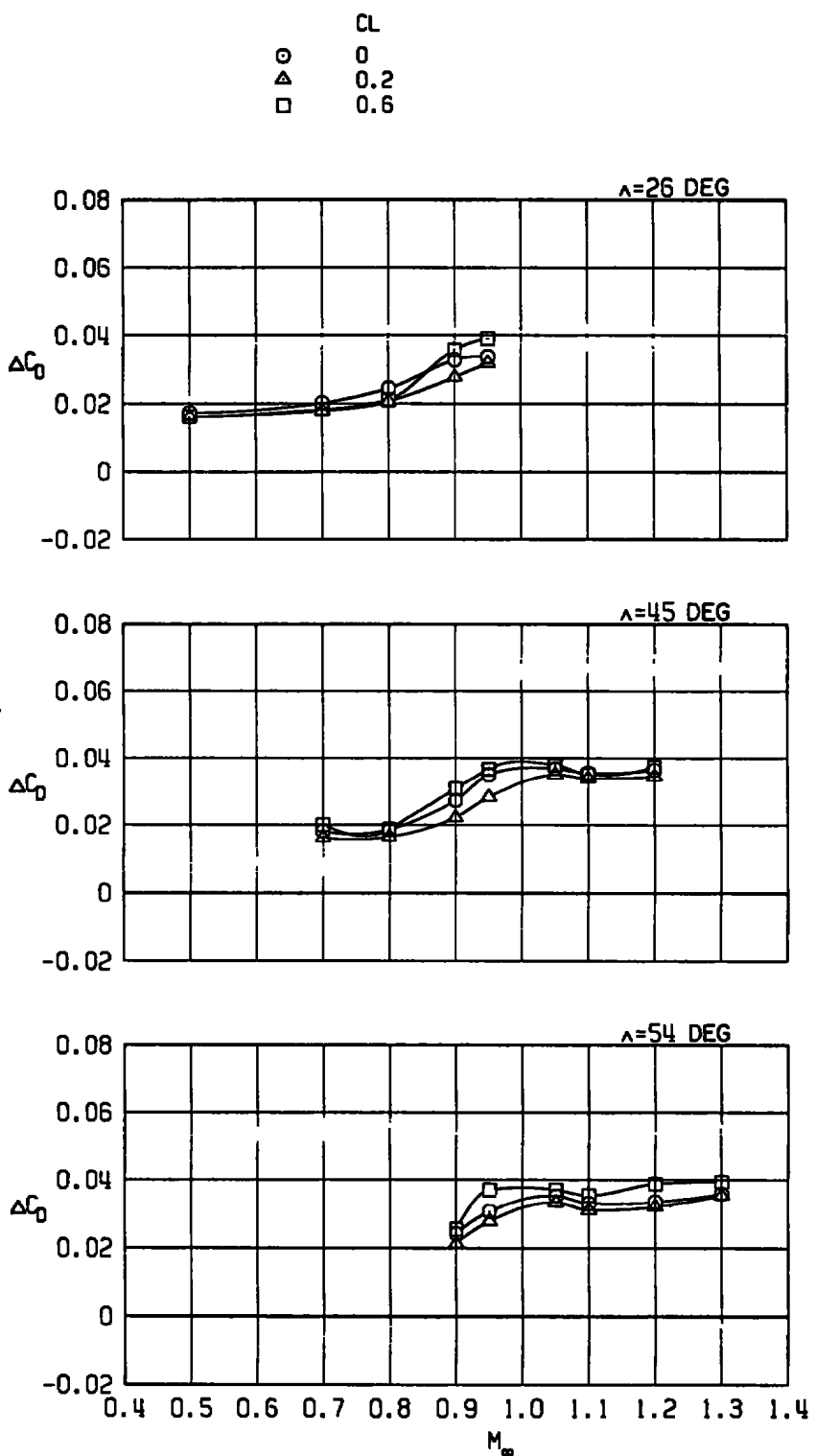
e. 12 AGM-65 stores
Figure 15. Continued.



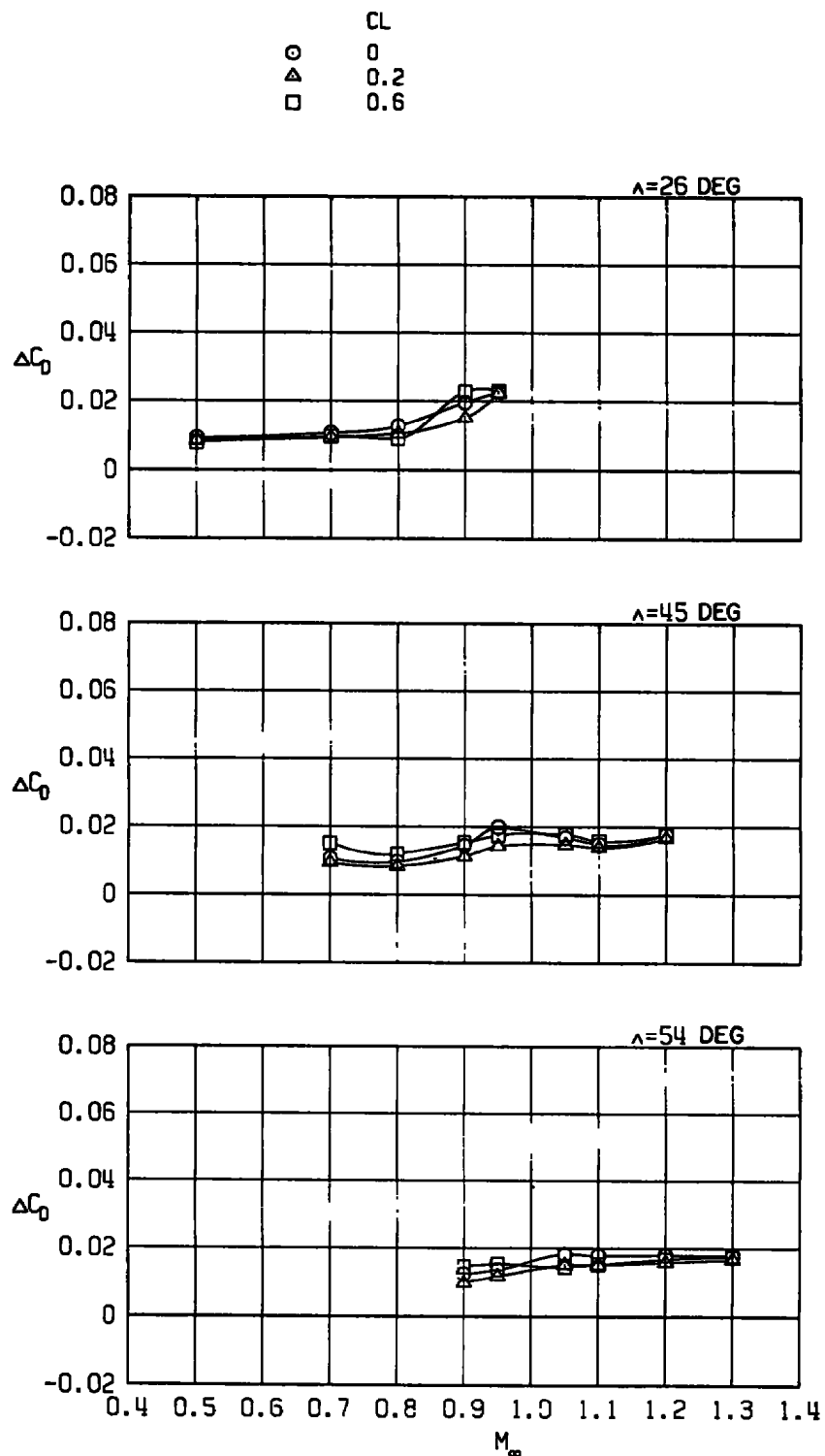
f. 16 Rockeye stores (slant 4 loading)
Figure 15. Continued.



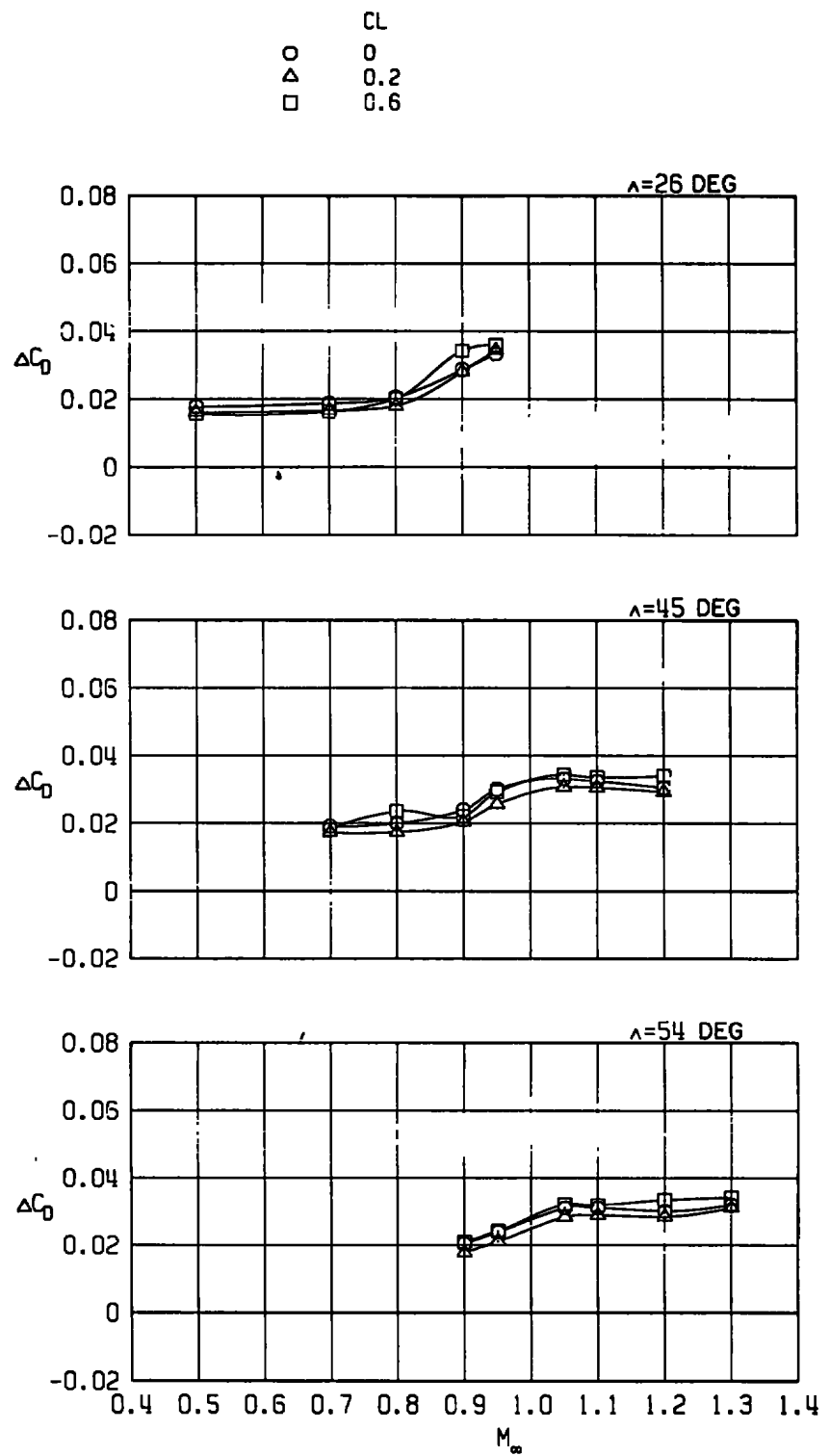
g. 12 Rockeye stores (outboard pylons)
Figure 15. Continued.



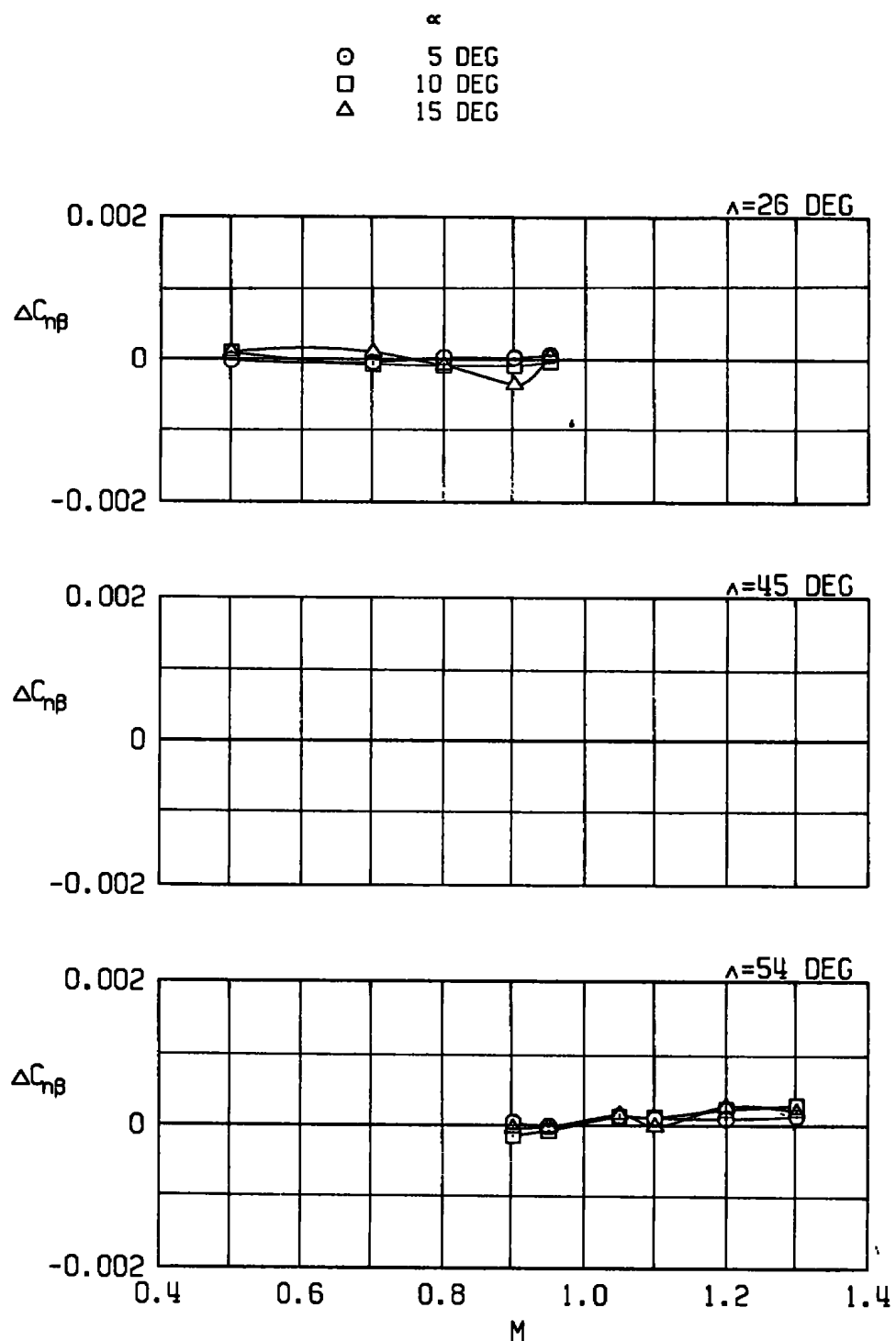
h. 12 SUU-30 stores (outboard pylons)
 Figure 15. Continued.



i. 12 MK-82SE stores (outboard pylons)
Figure 15. Continued.

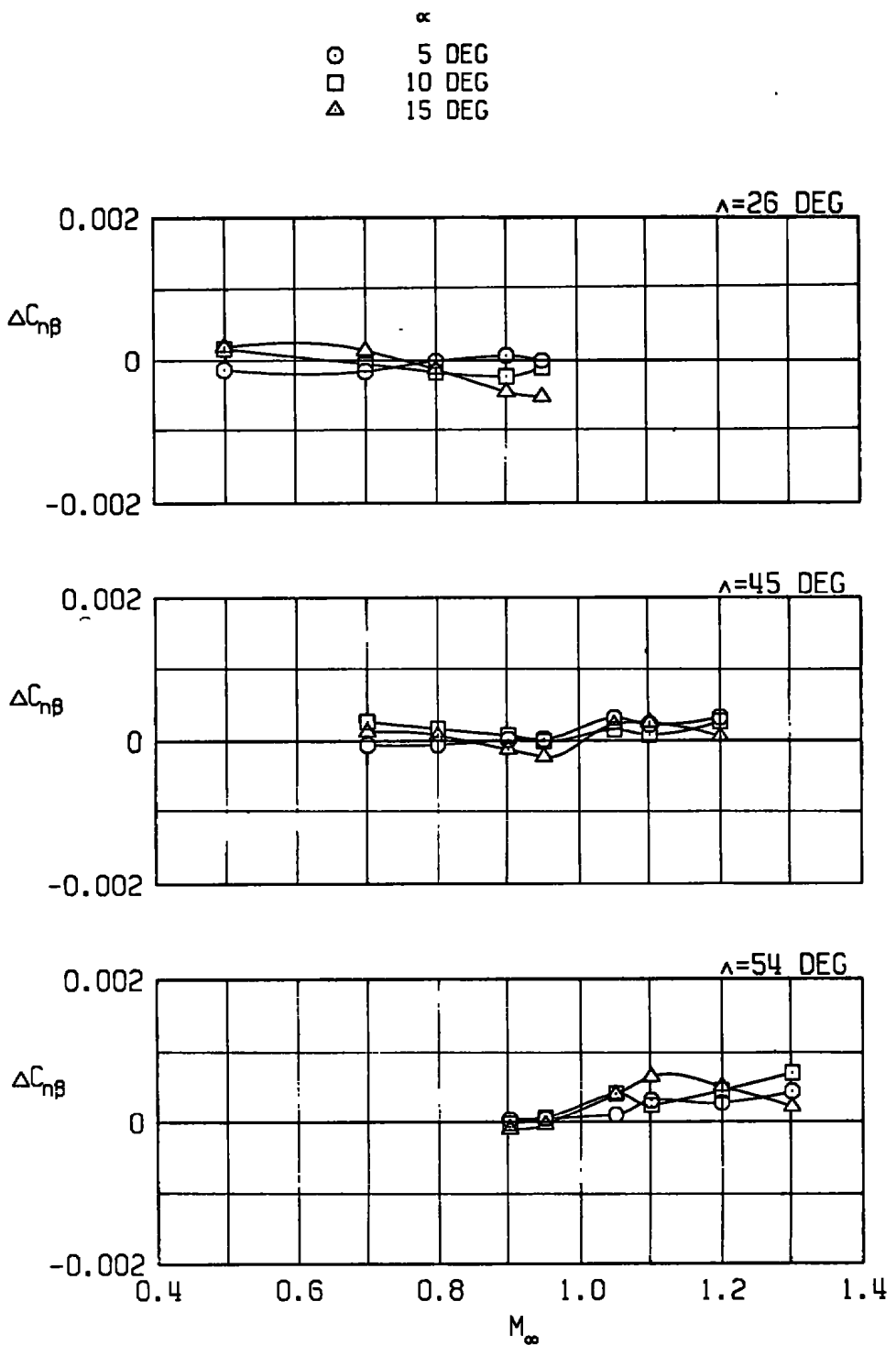


j. 22 MK-82SE stores
Figure 15. Concluded.

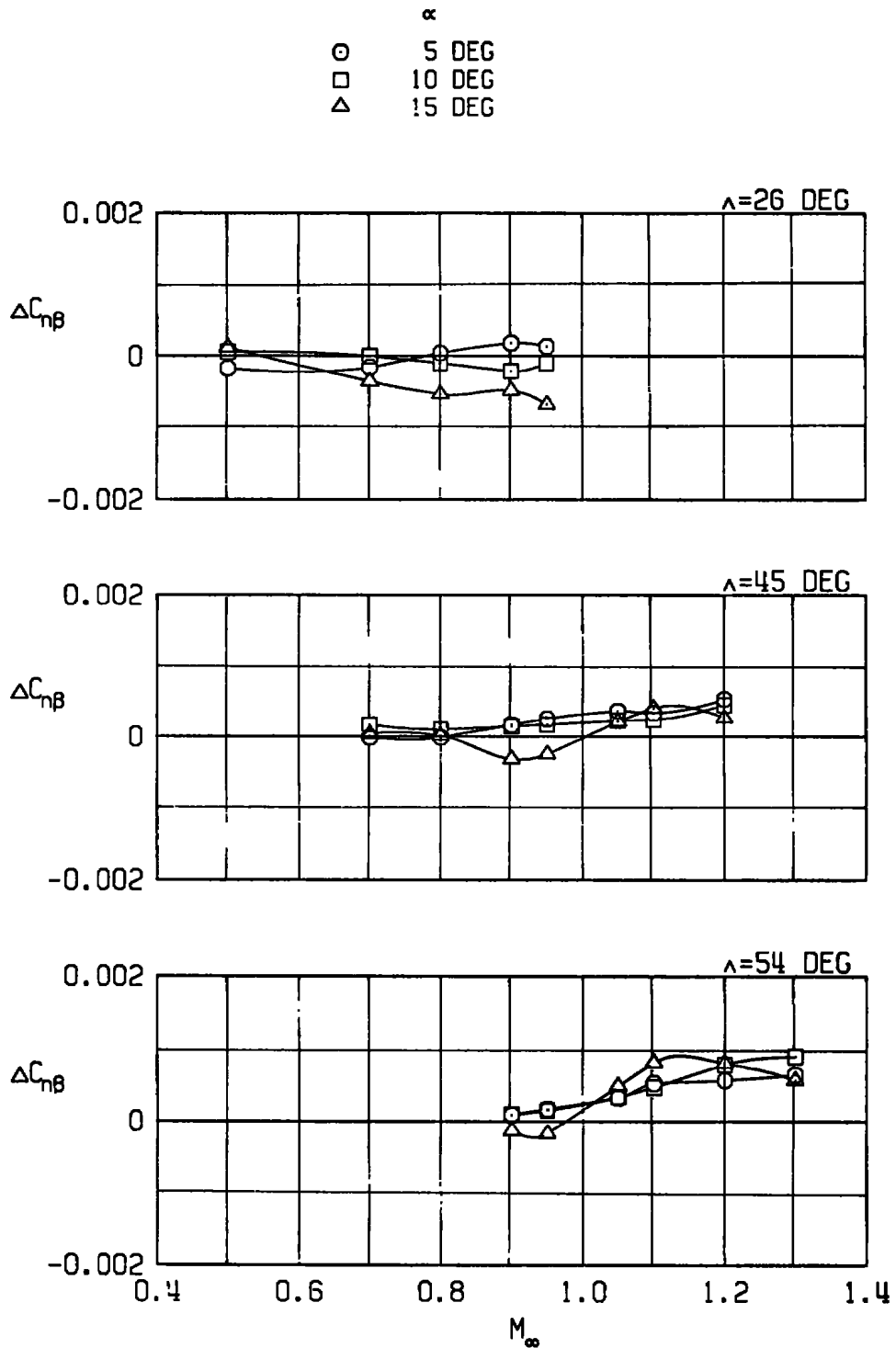


a. Pylons alone

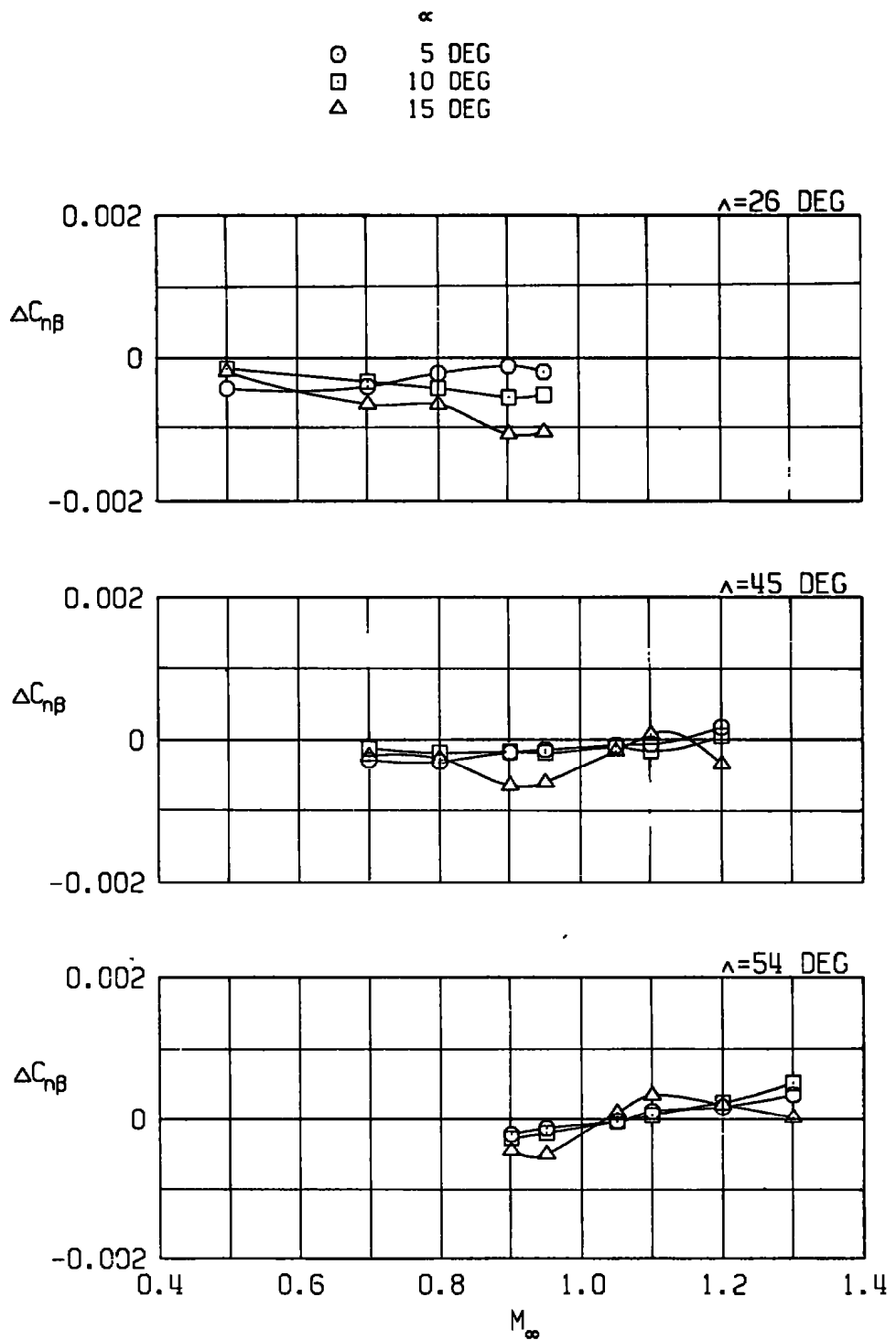
Figure 16. Effects of external stores on the static directional stability derivative.



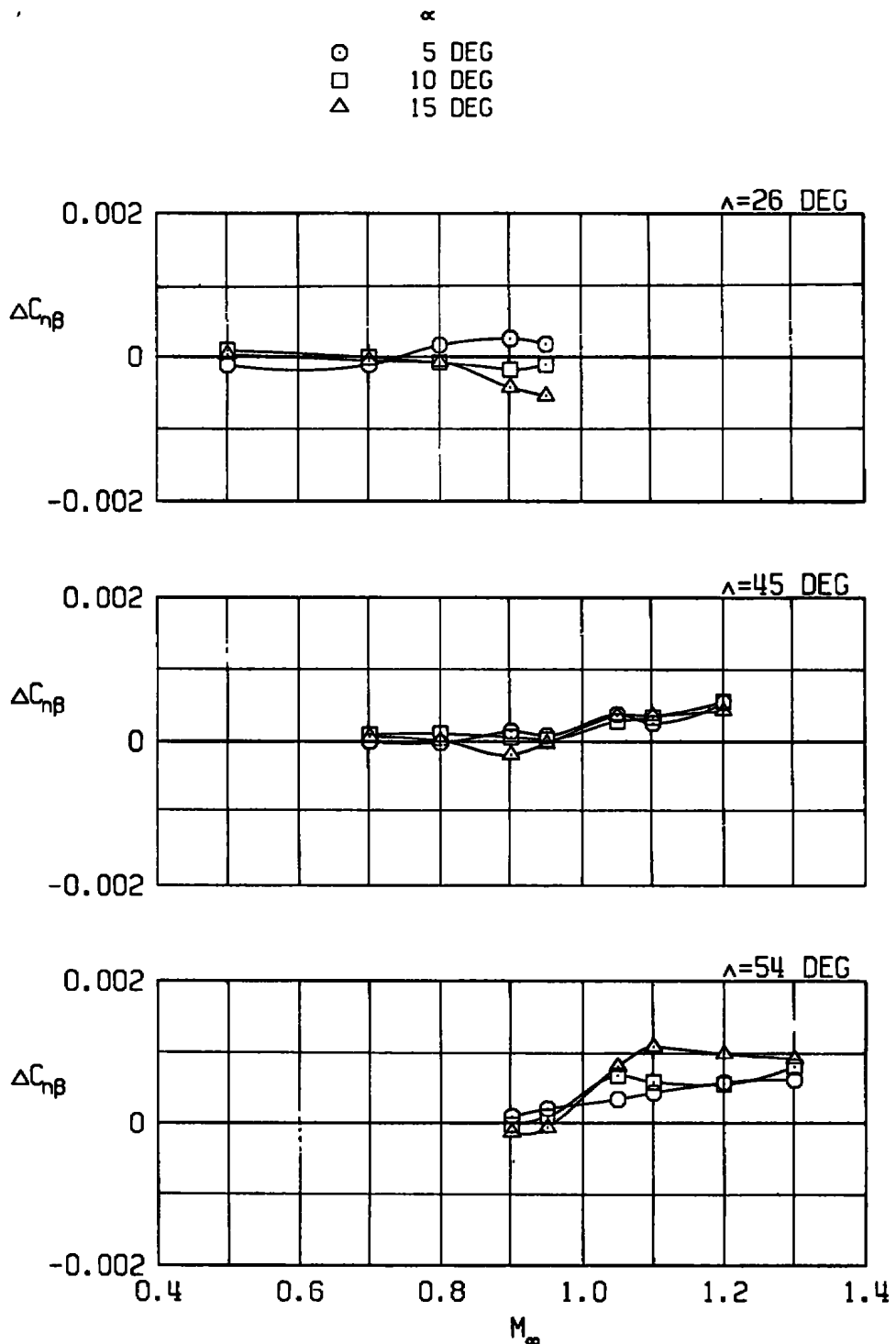
b. Four GBU-10 stores
Figure 16. Continued.



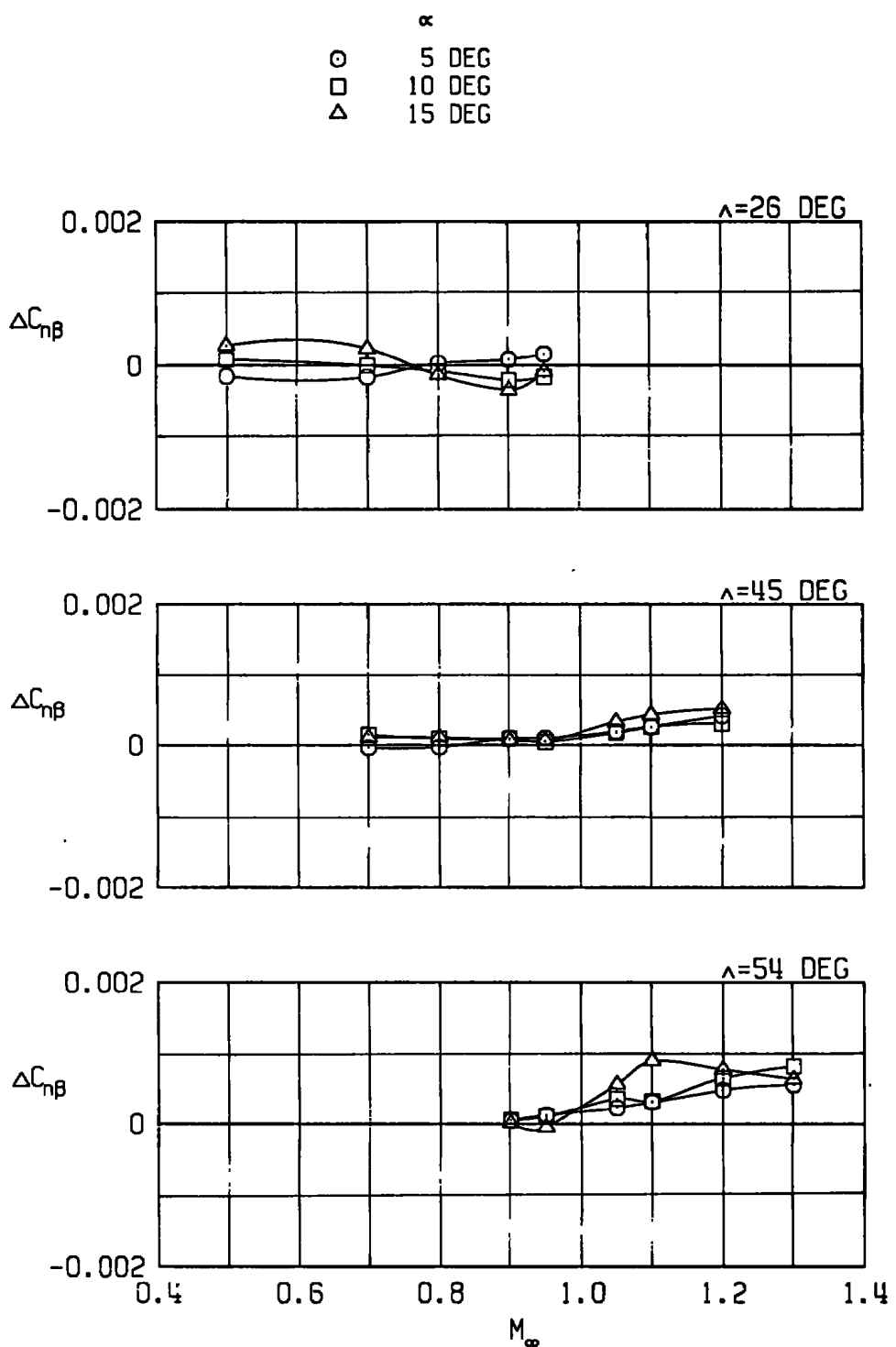
c. Four GBU-15CCW stores
 Figure 16. Continued.



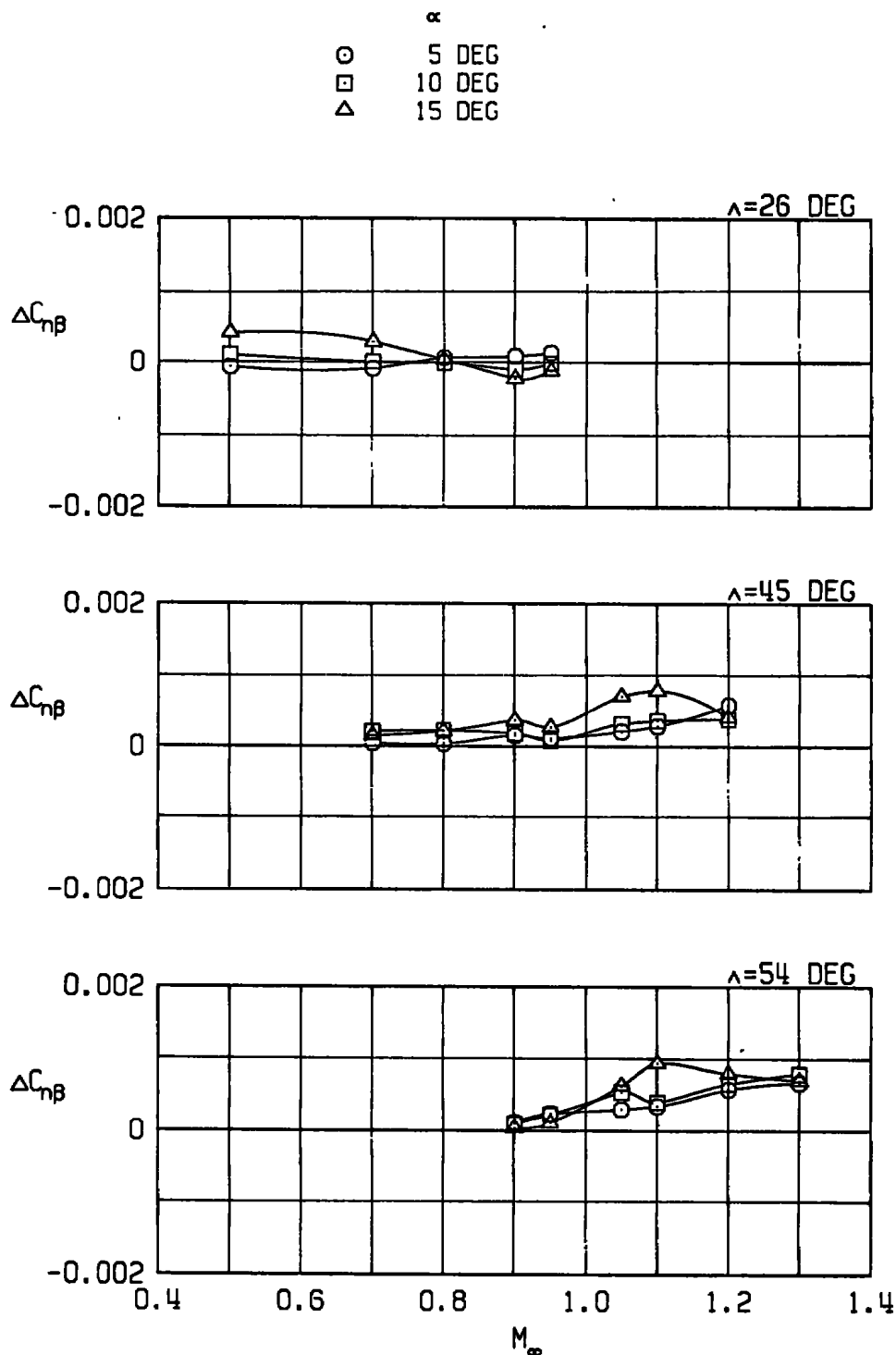
d. Four GBU-15CCW stores and extended
Pave Tack pod
Figure 16. Continued.



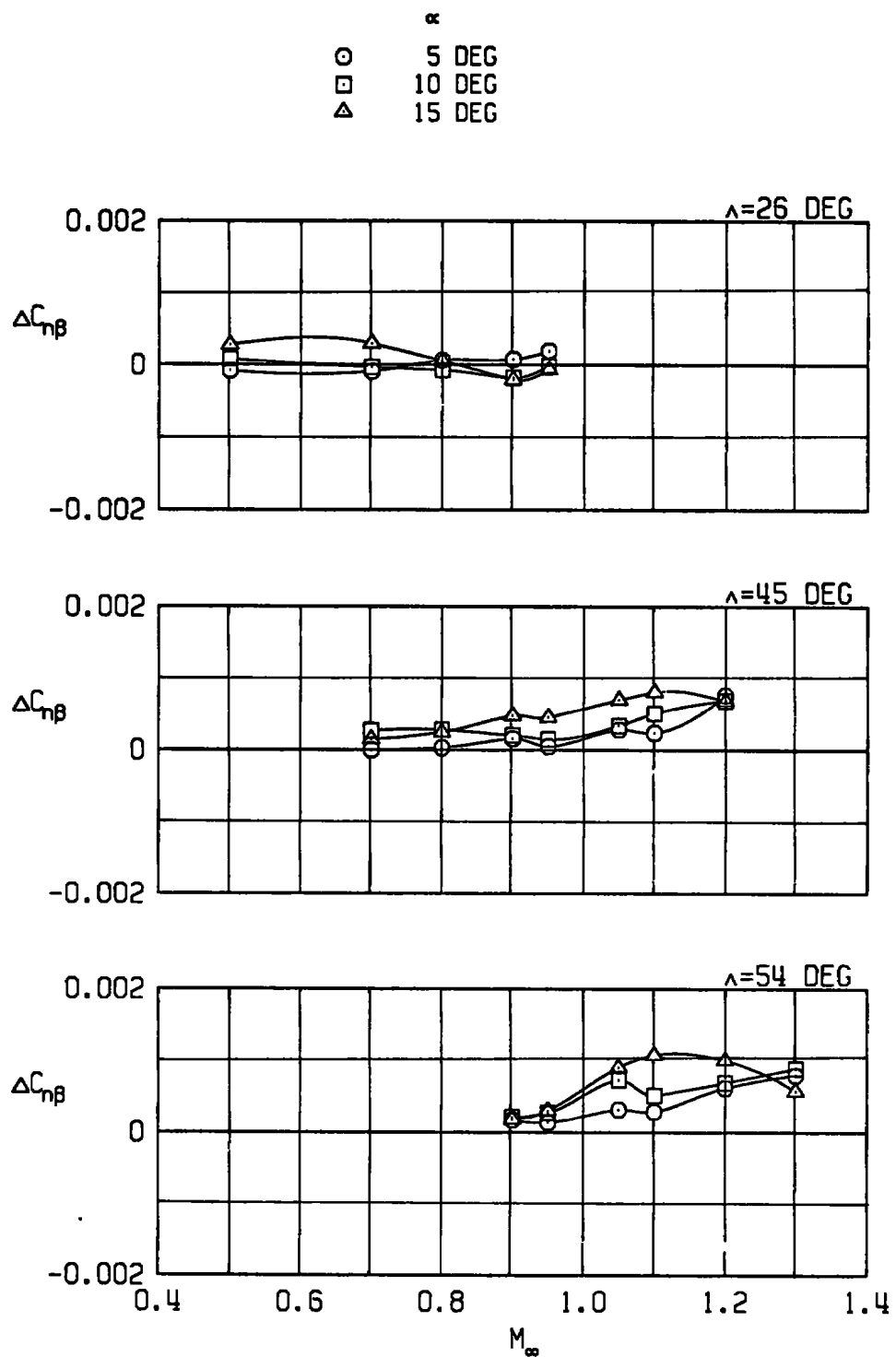
e. 12 AGM-65 stores
Figure 16. Continued.



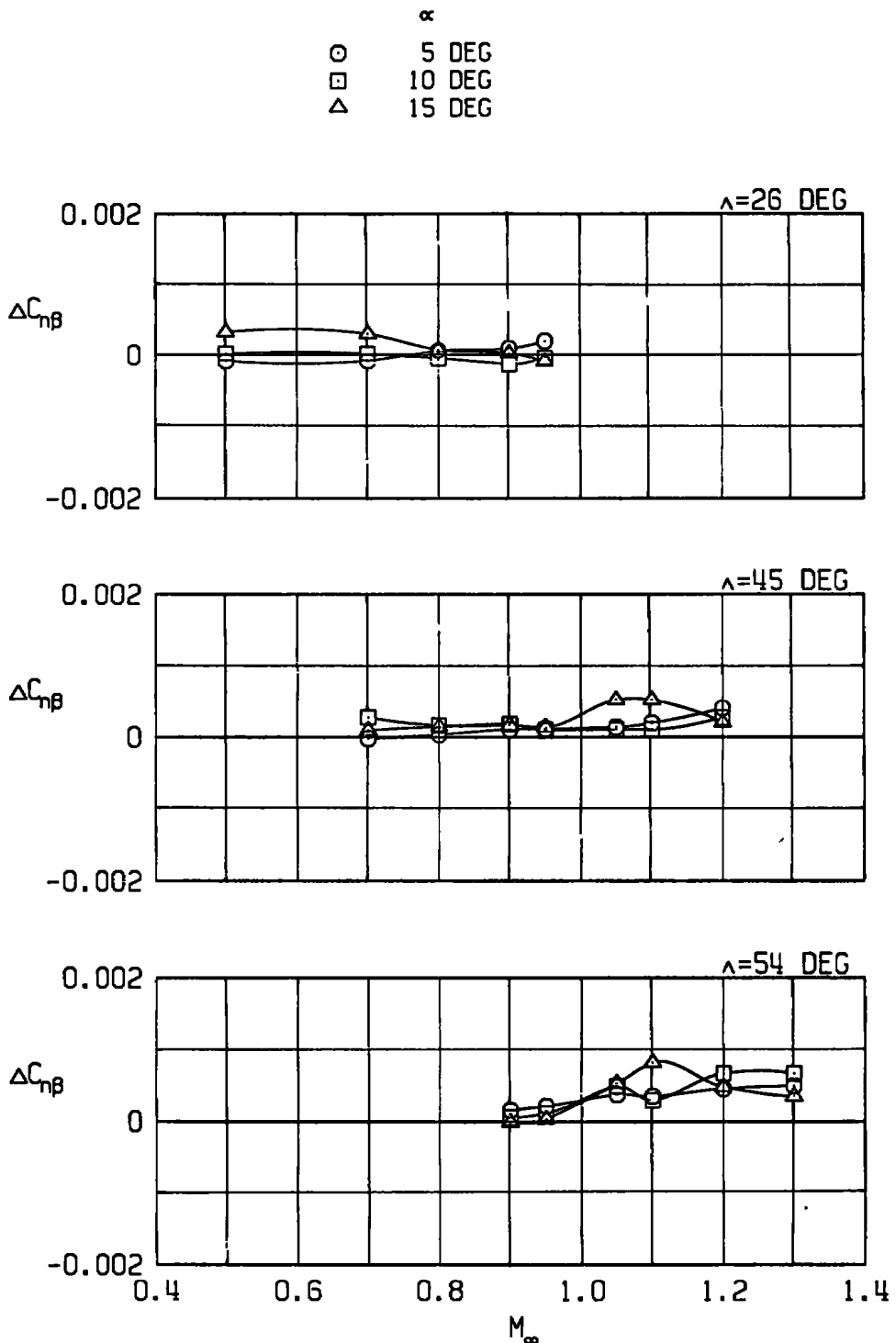
f. 16 Rockeye stores (slant 4 loading)
 Figure 16. Continued.



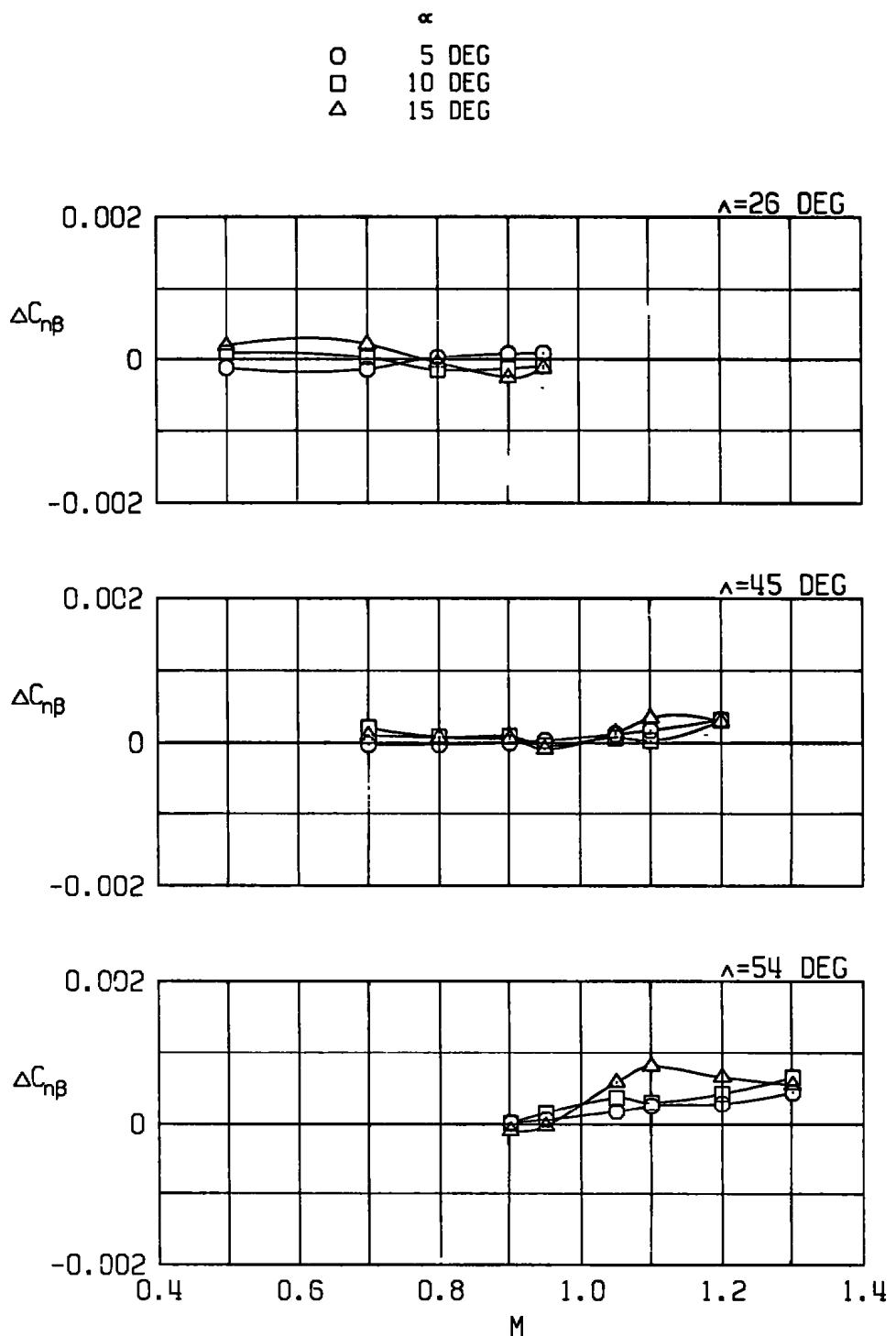
g. 12 Rockeye stores (outboard pylons)
Figure 16. Continued.



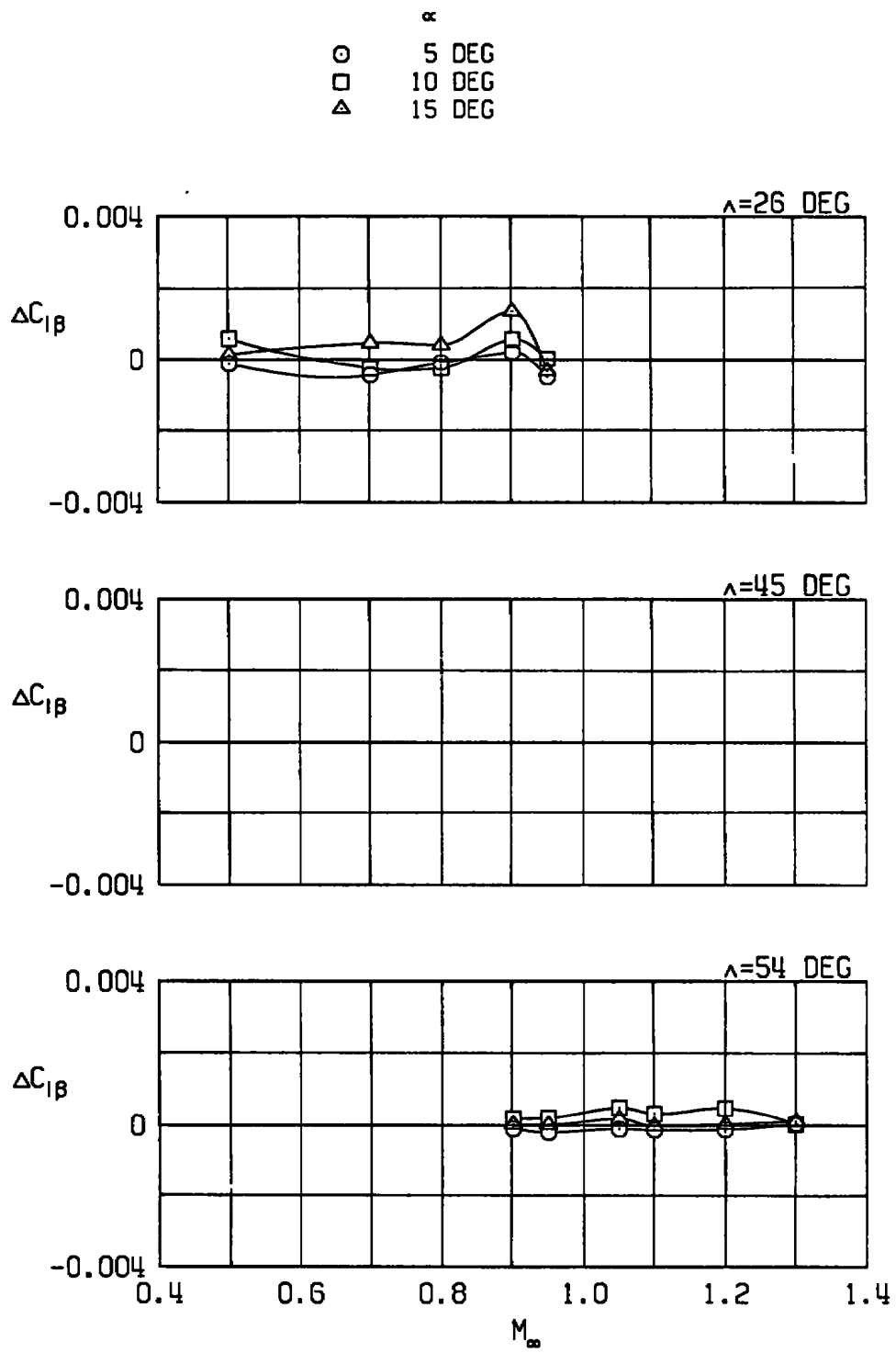
h. 12 SUU-30 stores (outboard pylons)
Figure 16. Continued.



i. 12 MK-82SE stores (outboard pylons)
Figure 16. Continued.

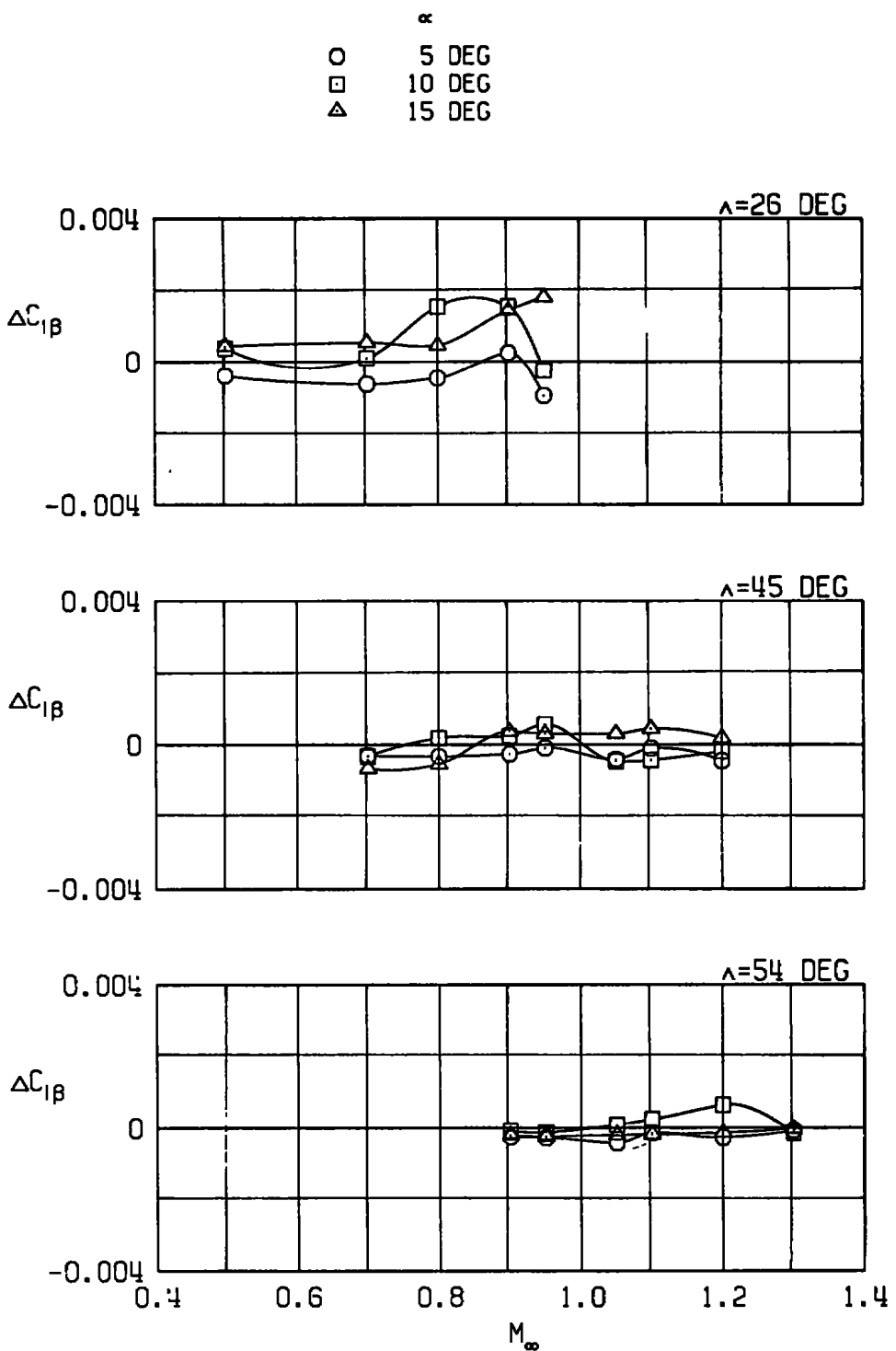


j. 22 MK-82SE stores
Figure 16. Concluded.

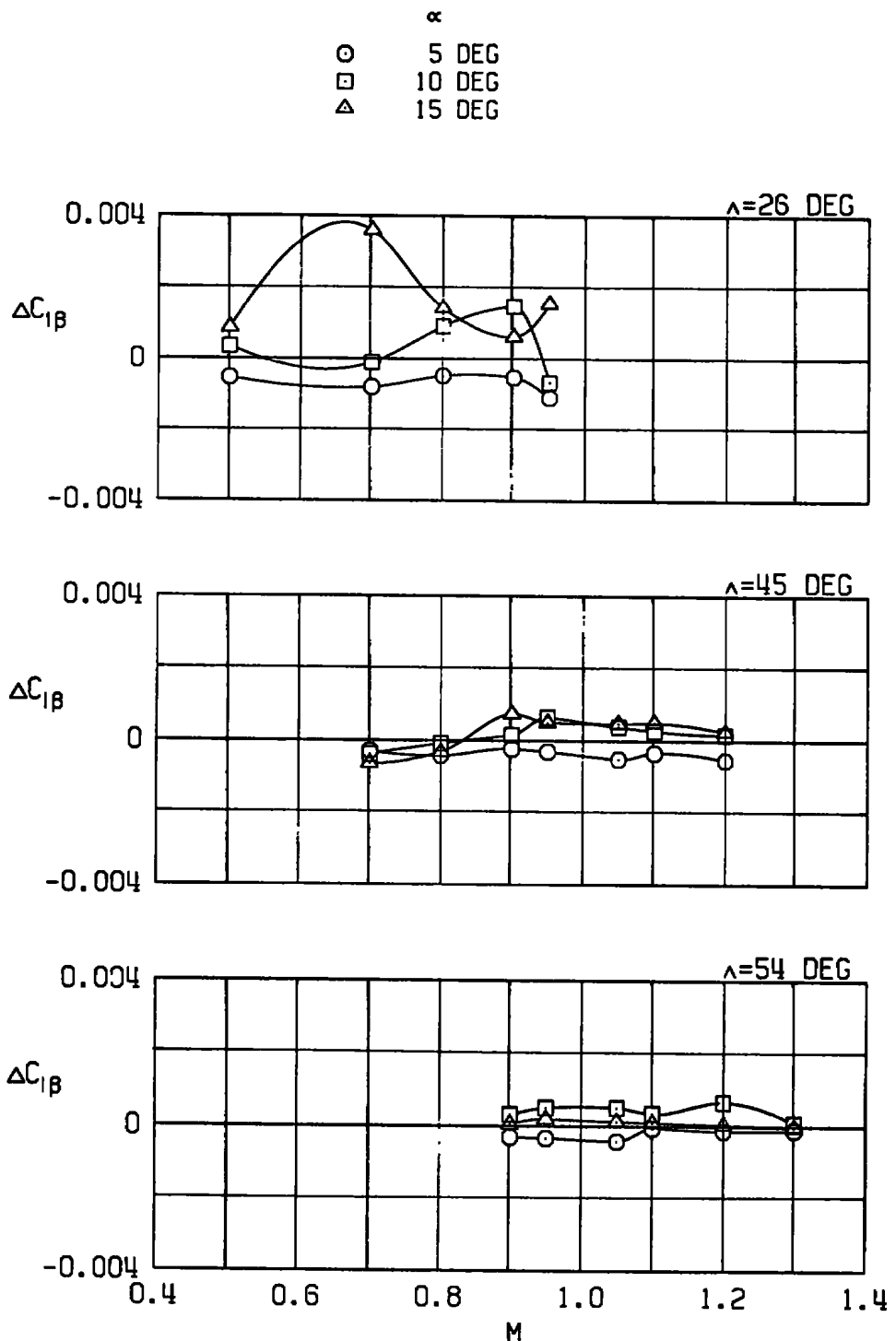


a. Pylons alone

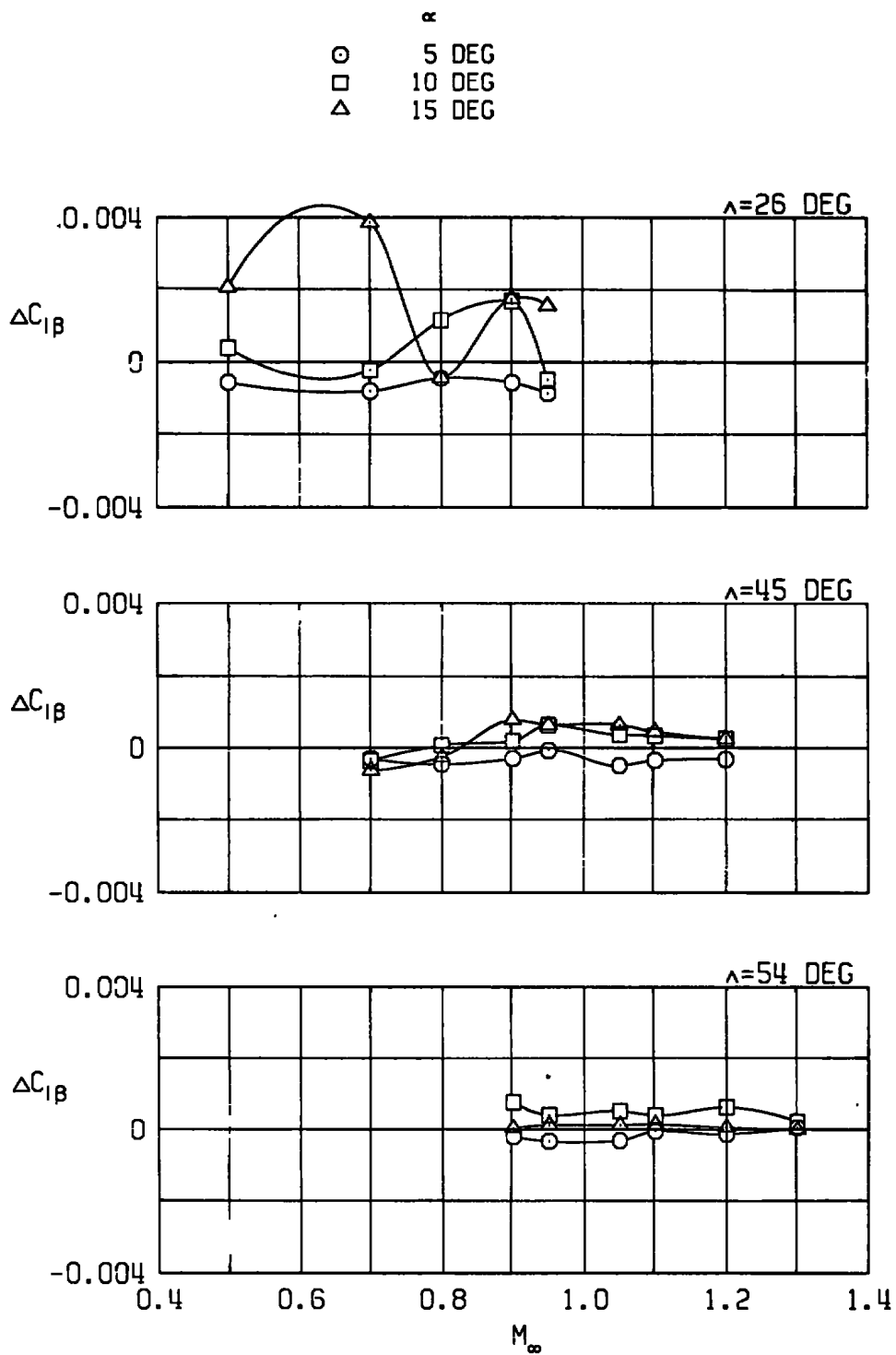
Figure 17. Effects of external stores on the effective dihedral.



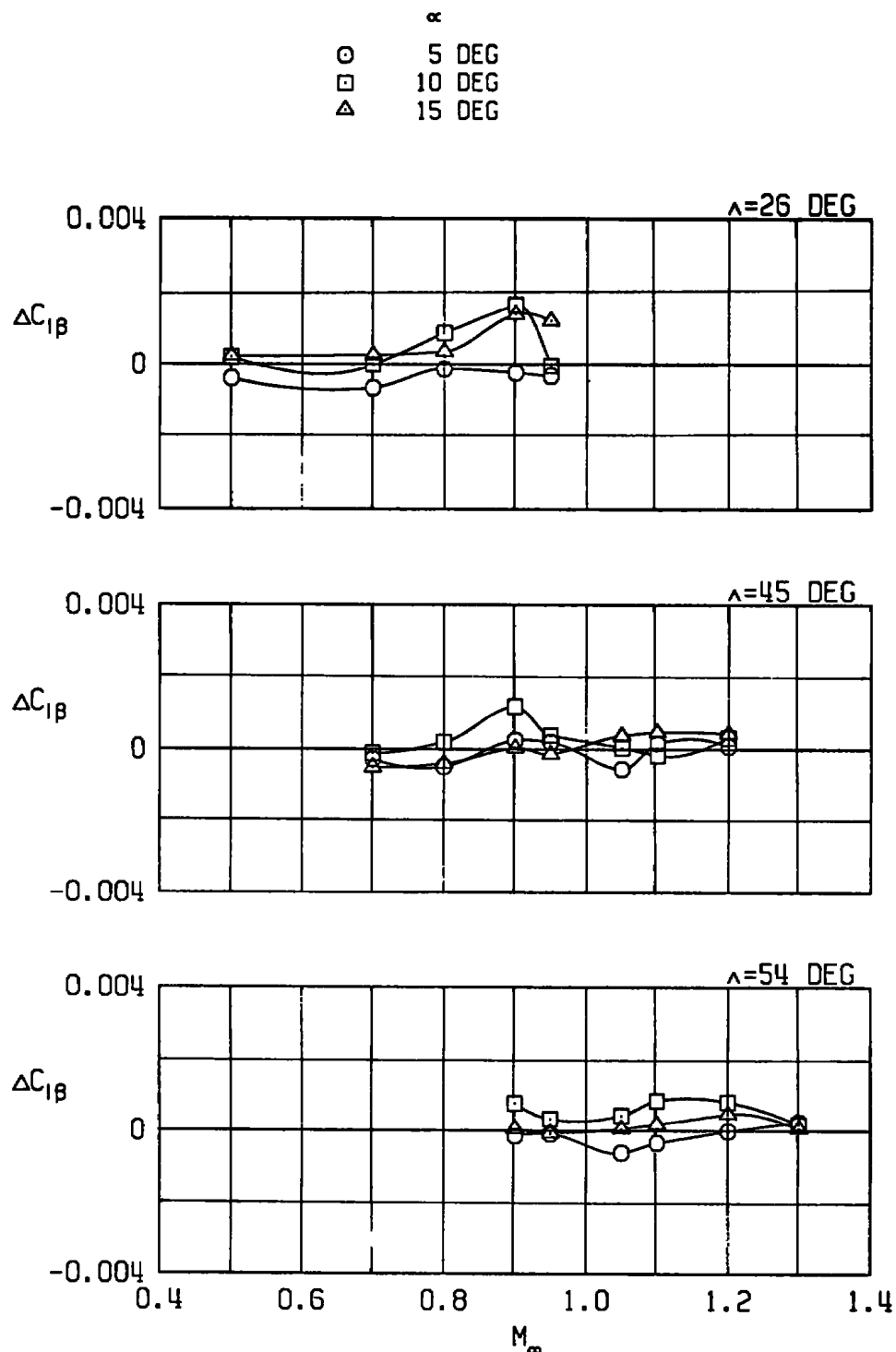
b. Four GBU-10 stores
Figure 17. Continued.



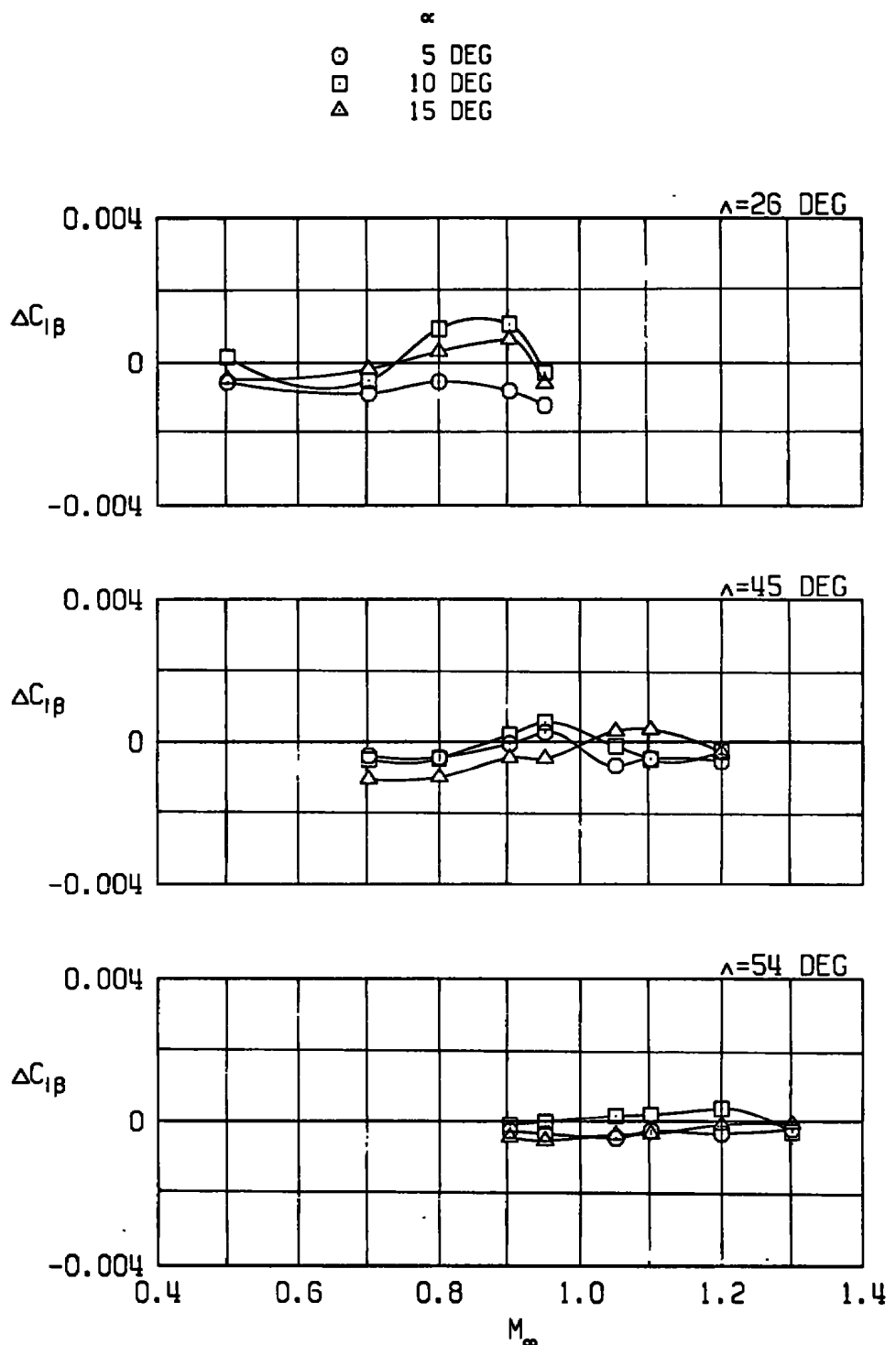
c. Four GBU-15CCW stores
Figure 17. Continued.



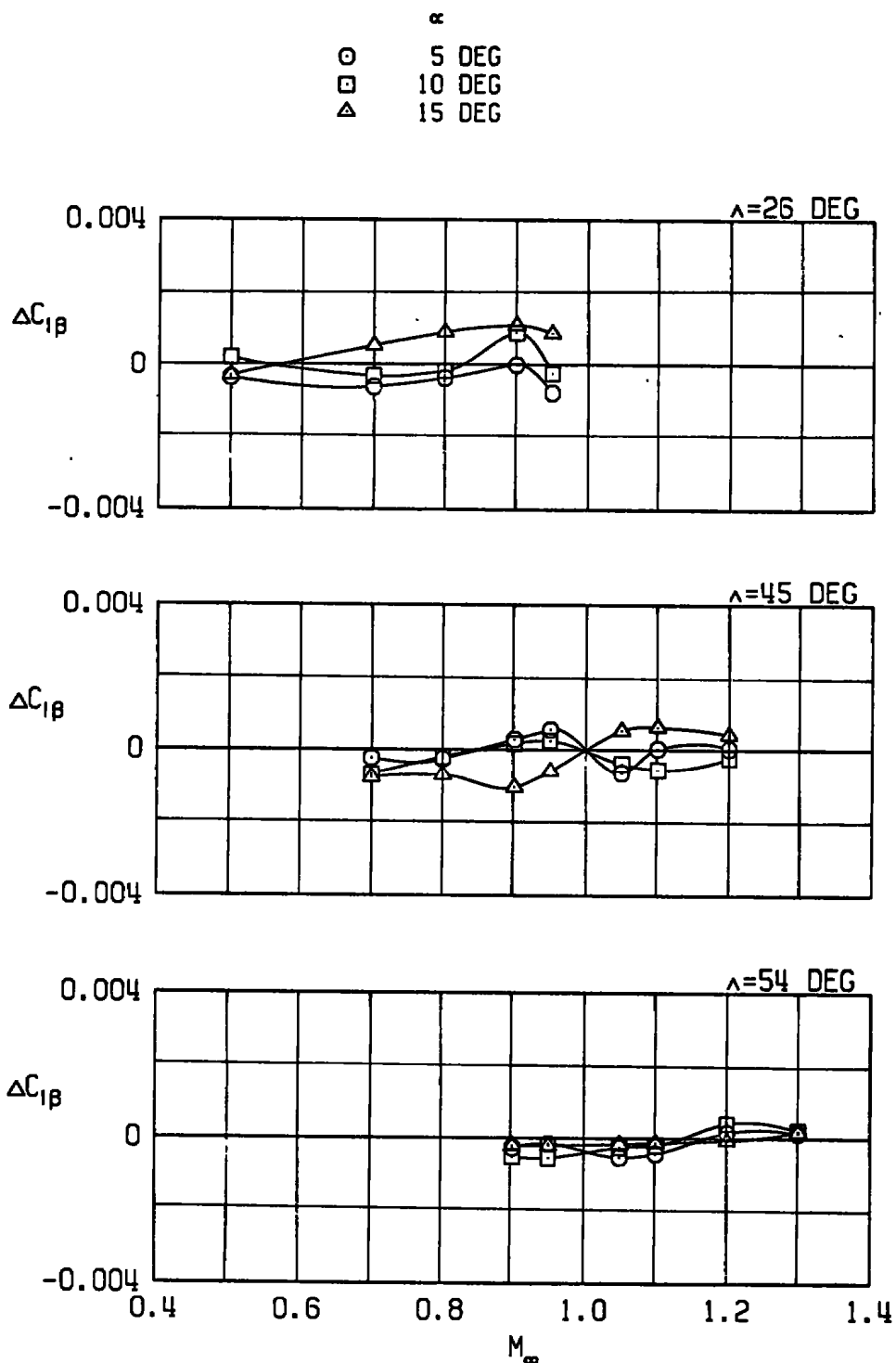
d. Four GBU-15CCW stores and extended
Pave Tack pod
Figure 17. Continued.



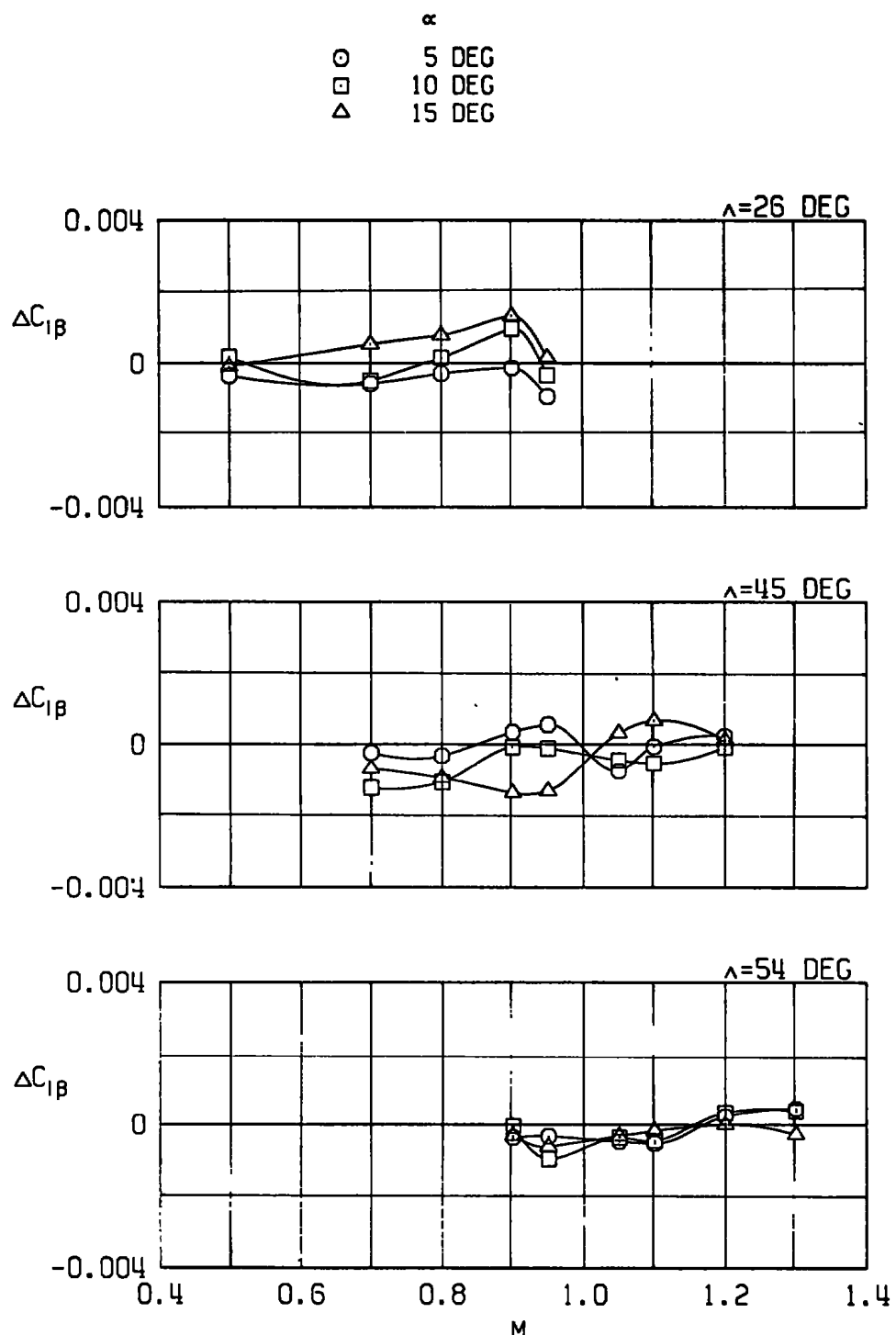
e. 12 AGM-65 stores
Figure 17. Continued.



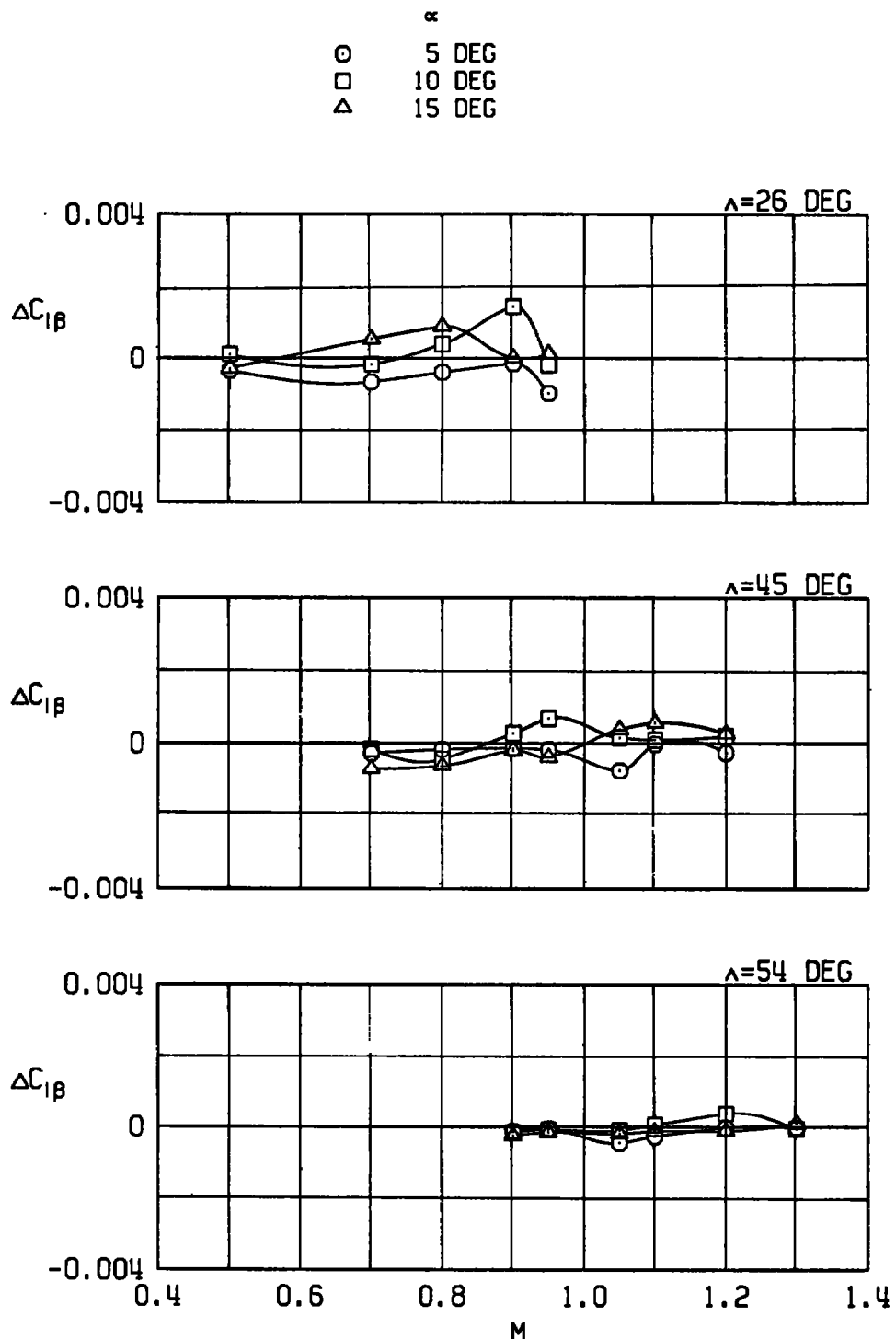
f. 16 Rockeye stores (slant 4 loading)
Figure 17. Continued.



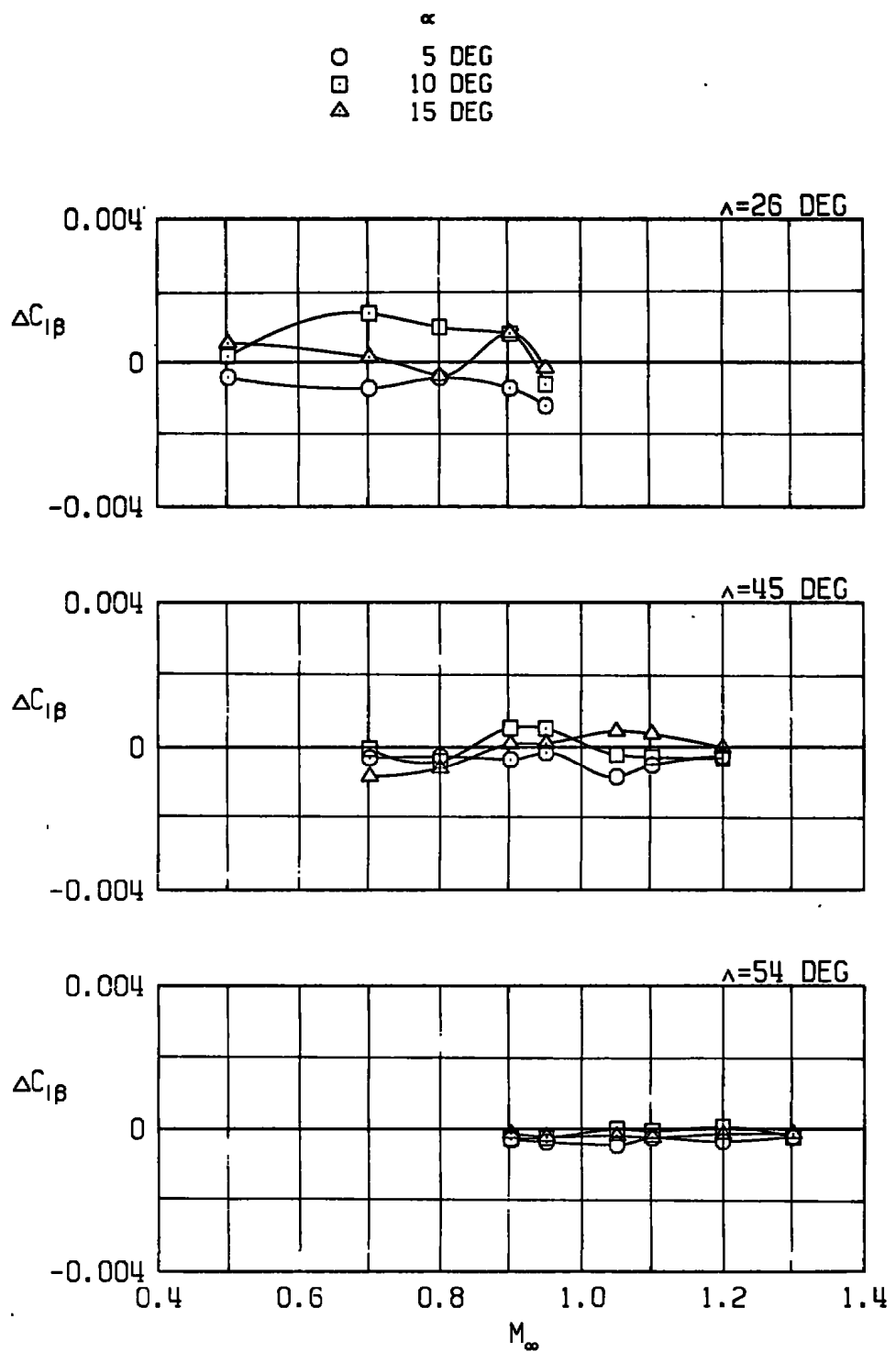
g. 12 Rockeye stores (outboard pylons)
Figure 17. Continued.



h. 12 SUU-30 stores (outboard pylons)
Figure 17. Continued.



i. 12 MK-82SE stores (outboard pylons)
 Figure 17. Continued.



j. 22 MK-82SE stores
Figure 17. Concluded.

Table 1. Part Number Index

Config.	Store Loading			Wing Sweep, deg	α , deg	β , deg	Mach Number								
	Outboard	Inboard	CL				0.5	0.7	0.8	0.9	0.95	1.05	1.1	1.2	1.3
1	Clean	Clean	Clean	26	V	0	32	39	45	51	61	--	--	--	--
					V	0	38*	40*	47*	52*	62	--	--	--	--
					5	V	36	43	49	59	64	--	--	--	--
					10	V	37	44	50	60	65	--	--	--	--
					15	V	**34	**41	**48	**55	**63				
				45	V	0	--	217	222	227	233	238	243	248	--
					V	0	--	218*	223*	228*	234*	239*	244*	249*	--
					5	V	--	220	225	231	236	241	246	251	--
					10	V	--	221	226	232	237	242	247	252	--
					15	V	--	219**	224**	230**	235**	240**	245**	250**	--

*Model inverted for tunnel flow angularity check.

**Model yawed from 0 to -10 to +10 to -10 deg for yaw hysteresis check.

***Model pitched from -2 to 18 to 0 deg for pitch hysteresis check.

Table 1. Continued

Config.	- Store Loading			Wing Sweep, deg	α , deg	β , deg	Mach Number								
	Outboard	Inboard	CL				0.5	0.7	0.8	0.9	0.95	1.05	1.1	1.2	1.3
1	Clean	Clean	Clean	54	V	0	--	--	--	*** 450	460	*** 465	470	*** 475	480
					V	0	--	--	--	456 [*]	461 [*]	466 [*]	471	476 [*]	481 [*]
					5	V	--	--	--	459	464	469	474	479	484
					10	V	--	--	--	458	463	468	473	478	483
					15	V	--	--	--	457 ^{**}	462 ^{**}	467 ^{**}	472 ^{**}	477 ^{**}	482 ^{**}
1 ^a	Clean	Clean	Clean	26	V	0	29	--	--	30	--	--	--	--	--
					V	0	--	--	--	770	--	--	--	--	774
					V	0	--	--	--	773	--	--	--	--	775
13 ^b	Clean	Clean	Clean	26	V	0	974	975	976	977	978	--	--	--	--
14 ^c	Clean	Clean	Clean	26	V	0	982	984	986	988	990	--	--	--	--
					V	0	983	985	987	989	991 ^{**}	992 ^{**}	993	--	--

^a $p_T = 2,000$ for Reynolds number effects.

^bAfterbody modification.

^cAfterbody modification and transition grit.

Table 1. Continued

Config.	Store Loading			Wing Sweep, deg	α , deg	β , deg	Mach Number								
	Outboard	Inboard	CL				0.5	0.7	0.8	0.9	0.95	1.05	1.1	1.2	1.3
2	3 AGM65	3 AGM65	Clean	26	V	0	69	73	77	81	85	--	--	--	--
					5	V	70	74	78	82	86	--	--	--	--
					10	V	71	75	79	83	87	--	--	--	--
					15	V	72	76	80	84	88	--	--	--	--
					45	V	0	--	256	260	264	268	272	276	280
				45	5	V	--	257	261	265	269	273	277	281	--
					10	V	--	258	262	266	270	274	278	282	--
					15	V	--	259	263	267	271	275	279	283	--
					54	V	0	--	--	--	491	495	499	503	507
					5	V	--	--	--	492	496	500	504	508	512
					10	V	--	--	--	493	497	501	505	509	513
					15	V	--	--	--	494	498	502	506	510	514

Table 1. Continued

Config.	Store Loading			Wing Sweep, deg	α , deg	β , deg	Mach Number								
	Outboard	Inboard	CL				0.5	0.7	0.8	0.9	0.95	1.05	1.1	1.2	1.3
3	4 Rockeye	4 Rockeye	Clean	26	V	0	146	150	154	158	162	--	--	--	--
					5	V	147	151	155	159	163	--	--	--	--
					10	V	148	152	156	160	164	--	--	--	--
					15	V	149	153	157	161	165	--	--	--	--
					45	V	0	--	349	353	357	364	368	372	376
						5	V	--	350	354	361	365	369	373	377
						10	V	--	351	355	362	366	370	374	378
						15	V	--	352	356	363	367	371	375	379
						54	V	0	--	--	572	576	580	584	588
							5	V	--	--	573	577	581	585	589
							10	V	--	--	574	578	582	586	590
							15	V	--	--	575	579	583	587	591
															595

Table 1. Continued

Config.	Store Loading			Wing Sweep, deg	α , deg	β , deg	Mach Number								
	Outboard	Inboard	CL				0.5	0.7	0.8	0.9	0.95	1.05	1.1	1.2	1.3
4	GBU-15 CCW	GBU-15 CCW	Clean	26	V	0	120	124	128	132	136	--	--	--	--
					5	V	121	125	129	133	137	--	--	--	--
					10	V	122	126	130	134	138	--	--	--	--
					15	V	123	127	131	135	139	--	--	--	--
				45	V	0	--	318	322	326	330	334	338	342	--
					5	V	--	319	323	327	331	335	339	343	--
					10	V	--	320	324	328	332	336	340	344	--
					15	V	--	321	325	329	333	337	341	345	--
				54	V	0	--	--	--	545	549	553	557	561	565
					5	V	--	--	--	546	550	554	558	562	566
					10	V	--	--	--	547	551	555	559	563	567
					15	V	--	--	--	548	552	556	560	564	568

Table 1. Continued

Config.	Store Loading			Wing Sweep, deg	α , deg	β , deg	Mach Number								
	Outboard	Inboard	CL				0.5	0.7	0.8	0.9	0.95	1.05	1.1	1.2	1.3
5	GBU-15 CCW	GBU-15 CCW	Pave Tack	26	V	0	92	96	102	106	110	--	--	--	--
					5	V	93	97	103	107	111	--	--	--	--
					10	V	94	98	104	108	112	--	--	--	--
					15	V	95	99 **	105	109	113	--	--	--	--
	45			45	V	0	--	287	291	295	299	303	307	311	--
					5	V	--	288	292	296	300	304	308	312	--
					10	V	--	289	293	297	301	305	309	313	--
					15	V	--	290	294	298	302	306	310	314	--
	54			54	V	0	--	--	--	518	522	526	530	534	538
					5	V	--	--	--	519	523	527	531	535	539
					10	V	--	--	--	520	524	528	532	536	540
					15	V	--	--	--	521	525	529	533	537	541

Table 1. Continued

Config.	Store Loading			Wing Sweep, deg	α , deg	β , deg	Mach Number								
	Outboard	Inboard	CL				0.5	0.7	0.8	0.9	0.95	1.05	1.1	1.2	1.3
6	6 MK-82SE	Pylon	Clean	26	V	0	169	173	177	181	185	--	--	--	--
					5	V	170	174	178	182	186	--	--	--	--
					10	V	171	175	179	183	187	--	--	--	--
					15	V	172	176	180	184	188	--	--	--	--
				45	V	0	--	383	387	391	395	399	403	408	--
					5	V	--	384	388	392	396	400	404	409	--
					10	V	--	385	389	393	397	401	405	410	--
					15	V	--	386	390	394	398	402	406	411	--
				54	V	0	--	--	--	708	712	719	723	727	731
					5	V	--	--	--	709	713	720	724	728	732
					10	V	--	--	--	710	714	721	725	729	733
					15	V	--	--	--	711	715	722	726	730	734

Table 1. Continued

Config.	Store Loading			Wing Sweep, deg	α , deg	β , deg	Mach Number								
	Outboard	Inboard	CL				0.5	0.7	0.8	0.9	0.95	1.05	1.1	1.2	1.3
7 ↓	6 SUU 30 ↓	Pylon ↓	Clean ↓	26 ↓	V	0	193	197	201	205	209	--	--	--	--
					5	V	194	198	202	206	210	--	--	--	--
					10	V	195	199	203	207	211	--	--	--	--
					15	V	196	200	204	208	212	--	--	--	--
				45 ↓	V	0	--	415	419	423	427	435	439	443	--
					5	V	--	416	420	424	428	436	440	444	--
					10	V	--	417	421	425	429	437	441	445	--
					15	V	--	418	422	426	430	438	442	446	--
				54 ↓	V	0	--	--	--	599	603	607	611	615	619
					5	V	--	--	--	600	604	608	612	616	620
					10	V	--	--	--	601	605	609	613	617	621
					15	V	--	--	--	602	606	610	614	618	622

Table 1. Continued

Config.	Store Loading			Wing Sweep, deg	α , deg	β , deg	Mach Number								
	Outboard	Inboard	CL				0.5	0.7	0.8	0.9	0.95	1.05	1.1	1.2	1.3
8 ↓	6 Rockeye ↓	Pylon ↓	Clean ↓	26 ↓	V	0	856	860	864	868	873	--	--	--	--
					5	V	857	861	865	870	874	--	--	--	--
					10	V	858	862	866	871	875	--	--	--	--
					15	V	859	863	867	872	876	--	--	--	--
				45 ↓	V	0	--	880	884	888	892	896	900	904	--
					5	V	--	881	885	889	893	897	901	905	--
					10	V	--	882	886	890	894	898	902	906	--
					15	V	--	883	887	891	895	899	903	907	--
				54 ↓	V	0	--	--	--	626	630	634	638	642	646
					5	V	--	--	--	627	631	635	639	643	647
					10	V	--	--	--	628	632	636	640	644	648
					15	V	--	--	--	629	633	637	641	645	649

Table 1. Continued

Config.	Store Loading			Wing Sweep, deg	α , deg	β , deg	Mach Number								
	Outboard	Inboard	CL				0.5	0.7	0.8	0.9	0.95	1.05	1.1	1.2	1.3
10	GBU-10	GBU-10	Clean	36	V	0	832	836	840	844	848	--	--	--	--
					5	V	833	837	841	845	849	--	--	--	--
					10	V	834	838	842	846	850	--	--	--	--
					15	V	835	839	843	847	851	--	--	--	--
	GBU-10	GBU-10	Clean	45	V	0	--	911	915	919	924	928	932	936	--
					5	V	--	912	916	920	925	929	933	937	--
					10	V	--	913	917	921	926	930	934	938	--
					15	V	--	914	918	922	927	931	935	939	--
	GBU-10	GBU-10	Clean	54	V	0	--	--	--	653	657	661	665	669	673
					5	V	--	--	--	654	658	662	666	670	674
					10	V	--	--	--	655	659	663	667	671	675
					15	V	--	--	--	656	660	664	668	672	676

Table 1. Continued

Config.	Store Loading			Wing Sweep, deg	α , deg	β , deg	Mach Number								
	Outboard	Inboard	CL				0.5	0.7	0.8	0.9	0.95	1.05	1.1	1.2	1.3
11	Pylon	Pylon	Clean	26	V	0	786	790	794	798	802	--	--	--	--
					5	V	787	791	795	799	803	--	--	--	--
					10	V	788	792	796	800	804	--	--	--	--
					15	V	789	793	797	801	805	--	--	--	--
					54	V	0	--	--	--	680	684	688	692	696
						5	V	--	--	--	681	685	689	693	698
						10	V	--	--	--	682	686	690	694	699
						15	V	--	--	--	683	687	691	695	700
															704

Table 1. Concluded

Config.	Store Loading			Wing Sweep, deg	α , deg	β , deg	Mach Number								
	Outboard	Inboard	CL				0.5	0.7	0.8	0.9	0.95	1.05	1.1	1.2	1.3
12	5 MK-82SE	6 MK-82SE	Clean	26	V	0	808	813	817	821	825	--	--	--	--
					5	V	809	814	818	822	826	--	--	--	--
					10	V	811	815	819	823	827	--	--	--	--
					15	V	812	816	820	824	828	--	--	--	--
					45	V	0	--	943	947	951	955	959	963	967
						5	V	--	944	948	952	956	960	964	968
						10	V	--	945	949	953	957	961	965	969
						15	V	--	946	950	954	958	962	966	970
						54	V	0	--	--	--	738	742	746	750
							5	V	--	--	--	739	743	747	751
							10	V	--	--	--	740	744	748	752
							15	V	--	--	--	741	745	749	753

Table 2. Aerodynamic Coefficient Uncertainties

M_{∞}	q_{∞} , psf	$\pm \delta C_L$	$\pm \delta C_m$	$\pm \delta C_D$	$\pm \delta C_Y$	$\pm \delta C_n$	$\pm \delta C_l$
0.50	180	0.0350	0.0136	0.0124	0.0101	0.0016	0.0010
0.70	295	0.0188	0.0084	0.0071	0.0060	0.0010	0.0006
0.80	350	0.0144	0.0071	0.0057	0.0050	0.0008	0.0005
0.90	400	0.0122	0.0064	0.0050	0.0043	0.0007	0.0005
0.95	425	0.0117	0.0062	0.0048	0.0041	0.0007	0.0005
1.05	460	0.0100	0.0063	0.0043	0.0037	0.0006	0.0004
1.10	475	0.0093	0.0059	0.0041	0.0036	0.0006	0.0004
1.20	500	0.0082	0.0055	0.0038	0.0034	0.0006	0.0004
1.30	515	0.0073	0.0051	0.0035	0.0033	0.0006	0.0004

Table 3. Incremental Drag Coefficients

Stores	Pylon Loading	Rack	ΔC_D		
			$\Lambda = 26^\circ$ $M_\infty = 0.7$ $C_L = 0.6$	$\Lambda = 45^\circ$ $M_\infty = 0.9$ $C_L = 0.4$	$\Lambda = 54^\circ$ $M = 1.2$ $C_L = 0.2$
Pylons alone	-	-	0.004	-	0.005
4 GBU-10	Single	-	0.011	0.014	0.019
4 GBU-15CCW	Single	-	0.013	0.017	0.025
4 GBU-15CCW Pave Tack Pod	Single	-	0.018	0.023	0.031
12 AGM-65	Multiple	LAU-88	0.022	0.031	0.035
16 Rockeye	Multiple Slant 4	BRU-3A/A	0.017	0.019	0.023
12 Rockeye	Multiple Outboard	BRU-3A/A	0.010	0.012	0.021
12 SUU-30H/B	Multiple Outboard	BRU-3A/A	0.018	0.021	0.032
12 MK-82SE	Multiple Outboard	BRU-3A/A	0.010	0.011	0.016
22 MK-82SE	Multiple	BRU-3A/A	0.016	0.019	0.028

NOMENCLATURE

b	Model reference span, 31.500 in.
BL	Model buttline, in.
C_A	Axial-force coefficient, axial force/ $q_\infty S$
C_D	Drag coefficient, drag/ $q_\infty S$
C_{D_0}	Drag coefficient at zero lift
ΔC_D	Incremental changes in drag coefficient caused by adding external stores; positive values indicate a drag increase
C_L	Lift coefficient, lift/ $q_\infty S$
$C_{L\alpha}$	Lift curve slope, slope of a linear least-squares curve fit of the lift coefficient versus angle of attack from $-2 \leq \alpha \leq 6$ deg, per degree
C_L	Centerline
C_Q	Rolling-moment coefficient, rolling moment/ $q_\infty Sb$
$C_{Q\beta}$	Effective dihedral, slope of a linear least-squares curve fit of the rolling-moment coefficient versus sideslip angle from $-4 \leq \beta \leq 4$ deg, per degree
$\Delta C_{Q\beta}$	Incremental change in the effective dihedral caused by adding external stores; positive values indicate a favorable dihedral effect
C_m	Pitching-moment coefficient, pitching moment/ $q_\infty S\bar{c}$ (see Fig. 2 for moment reference location)
C_N	Normal-force coefficient, normal force/ $q_\infty S$
C_n	Yawing-moment coefficient, yawing moment/ $q_\infty Sb$
$C_{n\beta}$	Static directional stability derivative, slope of a least-squares curve fit of the yawing-moment coefficient versus sideslip angle from $-4 \leq \beta \leq 4$ deg, per degree
$\Delta C_{n\beta}$	Incremental changes in the static directional stability derivative caused by adding external stores; positive values indicate a destabilizing effect

C_Y	Side-force coefficient, side force/ $q_\infty S$
$C_{Y\beta}$	Side-force derivative, slope of a linear least-squares curve fit of the side-force coefficient versus angle of sideslip from $-4 \leq \beta \leq 4$ deg, per degree
\bar{c}	Theoretical mean aerodynamic chord at $\Lambda = 16$ deg, 4.521 in.
FS	Model fuselage station, in.
M_∞	Free-stream Mach number
p_t	Free-stream total pressure, psfa
q_∞	Free-stream dynamic pressure, psf
Re	Unit Reynolds number, per foot
S	Model reference area, wing area, 0.911 ft ²
SM	Static margin, slope of a linear least-squares curve fit of the pitching-moment coefficient versus lift coefficient from $-2 \leq \alpha \leq 6$ deg, fraction of \bar{c} ; negative when the center of pressure is aft of the moment reference center
ΔSM	Incremental change in static margin caused by adding external stores; positive values indicate a destabilizing effect
WL	Model waterline from reference horizontal plane, in.
α	Model waterline angle of attack, deg
$\Delta\alpha$	Tunnel flow angle, deg, positive for flow upwash
β	Angle of sideslip, deg
Λ	Wing leading-edge sweep angle, deg

ERRATA

AEDC-TR-78-35, July 1978
(UNCLASSIFIED REPORT)

AERODYNAMIC CHARACTERISTICS OF A 1/24-SCALE F-111 AIRCRAFT WITH VARIOUS EXTERNAL STORES AT MACH NUMBERS FROM 0.5 TO 1.3

C. F. Anderson, ARO, Inc.

Arnold Engineering Development Center
Air Force Systems Command
Arnold Air Force Station, Tennessee 37389

Recent tests with the 1/24-scale F-111 model used to obtain the data presented in AEDC-TR-78-35 revealed that the model can foul the sting internally ahead of the fouling strip installed for that test. Therefore, all data obtained with the 1/24-scale F-111 model were examined for possible fouling. The data indicate that fouling may have been present for most configurations at high angles of attack at Mach numbers above 1.0. The maximum angle of attack for which no indication of fouling was observed is presented in the table below for each test configuration. All data at angles of attack above those listed should be used with caution.

Maximum Angle of Attack without Possible Fouling

Config	$\Delta = 45$ deg			$\Delta = 54$ deg			
	M = 1.05	M = 1.1	M = 1.2	M = 1.05	M = 1.1	M = 1.2	M = 1.3
1	12	10	10	12	10	10	10
2	14	14	14				14
3						14	14
4			14			14	14
5	14	14	14		14	14	14
6			14	14	14	14	12
7	14	14	14				14
8	14	14	14				14
10	14	14	14	14	14	14	12
11	--	--	--	12	12	12	10
12							14

Note: No evidence of fouling was observed in the data where angles are not shown. (Symbol -- indicates no data taken.)